IN VIVO MONITORING OF NEUROTRANSMITTER SEROTONIN AND DOPAMINE IN THE STRIATUM OF FREELY-MOVING RATS WITH ONE MINUTE TEMPORAL RESOLUTION BY ONLINE MICRODIALYSIS COUPLED WITH CAPIILARY HPLC

by

Jing Zhang

Bachelor of Science, Peking University, 2007

Submitted to the Graduate Faculty of

The Kenneth P. Dietrich School of Arts and Sciences

in partial fulfillment of the requirements for the degree of

Doctor of Philosophy

University of Pittsburgh

2016

UNIVERSITY OF PITTSBURGH

THE KENNETH P. DIETRICH SCHOOL OF ARTS AND SCIENCES

This dissertation was presented

by

Jing Zhang

It was defended on

March 30th, 2016

and approved by

Shigeru Amemiya, Associate Professor, Department of Chemistry

Adrian C. Michael, Professor, Department of Chemistry

Jeffrey K. Yao, Research Professor, Department of Psychiatry

Dissertation Advisor: Stephen G. Weber, Professor, Department of Chemistry

Reprinted with permission from

Zhang, J.; Liu, Y.; Jaquins-Gerstl, A.; Shu, Z.; Michael, A. C.; Weber, S. G. *Journal of Chromatography A.* 2012, 1251, 54-62. Copyright (2012) Elsevier.
Zhang, J.; Jaquins-Gerstl, A; Nesbitt, K. M.; Rutan, S. C.; Michael, A. C.; Weber, S. G. *Analytical Chemistry*, 2013, 85, 9889-9897. Copyright (2013) American Chemical Society.

IN VIVO MONITORING OF NEUROTRANSMITTER SEROTONIN AND DOPAMINE IN THE STRIATUM OF FREELY-MOVING RATS WITH ONE MINUTE TEMPORAL RESOLUTION BY ONLINE MICRODIALYSIS COUPLED WITH CAPIILARY HPLC

Jing Zhang, PhD

University of Pittsburgh, 2016

Dopamine and serotonin are widely studied monoamine neurotransmitters which are heavily involved in many physiological functions and pathological conditions. One method used to investigate the normal or abnormal functioning of the monoaminergic systems is to monitor the extracellular dopamine and serotonin concentrations by using microdialysis followed by liquid chromatography (LC), the temporal resolution of which is usually low, about 5-30 minutes. Thus, an online microdialysis/LC system was developed with one-minute temporal resolution for *in vivo* dopamine and serotonin monitoring.

One-minute LC separations of dopamine and serotonin were achieved by using short columns packed with 1.7 μm particles, working at 7-8000 psi and 70 ℃. Parameters of the LC-electrochemical detection system were optimized to achieve the best sensitivity and highest separation speed simultaneously under conditions where a small amount of band broadening occurs due to injection of a relatively large sample volume. Detection sensitivity is a function of void time, t_0, and column diameter, d_c, where optimum sensitivity is achieved at certain t_0 when d_c is chosen to fulfill the predetermined requirements of sample volume and apparent number of theoretical plates. To control dispersion during solute transport to and from the microdialysis probe, capillary tubing (75 μm inside diameter, 70 cm long) was used as probe inlet and outlet.

In vitro assessment based on the Taylor dispersion model showed that solute dispersion was well under one minute with a dispersion standard deviation of 7-12 s. *In vivo* monitoring of basal levels and fast changes of the extracellular serotonin in the striatum of freely-moving rats were performed. The longest monitoring lasted for 16.7 hours with one-minute temporal resolution. The superior temporal resolution revealed dynamic details in response to stimulation by 120 mM K^+ and fluoxetine intake. *In vivo* monitoring of the dopaminergic system with one-minute temporal resolution was also carried out. Maximum dopamine released during a 20-minute K^+ stimulation increased exponentially with K^+ concentration from 20 to 100 mM. Periodic dopamine fluctuations were observed starting at 100 mM K^+. The stability and temporal resolution of this system enables continuous sequential experiments with fine dynamic details within the same animal.

TABLE OF CONTENTS

LIST OF TABLES

LIST OF FIGURES

LIST OF SCHEMES

PREFACE

I would like to take a moment to acknowledge the following individuals in my life who influenced and encouraged me throughout the course of my graduate study. I couldn't complete the project without their supports. I am most grateful to my parents for their love and support. They taught me the value of education and being an independent woman. I would like to thank my loving husband Wanli and my beloved daughter who makes me become a better and happier person every day.

I am deeply grateful to my advisor and mentor, Prof. Stephen Weber, for his continuous guidance and supports both in research and in life. He gave me the opportunity to carry out this great project, always being patient and providing expertise when I met scientific challenges. He allowed me to pursue the research direction that I was interested and guided me to grow into an independent scientist.

I would like to express my gratitude to our collaborator, Prof. Adrian Michael for his expertise in neuroscience. Our discussion inspired me in my research work. He allowed me to use his lab space and resources for three years. I felt like I was a member of the Michael's group too.

Many thanks go to my superb colleagues, Yansheng Liu, Xiaomi Xu and Andrea Jaquins-Gerstl for their mentorship, great teamwork and friendship. I learnt a lot from them. I would like to thank the past and present members of the Weber group for their comments and inputs in my

research work. Thanks go to Yifat Guy for helping us initiating this project; thanks go to Juanfang Wu and Dujuan Lu for helping me settle down in Pittsburgh; thanks go to Hong for being a good friend and supporter.

I would like to express my appreciation to the members of my committee, Prof. Shigeru Amemiya and Prof. Jeffrey Yao for their supports and help in preparation of my dissertation.

Moreover, I would like to thank staff members in electronic shop and machine shop for the excellent work of heater design and manufacture.

Finally, I would like to dedicate my dissertation to my dearest grandfather, who inspired me and showed me the power of knowledge when I was a kid. His trust and understanding provide me with inner strength whenever I need it most.

1.0 INTRODUCTION

1.1 METHODS FOR MONOAMINE NEUROTRANSMITTER MEASUREMENT

Monoamine neurotransmitters, dopamine (DA), norepinephrine (NE) and serotonin (5-HT), are heavily involved in a variety of functions including emotion, cognition, motor activity, sleep and hormone secretion.[1-5] Neurotransmitter synthesis, storage, release, metabolism and reuptake greatly influence monoaminergic signaling, the abnormal of which may cause a number of brain disorders, such as Parkinson's disease, depression and drug abuse. Monitoring of the extracellular monoamine neurotransmitters, which directly reflects neurotransmitter release and uptake, is especially valuable for us to understand how the neurotransmitter dynamics is associated with the brain functions and disorders.

In vivo study of the monoamine neurotransmitter system requires quantitative and accurate measurement with high selectivity and sensitivity, high temporal and spatial resolution and proper interpretations of results. Two major tools[6-9] used are (1) microdialysis coupled with analytical techniques like high performance liquid chromatography (HPLC) or capillary electrophoresis (CE) using electrochemical (EC), laser-induced fluorescence or mass spectrometric detection and (2) fast scan cyclic voltammetry (FSCV) or amperometry using a carbon fiber microelectrode.

FSCV or amperometry using a carbon fiber microelectrode features relative fast and direct measurement on the time scale from s to ms.[10,11] The fast measurement allows the study of release and uptake dynamics.[12,13] It also excels in small neuron system like *Drosophila* Brain[14] or where high spatial resolution is required[15,16] because of the small diameter of the microelectrode. However, it has its own drawbacks like lack of selectivity[17] and electrode fouling problem.[18,19] FSCV, the widely used technique, suffers from the length of detection time and cannot detect the basal concentrations.

On the other hand, microdialysis followed by analytical techniques allows the detection of basal conditions and long term observations which are important for physiological and pharmacological study. There are two ways to couple microdialysis with analytical techniques: online and offline. For the offline measurements, sampling and analysis are independent processes which offer flexibility and versatility on method development and experiment implementation. But one extra step of proper sample storage is required which needs careful planning due to sample degradation, contamination and the feasibility of small volume handling. On the other hand, the online measurement is more efficient and avoids these problems. Furthermore, direct response from analysis results allows the synchronous behavior study.

HPLC and CE are two frequently used techniques for monoamine detection. HPLC has sufficient sensitivity to quantify basal concentrations of both dopamine and serotonin in the extracellular space and the separation step before detection allows accurate multi-analyte detection.[20-22] One major problem of this technique is the limited temporal resolution. The time intervals for sampling are typically 10-30 minutes (5-30 μL dialysate).[23,24] The lack of temporal resolution prohibits the study of dynamic release and uptake of the extracellular neurotransmitters. Research towards scaling down the dialysate volume (0.5-1 μL) by using

small i.d. column (i. d. < 1 mm) has been developed recent years.[25-28] The reduced sample consumption helps reduce sampling time and improve temporal resolution. Newton and Justice[27] demonstrated one-minute temporal resolution of dopamine monitoring using microdialysis-HPLC system. But this was done offline. Storing 0.5 or 1 μL sample in a 250 μL vial and loading it using a 10 μL syringe is awkward and may cause sample recovery and reproducibility problem. Jung et al.[28] also determined dopamine and serotonin with 0.5 μL dialysate sample consumption using capillary column coupled with photoluminescence following electron transfer (PFET) detection system in an offline way. To fully take advantage of this technique, online measurement is preferred. In fact, Wang et al. recently reported 2-s offline microdialysis sampling of amino acid standards and 10 s temporal resolution of offline *in vivo* measurements of six neuroactive amino acids.[29] Therefore fast determination of monoamines by HPLC with good detection limit is the key to achieve high temporal resolution for online analysis.

Microdialysis coupled to CE is another option for neurotransmitter determination.[6,30] CE is popular because of its high mass sensitivity, high separation speed and the potential to achieve high throughput. One successful application area is the determination of amino acid neurotransmitters in the brain. The Kennedy group developed an on-line CE system in which amines were derivatized with a fluorescent tag before injected onto an electrophoresis capillary using a flow-gate interface with laser-induced fluorescence detection.[31,32] Using this device, *in vivo* determination of dopamine in dialysate with 2 nM detection limit and 90 s temporal resolution has been done.[32] Determination of serotonin by microdialysis/CE has been carried out.[33-35] But none of them is comparable to or better than current HPLC techniques. The separation time is usually long and the concentration detection limit is usually poor. To improve the poor concentration sensitivity, online concentration by stacking is carried out which usually

takes several minutes.[33] One more problem with CE technique is the irreproducible migration times because of the zeta potential changes caused by substance adsorption onto the capillary wall. Rinsing between runs is necessary to keep constant zeta potential but this extra step is a limitation for high speed and continuous analysis. Therefore, HPLC, instead of CE, is more suitable for *in vivo* monitoring of serotonin given the better detection sensitivity, stable separation condition and reproducible results.

1.2 TEMPORAL RESOLUTION OF *IN VIVO* NEUROTRANSMITTER MONITORING BY MICRODIALYSIS

Microdialysis sampling coupled with analytical techniques or biosensors enables the monitoring of monoamines, amino acids, neuropeptides and other molecules in the extracellular environment.[36] The semipermeable membrane with a specific molecular weight cutoff at the microdialysis probe tip allows molecular exchange between microdialysate inside the probe and the surrounding environment, mostly the extracellular space in the brain and periphery. The rational design of dialysis probe makes microdialysis a better technique with low disturbance of local environment, exclusion of high-molecular-weight substances and well-predicted recovery compared with other *in vivo* sampling techniques.[37-40] Quantifications of neuro-active molecules by microdialysis can reflect neurochemical activities in the extracellular space which helps understand normal and abnormal brain functions.[41,42] Although microidialysis coupled with analytical techniques has many advantages like the merit of versatility, multiple analyte detection and measurements of both basal concentrations and transient changes, it does have disadvantages: limited temporal resolution, molecule-depleted local environment, low spatial

resolution and flow rate dependent molecular recovery. Many neurochemical activities in brain happen in a relatively short period of time (e.g. milliseconds to minutes) and in a defined small space (e.g. between several brain cells). *In vivo* experiment with accurate and precise spatial and temporal resolution is very important to advance the utilization of this method in the neuroscience study.

Temporal resolution of mcirodialysis coupled with analytical techniques is determined by the sampling frequency, the analysis frequency and zone dispersion of solute during sampling and transport.[6] The sampling frequency is set by the microdialysis flow rate and the mass detection limit of the analytical method. The extracted solute concentration in microdialysate is determined by solute diffusivity, extracellular solute concentration, probe membrane permeability and microdialysis flow rate. At a constant microdialysis flow rate, solute concentration in microdialysate is determined and the minimum collection of sample mass/volume, which is the best possible temporal resolution, is determined by the HPLC mass detection sensitivity. The minimization of column diameter synchronously reduces many parameters such as mobile phase flow rate and sample volume, significantly improving the mass detection sensitivity of a variety of detectors.[30,43,44] Microdialysis sampling time for monoamine neurotransmitters is greatly reduced from 10 to 20 minutes to sub-minute level when switching from conventional HPLC to capillary/microbore HPLC. Another factor, preconcentration by on-column focusing,[45] also contributes to the improvement of the detection limit. Capillary/microbore HPLC has very small column volume which is comparable to the typical microdialysate sample size (nL to μL). Microdialysate is usually very clean because of the exclusion of high molecular weight substances and can be directly injected to the HPLC column without further sample preparation. The water-based dialysate matrix (nL to μL) has less eluting

strength than the mobile phase but significantly large enough volume to serve as temporary mobile phase which generates a phenomenon called on-column focusing, greatly improving the concentration detection sensitivity (further discussion in Chapter 4).

Analysis frequency can be the limiting factor for the temporal resolution when doing online coupling of microdialysis sampling and dialysate analysis by analytical techniques like HPLC, CE or microchip. Increasing the temporal resolution for online measurements results in less analyte quantity in the dialysate sample and more sample collections per time,[6] pushing the advances in speed and sensitivity of analytical techniques. When analysis frequency cannot match sampling frequency, local enlargement of the temporal resolution is very useful to gather information from the zone of interest, transient changes of neurotransmitters in response to stimuli. Development in valve technology allows capture of six sample fractions in the first dimensional flowing stream (1DLC eluent) which are injected and analyzed later in 2DLC.[46] Collecting and transiently storing a series of dialysates using this new valve technology can enlarge the temporal resolution for the targeting time period of sampling. The analysis of these samples can be done when collecting dialysate with no information (basal levels).

1.3 ONLINE HIGH SPEED HPLC ANALYSIS

1.3.1 Improvement of analysis speed

Three types of dispersion contribute to the peak variance (σ^2) and band broadening during a chromatographic run: eddy diffusion, longitudinal diffusion and resistance to mass transfer in the

mobile phase, stationary phase and stagnant mobile phase. The van Deemter equation[47,48] is used to quantify the effect of these factors:

$$h = A + \frac{B}{\nu} + C\nu \quad (1)$$

Where h is the reduce form of the height equivalent to a theoretical plate (HETP) H ($h = \frac{H}{d_p}$); ν is the reduced form of interstitial linear velocity u_e ($\nu = \frac{u_e d_p}{D_m}$); A, B and C are constants which are related to the different types of dispersion. The A, B and C terms are typically experimentally determined by building a van Deemter plot (h against ν) for a specific solute, column and experiment conditions.[49] A term describes eddy diffusion. It relates to the particle size, shape and packing quality. B term describes longitudinal diffusion and it is most important when ν is small. C term describes the mass transfer resistance in the mobile phase, stationary phase and stagnant mobile phase. It dominates in the high ν region. Based on the van Deetmer equation, the minimum HETP can be reached as $h_{\min} = A + 2\sqrt{BC}$ at the optimum reduced velocity $\nu_{opt} = \sqrt{\frac{B}{C}}$. Traditional HPLC usually runs at a velocity slightly higher than optimum velocity. For high speed separation, the reduced linear velocity is set at a much higher value than ν_{opt} and C term (resistance to mass transfer) contributes the most to the band broadening process.

1.3.1.1 Particle size and configuration

In response to the high demand of high throughput analysis in the pharmaceutical and fine chemical industry, manufacturers developed and commercialized short columns packed with very fine particles which features superior separation speed and efficiency. The use of sub-2 μm

particles reduces eddy diffusion and mass transfer resistance which improves the column efficiency when working at high linear velocity. Therefore, short column packed with sub-2 μm particles offers faster separations, keeping equivalent separation power/column efficiency.[50] Besides particle diameter, the particle configuration is also a key factor in terms of separation speed and efficiency. The design of nonporous particles eliminates the stagnant mobile phase in the intraparticle void volume. Small *C* term (no mass transfer resistance in the stagnant mobile phase) helps improve the column efficiency for high speed separations.[51] The downside of nonporous particles is the small sample loading capacity and retention due to a low surface area. Fused core particles[52,53] consist of a thin porous shell and a solid core. The thin layer of shell shortens the diffusion distance of solutes in the pores and exhibits better mass transfer kinetics at high velocities. Also the existence of porous layer ensures a sufficient amount of stationary phase and adequate sample loading capacity and retention time. The minimum HETP of commercial 2.7 μm HALO Fused-Core C 18 particles is as low as 3.4 μm which is comparable to the sub-2 μm fully porous particles.[52] Remarkably, their relatively larger permeability and reduced heat friction effect permits very fast separation using conventional HPLC pump, providing column efficiency compared to sub-2 μm particles.[54] Monolithic columns,[55] as an alternative to particle-packed column, employ a continuous porous column bed, featuring a bimodal pore size distribution of large through pores and mesopores which permits separations done at high flow rates and low pressures without losing column efficiency. Monolithic columns can be categorized into two types: silica monoliths and polymeric monoliths. Silica monoliths[56] are well-characterized and studied even though there are only a few choices of pore size and surface chemistry. Their high permeability and slow decrease of column efficiency at high flow rate makes them a strong competitor of conventional RPLC columns.[57] Polymeric monoliths are

intensively studied by many researchers.[58] A lot of columns with different pore size and surface chemistry emerged to separate a variety of samples, with an intensive focus on separations of biological samples.[59] However, that the batch to batch reproducibility of polymeric monoliths is not very consistent, together with the massive column choices, are the obstacles for commercialization.

1.3.1.2 Ultrahigh pressure liquid chromatography

The use of very fine particles to achieve high separation power was predicted as early as 1969 by Knox and Saleem.[60] However, the development was slow, limited by the column manufacture and instrument design. In 1997, Jorgenson group[61] first demonstrated the use of ultrahigh pressure (pressure as high as 60,000 psi) for efficient capillary column packing and chromatographic separations. Columns packed with 1.5 μm nonporous particles generate 300,000 theoretical plates. The first commercialized fully porous particle column, 1.8 μm Zorbax Rx by Agilent Technologies, was successfully introduced in early 2005 and followed by the introduction of Acquity UHPLC system from Waters.[41] It is quite a challenge to take fully advantages of the ultrahigh separation power generated by using sub-2 μm particles and ultrahigh operational pressure when using conventional HPLC columns. UHPLC using traditional 4.6-mm diameter column generates significant heat (24 W at a flow rate of 2 mL/min) which can't be completely dissipated.[36] The accumulated heat produces temperature radial gradient from the column core to the column wall which further caused radical gradient in mobile phase velocity and solute retention, leading to band broadening and loss of column efficiency. It is important to decrease the column diameter to 2.1 mm and 1.0 mm in commercial UHPLC system and employ capillary columns working at extremely high pressures. The high separation power from UHPLC system produces peaks with extremely narrow peak width in

volume and time. It is critical to avoid peak deterioration caused by relatively large extra-column broadening and slow data acquisition.

1.3.1.3 High temperature liquid chromatography

High column temperature has been an important factor for improving separation speed and column efficiency.[62-64] The low viscosity, η, of high temperature mobile phase will allow the use of higher flow rate for a given pressure and reduce the separation time. The high diffusion coefficient at high temperature will improve mass transfer of a solute and reduce band broadening at high flow rates. However, the development of high temperature liquid chromatography (HTLC) has been limited before 2000 because of three major hindrances: stationary phase stability, temperature mismatch[65] between the incoming mobile phase and the column, and analyte degradation[66] at high temperature. Novel stationary phases[67] with high thermal stability have been developed which can operate at or greater than 100 ^{0}C such as some silica or zirconia-based columns and porous graphitic carbon columns. Temperature difference larger than 5 ^{0}C between the incoming mobile phase and the column will cause column efficiency loss and peak splitting which is mostly due to a radial retention factor gradient instead of a radial viscosity gradient.[65] This could be reduced by pre-heating the mobile phase and using small diameter columns. It is demonstrated that most substances are stable enough during the separation time for high speed separations where the time is so short that very little degradation is observed.[68] Improved separation speed and efficiency was observed by using conventional,[69] narrow bore[68,70] and capillary columns[71] at high temperature. Eventually, the use of small diameter particles, high pressure and high temperature conditions will enhance the separation speed and column efficiency.[72-74]

1.3.2 Optimization of online microdialysis coupled with HPLC

Online microdialysis sampling is beneficial for continuous analysis with high temporal resolution/sample collection frequency. It also makes the study of neurochemistry and related animal behavior more direct and efficient. When coupled to analytical techniques like HPLC, several aspects need to be considered during the online integration of the sampling and analysis process. To avoid loss of biological information, all or most of the dialysate collected should be transferred to and analyzed by HPLC. HPLC analysis time should be equal to or smaller than the sampling time. When doing online microdialysis coupled with capillary HPLC, the sampling frequency is in the sub-minute level. Therefore, superior separation speed and detection sensitivity are very critical to the online analysis of dopamine and serotonin from the microdialysate matrix. One other major limitation may come from the solute zone dispersion during sampling and transport from the sampling site to the HPLC analysis system especially for experiments with freely-moving animals where long connection tubing is needed. We need to make sure that solute dispersion in time is much smaller than the sampling and analysis time. Solute dispersion increases with larger connection tubing i.d. and longer tubing length. Selection of tubing i.d. and length is a compromise between solute dispersion, pressure drop across the tubing and practical space between sampling site and analysis site. Another way to diminish solute dispersion during transport is to use segmented flow.[31,32,75] Oil phase is introduced and separates the microdialysates into each individual sample plug. There is no solute dispersion between dialysate sample plugs and the temporal resolution is defined by the sampling time of each sample plug. This method is very suitable when coupling with CE.

2.0 HIGH SPEED ANALYSIS OF NEUROTRANSMITTER SEROTONIN

2.1 HPLC INSTRUMENTATION

Capillary HPLC has superior mass sensitivity with small sample consumption which is ideal for high temporal resolution microdialysis sampling. Not like working with commercial HPLC instrument which comes as a whole package, we needs to customize different parts of our capillary HPLC system. It needs extra work but it does provide design flexibility and individuality for different applications. To achieve high temporal resolution online analysis of trace level neurotransmitters in microdialysate, the design of our capillary HPLC system focuses on separation speed, and detector sensitivity and selectivity.

2.1.1 Two factors for high speed HPLC: elevated column temperature and ultrahigh pressure drop

Two key features of high speed separations are elevated column temperature and ultrahigh pressure drop. If we assume that the retention factor of the last eluting solute is predetermined as k_l', then the separation time is $t_0(1+k_l')$. If the void volume of the system is fixed, the void time t_0 is inversely proportional to the flow rate which means higher flow rate leads to smaller t_0 and faster separation. Both pressure and temperature can regulate the mobile phase flow rate. Eq. 2 indicates that mobile phase linear velocity u is proportional to the pressure drop P which means

high pressure generates high linear velocity and small t_0 when other parameters stay constant. Eq. 3 shows that the viscosity η of the mobile phase is temperature dependent. Increased temperature can reduce mobile phase viscosity, leading to higher linear velocity and smaller t_0 at constant pressure based on Eq. 2.

$$P = \frac{\phi \eta u L}{d_p^2} \tag{2}$$

$$\eta = \eta_0 \exp^{-bT} \tag{3}$$

A UHPLC pump, providing high precision flow rate in the range of nanoliter to microliter per minute, is highly desired for our capillary HPLC system in order to generate ultrahigh pressure drop. The NanoLC Ultra pump (Model nanoLC-Ultra 1D, Eksigent, Dublin, CA) with a maximum pressure of 10,000 psi and working flow rate range of 0.1 to 20 μL/min fulfilled the requirements.

In general, commercial HPLC system uses auto-sampler and connection tubing between the auto-sampler and the analytical column. But for our capillary HPLC system, the capillary column directly connected to the injection valve which loaded and injected samples to the column. This design reduced the extra-column broadening from the sample injection and minimized solvent dispersion between the mobile phase and the sample solvent. This was very important for our system since we took advantages of the eluting strength difference between the mobile phase and the sample solvent in order to concentrate a large volume of sample at the front of the column (see Chapter 3 for preconcentration by on-column focusing). The direct connection between injection valve and column avoided mixing at the interface between the sample solvent and the mobile phase while it increased the complexity of the design of the heating assemblies for the column. We needed to heat both the capillary column and the injection

valve to the same temperature since part of the column was inside the fittings in the injection valve. Two homemade heating assemblies were made to control the temperature of the injector and the capillary column. Two proportional-integral-derivative (PID) controllers (Model CT15122, Minco Products, inc., Minneapolis, MN) drove Kapton polyimide heat film (Minco Products, inc., Minneapolis, MN) to heat the column and injector separately. For the capillary column, the heat film covered the surface of an aluminum cylinder with insulation which transferred the heat to the capillary column. A temperature sensor inside the aluminum block monitored the heating power. For the injector, a standoff assembly was used to insulate the actuator from the valve which was covered by the heat film with insulation so the electronic part of the injector was not heated. Temperature sensor was set on the valve center. The precision of temperature control was about 0.1 ℃ in the range from room temperature to 100 ℃.

We systematically studied the change of t_0 at different pressures and temperatures of our system. In Figure 1, the green line shows the ratio of t_0 at different temperatures and t_0 at room temperature (constant pressure); the blue line shows the ratio of t_0 at different pressures and t_0 at 3000 psi (constant temperature). Both indicted that void time t_0 was reduced significantly by using either high pressure or high temperature. The star point is at the condition of 80 ^{0}C and 9000 psi and the void time t_0 was reduced about 8 times compared to that at room temperature and 3000 psi. Therefore, high pressure and high temperature are efficient tools to achieve high speed separation.

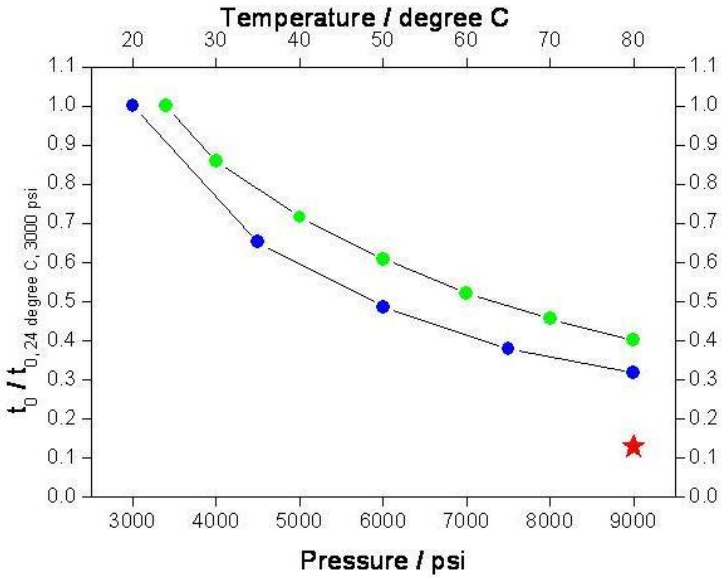

Figure 1. Void time t_0 at different working pressures and temperatures

2.1.2 Comparison of PFET and electrochemical detectors

To achieve fast analysis of neurotransmitters like serotonin and dopamine which was in sub-nM to nM level in complex biological sample, the detector of the capillary HPLC system should have good selectivity and sensitivity. To work with fast separation using capillary column, small void volume and low backpressure were also two key requirements for the detector.

Two types of detectors were used during method development. Initially, PFET detection system was used which was developed in our group and had high selectivity of electrochemical detection without electrode fouling problem.[76,77] The postcolumn reaction in the PFET system was the homogeneous oxidation of serotonin by $[Os(bpy)_3]^{3+}$ in the mixer. While it provided good selectivity and sensitivity, it did have disadvantages. As we increased the flow rate, the detection sensitivity decreased. This was due to incomplete postcolumn reactions at higher flow rate. We further studied the peak area at different flow rates and found that peak area decreased with flow rate increased at certain mixing length (Figure 2). Whether the postcolumn reaction

was complete or not was determined by the solute residence time in the mixer before detection. As we increased the flow rate, the residence time decreased and so did the peak area and the detection limit.

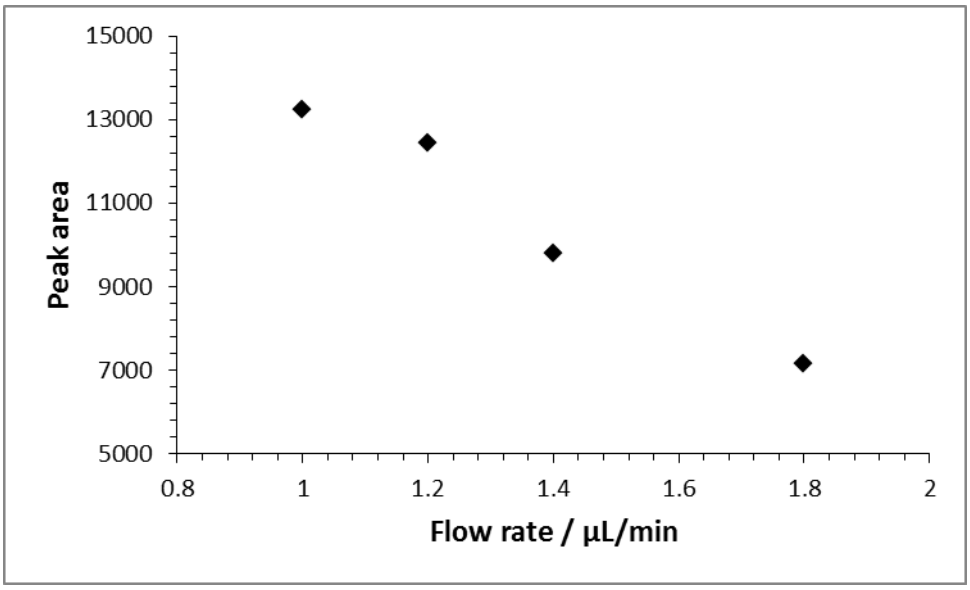

Figure 2. Peak are of serotonin at different mobile phase flow rates

To maintain the detection limit, we cannot simply increase the mixing length so that the residence time stayed the same as we increased the flow rate because the increase of the extracolumn dead volume resulted in column efficiency loss. Previous theoretical study[78] in our lab shows that for fast separation the optimized postcolumn mixer should be long and narrow in order to minimize efficiency loss. But this steals the available pressure from the column. In addition, the fabrication and operation are more difficult and the whole method is less robust. Electrochemical detector is one major detector for the detection of monoamine neurotransmitters. Electrochemical detection in a flow cell with small void volume is suitable for capillary HPLC.[79] The small dead volume of the detector minimizes the extra-column band spreading. Since the detector works in a flow cell, the mobile phase constantly renews the electrode surface and the

high flow rate actually benefits the signal. So we used electrochemical detector for fast separation after the initial attempt of PFET detector.

2.2 CHROMATOGRAPHIC CONDITIONS TOWARDS HIGH SPEED ANALYSIS

High speed separations are effective only when the resolving power of the system is sufficient which is evaluated by the peak resolution of the critical peak pair. For two peaks with similar retention like the critical peak pair, the peak resolution *R* is determined by the plate number *N*, the retention factor *k'* and selectivity α. We evaluate how different packing materials/stationary phase, mobile phase and temperature affect peak resolution/separation efficiency by regulating retention, selectivity and column efficiency/plate number.

$$R \approx \frac{\sqrt{N}}{4}(\alpha - 1)\frac{k'}{1+k'} \tag{4}$$

2.2.1 Evaluation of column packing materials for high speed separations

The properties of the packing materials of HPLC column such as particle diameter, stationary phase chemistry and particle sources can affect the separation performance. Columns packed with smaller diameter particles generate more plate number *N* because of the smaller eddy diffusion and mass transfer resistance. Stationary phase hydrophobicity and stationary phase density affect the retention factor of a solute. Stationary phases with high hydrophobicity and high density retain solutes longer. Also packing materials from different companies may have different performances due to different stationary phase densities, pore sizes and end cap

techniques. The five reversed-phase packing materials we evaluated were 2.6 μm XTerra MS C 18 (Waters), 2.7 μm HALO Fused-Core C 18 (Advanced Materials Technology), 1.7 μm BEH C 18, C 8, and Shield RP 18 particles (Waters).

1.7 μm BEH Shield RP 18 particles showed completely different behaviors from the other four packing materials. After optimization, separation in one minute was achieved at 35 ℃ and with a flow rate of 2.4 μL/min (Figure 3). However, it is found that the critical peak pair 5-HT and 3-MT was not well resolved at higher temperature. At 50 ℃, the 5-HT and 3-MT peaks completely overlapped with each other. 5-HT and 3-MT were not completely separated at temperature as high as 80 ℃. This limited the use of higher temperature which was a key factor to promote separation speed. Therefore, 1.7 μm BEH Shield RP 18 particles were not suitable for faster separations.

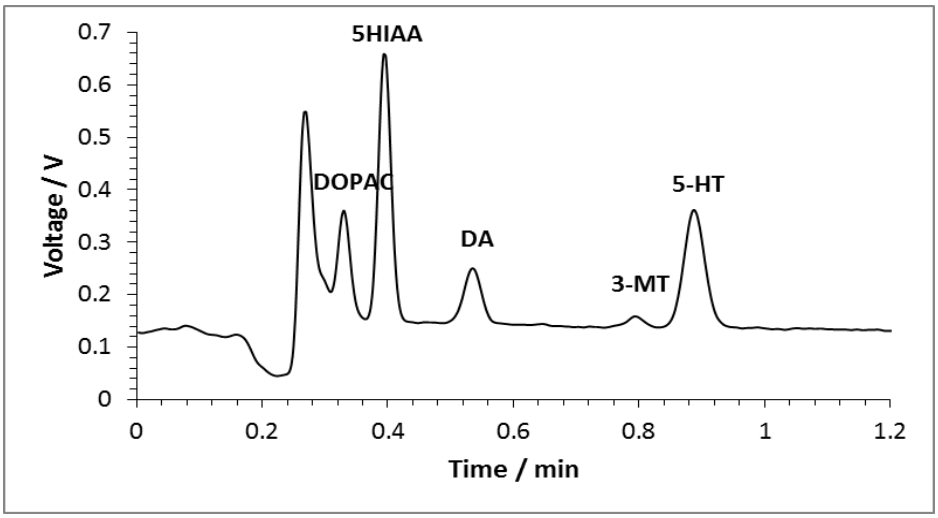

Figure 3. Chromatogram of a standard sample from the BEH Shield RP 18 column

Sample includes DOPAC, 5HIAA, DA, 5-HT, 3-MT, each at 100 nM. Injection volume: 500 nL. Column: 100-μ-i.d., 5.0-cm-length capillary column packed with BEH Shield RP 18 particles. Mobile phase: 100 mM sodium acetate, 0.15 mM disodium EDTA, 18.0 mM sodium 1-octanesulfonate (SOS), pH=4.0, mixed with 14% (v/v) acetonitrile. Flow rate: 2.4 μL/min. Column temperature: 35 ℃. PFET detection.

The chromatographic behaviors of the other four packing materials were quite similar. The separation performance was investigated at high pressure and high temperature conditions. Around 1-min separation was achieved after rough optimization of mobile phase, temperature and flow rate (Figure 4, Table 1**)**.

Table 1. Experiment conditions for the columns packed with different packing materials

	1.7 μm, BEH C18	1.7 μm, BEH C8	2.6 μm, XTerra	2.7 μm, HALO
T (℃)	70	70	75	70
Flow rate (μL/min)	4.0	4.0	5.5	5.5
Column length (cm)	4.9	5.0	7.6	7.6
Pressure (psi)	7249	7581	8300	7545

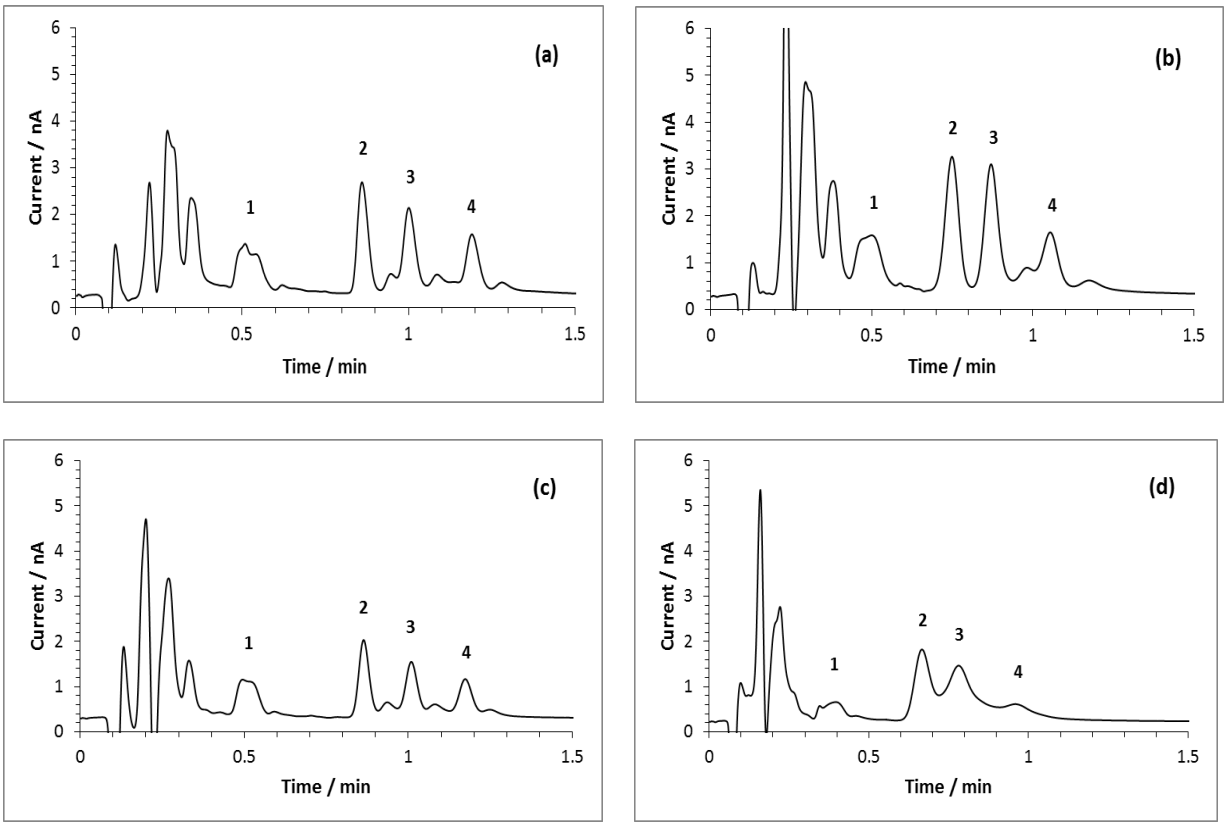

Figure 4. Chromatograms of standard samples from four different columns

Sample includes DOPAC, HIAA, HVA, (1) DA, (2) 5-HT, (3) N-Me-5-HT, (4) 3-MT, each at 100 nM. Injection volume: 500 nL. The separation conditions are described below. Column: (a) BEH C18, (b) BEH C8, (c) XTerra and (d) HALO. Mobile phase: 100 mM sodium acetate, 0.15 mM disodium EDTA, 10.0 mM SOS, pH=4, mixed with 4% (v/v) acetonitrile. Electrochemical detection.

Column efficiency and detection sensitivity were investigated for the four packing materials (Table 2). Large sample volumes (500 nL) were injected in order to gain sufficient detection sensitivity. The detection sensitivity of columns packed with 1.7 μm BEH C 18 and C 8 particles was better than the other two. Due to the large sample volume loading and insufficient on-column focusing (see Chapter 3 for detail) of the solutes, the column efficiency was unusually low for all the packing materials. The 2.7 μm HALO particles gave the lowest plate number. The 5-HT, N-Me-5-HT and 3-MT peaks overlapped with each other (Figure 4 d). The column efficiency of the HALO fused core particles was worst probably because of the low sample volume capacity compared to fully porous particles. The 2.7 μm HALO particles have a 1.7 μm diameter solid silica core with a 0.5 μm diameter porous shell. This unique structure allows faster mass transfer and offers better column efficiency especially at high flow rate.[52,53] But the structure of HALO particles also results in small sample volume capacity and severe sample overloading in the case of 500 nL injection. 1.7 μm BEH C 8 particles also showed much lower column efficiency than 1.7 μm BEH C 18 and 2.6 μm XTerra particles. The C 8 stationary phase has shorter hydrocarbon chain. Its ability to sorb ion pair reagent and interact with solutes is weaker compared to C 18 stationary phase. Therefore the sample capacity was not as good as C 18 stationary phase which caused more column efficiency loss. Since we pursue both high sensitivity and fast separation with acceptable column efficiency, columns packed with the 1.7 μm BEH C18 particles are an excellent choice from both detection sensitivity and column efficiency aspects.

Table 2. Evaluation of the performance of the columns packed with different packing materials

	1.7 μm, BEH C18	1.7 μm, BEH C8	2.6 μm, XTerra	2.7 μm, HALO
Sensitivity (nA)	2.35	2.87	1.72	1.57
$t_{5\text{-HT}}$ (s)	51.5	44.9	51.7	39.9
$W_{1/2,\,t}$ (s)	2.1	2.8	2.1	3.5
$W_{1/2,\,v}$ (μL)	0.14	0.19	0.19	0.32
N	2432	988	2687	537
H (μm)	20	51	28	112

2.2.2 Regulation of retention and selectivity

2.2.2.1 Mobile phase optimization

Mobile phase composition was regulated by adjusting the concentration of sodium 1-octanesulfonate (SOS) and organic modifier percentage. DA, 5-HT and 3-MT are cationic molecules in acidic mobile phase while DOPAC, HVA and 5HIAA are partially negative charged. SOS is an ion pair reagent for ion pair reverse phase HPLC. It increases the retention of cations and decreases the retention of anions by electrostatic interaction. During the optimization process, we found that the concentration of SOS could regulate the selectivity of 5-HT and 5-HIAA but had no influence on selectivity of 5-HT and 3-MT (Table 3). SOS adsorbs on the stationary phase and creates a surface potential ψ.[80] The value of ψ is altered with SOS

concentration. The selectivity of solutes is determined by Eq. 5 in the ion pair reverse phase HPLC mode.

$$\ln \alpha_{i,j} = \ln \frac{k_i'}{k_j'} = -\frac{\Delta G_{i,ch}^{o'} - \Delta G_{j,ch}^{o'}}{RT} + \frac{(Z_i - Z_j)F\psi}{RT} \quad (5)$$

In the equation, $\alpha_{i,j}$ is the selectivity of solute i and j, k_i and k_j are the retention factor of solute *i* and *j*, $\Delta G_{i,ch}^{o'}$ and $\Delta G_{j,ch}^{o'}$ are the free energies from non-Coulombic type of interaction, Z_i and Z_i are the charges of solute i and j. In acidic mobile phase, 5-HT and 3-MT are fully positively charged so that Z_i equals Z_j and the right term is zero. Therefore the selectivity of 5-HT and 3-MT is independent of surface potential ψ and SOS concentration. On the other hand, the charge difference between 5-HT and 5-HIAA is larger than zero. Therefore, the selectivity of 5-HT and 5-HIAA are SOS concentration dependent.

Table 3. Selectivity of two peak pairs at differen SOS concentration

SOS (mM)	$\alpha_{5\text{-HT,5-HIAA}}$	$\alpha_{5\text{-HT,3-MT}}$
12	2.6	1.3
15	2.7	1.3
20	4.4	1.3

2.2.2.2 Temperature optimization

During HPLC method development, the order of resolution optimization would be retention, selectivity and then column efficiency. Among the three parameters, selectivity α is the most effective one to regulate peak resolution. Modulation of selectivity by adjusting mobile phase and stationary phase is the most common way for chromatographers to achieve sufficient peak

resolution. Another efficient tool to change selectivity is temperature. The temperature effect on retention and selectivity can be explained using the van't Hoff equation.

$$\ln k' = -\frac{\Delta H}{RT} + \frac{\Delta S}{R} + \ln \beta \tag{6}$$

$$\ln \alpha_{(solute1,solute2)} = -\frac{(\Delta H_{solute1} - \Delta H_{solute2})}{RT} + \frac{(\Delta S_{solute1} - \Delta S_{solute2})}{R} \tag{7}$$

where ΔH and ΔS are the enthalpy change and entropy change associated with the solute transfer from the mobile phase to the stationary phase, β is the volume phase ratio. If enthalpy changes of two solutes are different, the selectivity of the two solutes could be regulated by temperature optimization. In a review article, Dolan[81] emphasized the importance of temperature effect on selectivity in reverse phase HPLC and pointed out that temperature regulation is a strong complementary tool to mobile phase optimization.

Retention and selectivity of the solutes are influenced by the column temperature.[81-83] The temperature effect on retention is mainly determined by the enthalpy term (ΔH) in the van't Hoff equation (Eq. 6). Most molecules have negative phase transfer enthalpies. This means retention factors decrease with increasing temperatures. The magnitude of ΔH determines how much temperature can affect retention.

We studied the retention behavior of 5-HT, DA and 3-MT in the temperature range between room temperature and the highest temperature that the column can endure. Figure 5 showed plots of ln$k$' against 1/T for 5-HT, DA and 3-MT in columns packed with four different particles. From right to left, the retention factors decreased with increasing temperatures.

The retention factor of an analyte is determined by the stationary phase chemistry, mobile phase composition, temperature and the volume phase ratio β. It also differs between different particle sources. From our results, the retention factors of the three solutes for BEH C 18, XTerra

and HALO particles were similar. On the other hand, the retention factors for BEH C 8 particles were relatively lower. This is because that the stationary phase of BEH C8 particles has shorter alkyl chain and its ability to sorb ion pair reagents and interact with solutes is weaker compared to C 18 stationary phase.

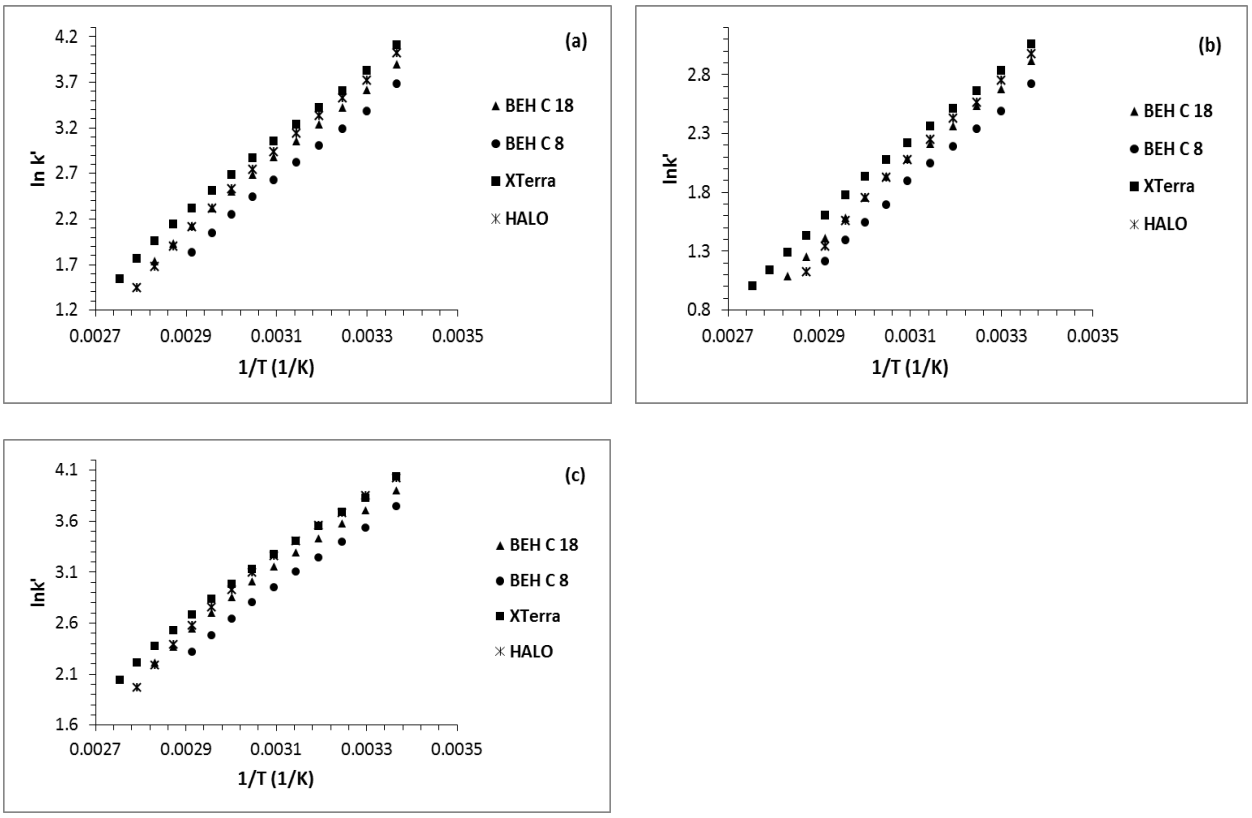

Figure 5. Temperature effect on retention factors of the three solutes: (a) 5-HT, (b) DA, (c) 3-MT

The date sets of ln*k'* and 1/*T* fitted well in linear regression analysis for all the stationapy phases and solutes (R^2 > 0.98). The average ΔH was calculated from the slope of linear regression analysis using Eq. 6 (Table 4). The phase transfer enthalpies of 5-HT, DA and 3-MT were similar for BEH C 18 and C 8 and XTerra columns. The phase transfer enthalpy for HALO particles was significantly different from the other three. The differences may result from that they were from different companies (Xterra and BEH from Waters). Xterra and BEH particles

were hybrid particles while HALO particles were not. So the microenvironment of the stationary phase of HALO particles was different from the other three.

Table 4. Calculated phase transfer enthalpies for 5-HT, DA and 3-MT

	$\Delta H_{5\text{-HT}}$ (kJ/mol)	ΔH_{DA} (kJ/mol)	$\Delta H_{3\text{-MT}}$ (kJ/mol)
BEH C18	-33.0 ± 0.5	-28.0 ± 0.6	-26.0 ± 0.6
BEH C8	-33.1 ± 0.5	-27.4 ± 0.5	-25.9 ± 0.5
XTerra	-33.9 ± 0.5	-27.7 ± 0.5	-26.6 ± 0.6
HALO	-36.6 ± 0.7	-30.3 ± 0.9	-29.2 ± 1.0

The importance of column temperature in controlling selectivity has been recognized recently. The selectivity can be expressed using the van't Hoff equation (Eq. 7). When $T = (\Delta H_{solute1} - \Delta H_{solute2})/ (\Delta S_{solute1} - \Delta S_{solute2})$, selectivity equals 1 which means that the retention of the two solutes are the same and the eluting peaks completely overlap with each other. Increasing or decreasing temperature from $T = (\Delta H_{solute1} - \Delta H_{solute2})/ (\Delta S_{solute1} - \Delta S_{solute2})$, selectivity of the solute pair will be improved. The extent of temperature effect is determined by the enthalpy difference of the two solutes.

Bolliet et al. reported that temperature in reverse phase HPLC has largest effect on selectivity of solutes which differ by size and H-bond basicity.[84] We observed strong temperature effect on selectivity of 3-MT and 5-HT solutes. The critical solute pair 3-MT and 5-HT cannot be resolved at room temperature using column packed with BEH C 18 particles. Adjustement on detergent SOS concentration and organic modifier concentration helped very little. However, as

we studied the retention behavior at high temperature, we found 3-MT and 5-HT can be resolved at high temperature and the band spacing increased with increased temperature.

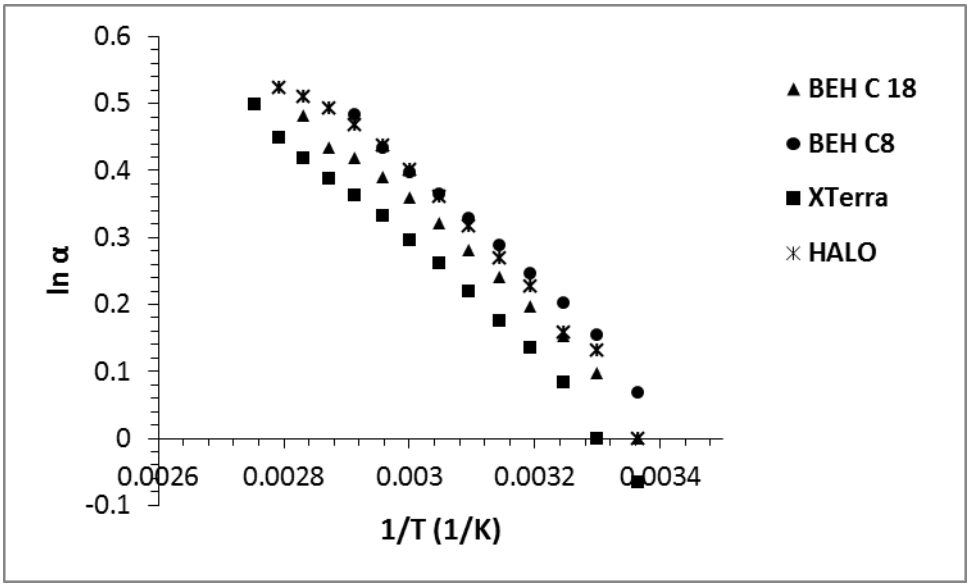

Figure 6. Selectivity-temperature dependence of 3-MT and 5-HT for the four particles

Figure 6 showed the selectivity of 3-MT and 5-HT ($\alpha=k_{3\text{-MT}}'/k_{5\text{-HT}}'$) at different temperature. The enthalpy and entropy differences were calculated using Eq. 7 after doing linear regression analysis. As seen in Table 5, the $\Delta\Delta H$ and $\Delta\Delta S$ were both positive. This indicated the separation with the solute order of 5-HT and 3-MT was favored at high temperature while the separation with solute order of 3-MT and 5-HT was favored at low temperature. When T=ΔΔH/ΔΔS, the selectivity equaled 1 and the two peaks completely overlapped. From our results, we concluded that for some solute pairs like 3-MT and 5-HT, temperature optimization is much more effective compared to regulation of mobile phase composition. Temperature regulation is a complementary tool to mobile phase optimization.

Table 5. Calculated enthalpy and entropy difference of 3-MT and 5-HT

	$\Delta H_{3\text{-MT}} - \Delta H_{5\text{-HT}}$ (kJ/mol)	$\Delta S_{3\text{-MT}} - \Delta S_{5\text{-HT}}$ (J/(mol*K))
BEH C18	7.1 ± 0.3	24.1 ± 0.8
BEH C8	7.2 ± 0.2	25.0 ± 0.6
XTerra	7.3 ± 0.2	24.2 ± 0.6
HALO	7.4 ± 0.4	25.2 ± 1.1

When analyzing trace level of serotonin like basal serotonin in microdialysates, peaks from inpurities in aCSF may interfere with serotonin peaks. Temperature regulation is powerful and convenient to separate serotonin from interfering peaks based on different enthalpy changes *ΔH*. In our initial experiment set up, the temperature was set at 80 ℃ (Figure 7a). Two interfering peaks coeluted with 5-HT peak. We tried to separate the 5-HT peak from the interfering peaks by changing temperature. At 70 ℃, the interfering peak and 5-HT peak achieved baseline separation (Figure 7b).

Temperature regulation is much more convenient than changing the mobile phase composition and column type especially for capillary columns which have small column inner diameter and are fast to reach thermal equilibrium. Further studying the retention behavior of one impurity and 5-HT (Figure 8), we found that temperature effect resulted from the difference of slope steepness (enthalpy difference). There was no selectivity at around 77 ℃. Temperature away from this region was good for the separation.

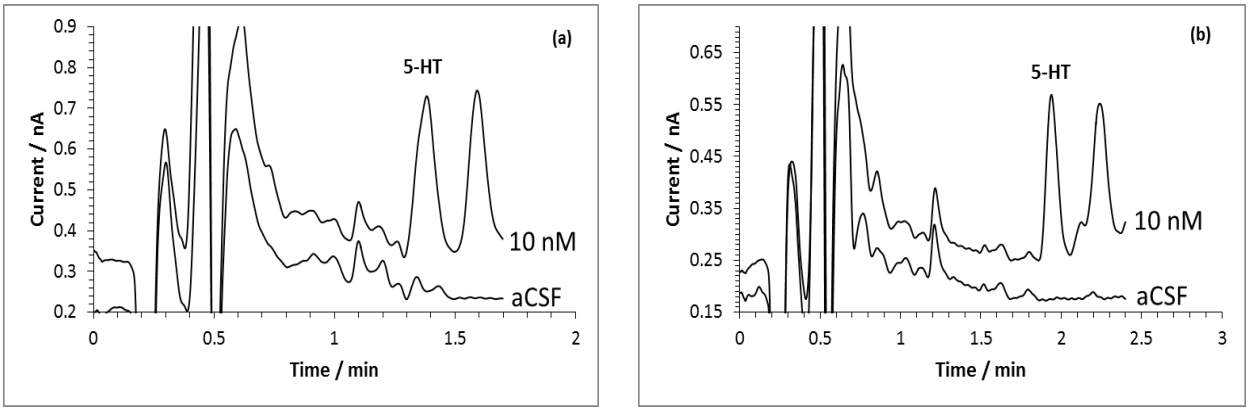

Figure 7. Chromatograms of 10 nM standard and aCSF blank

Column temperature: 80 °C (a), 70 °C (b). Flow rate: 4 µL/min (a), 3.7 µL/min (b).

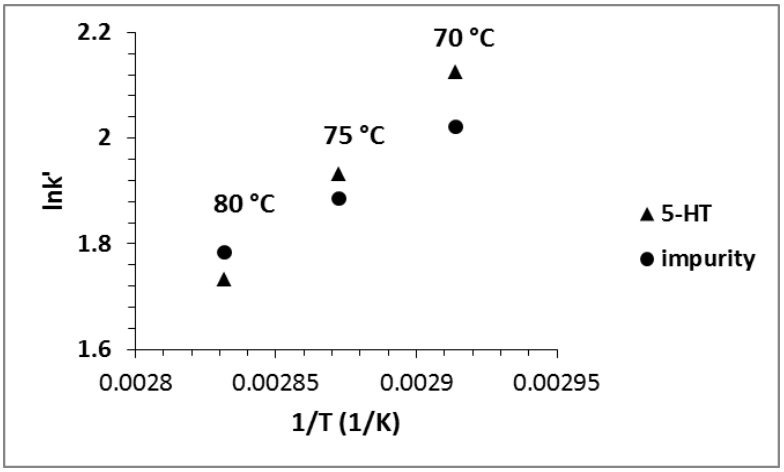

Figure 8. Temperature effect on retention of 5-HT and an impurity

3.0 OPTIMIZATION FOR SPEED AND SENSITIVITY IN CAPILLARY HIGH PERFORMANCE LIQUID CHROMATOGRAPHY. THE IMPORTANCE OF COLUMN DIAMETER IN ONLINE MONITORING OF SEROTONIN BY MICRODIALYSIS.

The following work has been published in *Journal of Chromatography A* **2012**, *1521*, 54-62.

The speed of a separation defines the best time resolution possible in online measurements using chromatography. The desired time resolution multiplied by the flow rate of the stream of analyte being sampled defines the maximum volume of sample per injection. The best concentration sensitivity in chromatography is obtained by injecting the largest volume of sample that is consistent with achieving a satisfactory separation, and thus measurement accuracy. Taking these facts together, it is easy to understand that separation speed and concentration sensitivity are linked in this type of measurement. To address the problem of how to achieve the best sensitivity and shortest measurement time simultaneously, we have combined recent approaches to the optimization of the separation itself with an analysis of method sensitivity. This analysis leads to the column diameter becoming an important parameter in the optimization process. We use these ideas in one particular problem presented by online microdialysis sampling/liquid chromatography/electrochemical detection for measuring concentrations of serotonin in the dialysate. In this case the problem becomes the optimization of conditions to yield maximum

signal for a given sample volume under the highest speed conditions with a certain required number of theoretical plates. It turns out that the observed concentration sensitivity at an electrochemical detector can be regulated by temperature, particle size, injection volume/column diameter and void time. The theory was successfully used for optimization of neurotransmitter serotonin measurement by capillary HPLC when sampling from a microdialysis flow stream. The final conditions are: 150 μm i.d., 3.1 cm long columns with 1.7 μm particle diameter working at a flow rate of 12 μL/min, an injection volume of 500 nL, and a temperature of 343 K. The retention time for serotonin is 22.7 s, the analysis time is about 36 s (which allows for determination of 3-methoxytyramine), and the sampling time is about 0.8 minutes with a perfusion flow rate of 0.6 μL/min.

3.1 INTRODUCTION

There are many important examples of flowing streams that are sampled periodically for analysis, for example microdialysis,[6-8] microreactors,[85-90] and even a chromatographic effluent as a first stage in a two- or three-dimensional separation.[91-93] When analysis of a flowing stream requires taking samples from the flowing stream, the sample volume is a key parameter in defining the attributes of the system. The time resolution of the measurement is related to the stream's flow rate and the sample volume. A larger sample volume dictates poorer time resolution. An exemplary demonstration of this is the early work from the Justice group[27] showing 1-minute time resolution in microdialysis at a time when the typical time resolution was 20 minutes.[94-96] They achieved this by taking 1 μL samples and using a 1 mm column ID for the separation in contrast to the typical 20 μL sample used with a then normal 4.6 mm ID column.

The smaller column volume permitted the use of a smaller sample without decreasing the concentration of the analyte, dopamine, in the detector. The Justice group used off-line HPLC for analysis of the captured microdialysate. The problem becomes considerably more interesting if *online*, near-real time measurements are required.

When online analysis is required, the speed of the separation must equal or exceed the rate of sample acquisition. In this case, the time resolution of the measurement dictates the separation speed, or vice versa. Fortunately, there are developments in liquid chromatographic optimization that focus on achieving minimum time-per-plate that we can use to guide us.[60,97,98] These approaches allow workers to discover the combination of chromatographic parameters such as particle diameter d_p, column length L, and mobile phase linear velocity u for the smallest t_0 with a certain N (high speed separation). In addition, Carr et al.[99] demonstrated that an algebraic approach can be used to carry out the optimization, simplifying the process. But these strategies focus on the separation itself. They do not consider other figures of merit that may be important in the application of the separation to an analytical problem.

There is a need for an optimization approach that includes both separation and detection figures of merit. We face this problem when we consider the monitoring of serotonin (5-hydroxytryptamine, 5-HT) by microdialysis coupled to online HPLC. Our motivation is to improve significantly the speed of the chromatographic determination of 5-HT to improve the temporal resolution of the measurement. This is a challenge, because the concentrations expected for 5-HT in dialysate under resting conditions are less than 1 nM. The separation must be good enough to avoid interferences from solutes with much higher concentrations (by factors of 10^3 – 10^4). Our group has successfully determined 5-HT with a retention time less than one minute in mouse microdialysate samples using capillary columns under high pressure, high temperature

conditions.[100] In that work, 500 nL were injected onto a column with approximately 133 nL of fluid volume. This provided adequate concentration sensitivity. However, the large volume injection, while improving the analytical signal, decreased the number of theoretical plates. We therefore asked the question, "Knowing that a certain number of theoretical plates are sufficient for the separation, can we gain speed without compromising the detection limit?" We have a budget of excess plates (difference between plate number generated by the column with a small injection volume, N and number of theoretical plates achieved with the larger injection volume, N_a). What is the best way to spend the budget?

We will approach this problem conceptually in two steps. First, we recapitulate Carr's algebraic approach that determines N as a function of the void time, t_0, and the particle diameter, d_p, for fixed pump pressure and column temperature.[99] In this portion of the analysis we do not include the injection volume and the band spreading it creates, called volume overload in the preparative chromatography literature,[101,102] nor do we include the column diameter. Based on work of Guiochon and Colon[103] and Poppe et al.,[104] we then incorporate the sacrifice in N caused by volume overload. Based on well-known detector properties,[105-107] we incorporate how the concentration sensitivity of the method is altered by changes in the void time, particle diameter, and column diameter at fixed injection volume, pump pressure, and column temperature. We note that both concentration sensitivity, signal per unit concentration of analyte injected, and mass sensitivity, signal per unit mass injected, could be used as the "detection sensitivity". In the application we are pursuing, the concentration sensitivity is more relevant.

Under the optimum conditions determined by the analysis, the separation time for 5-HT was reduced to about 22.7 s while maintaining the column performance and concentration

sensitivity. Further, we simulated online analysis by making repeated injections to demonstrate the feasibility of online analysis with a time resolution of 36 s.

3.2 EXPERIMENTAL

3.2.1 Chemicals and materials

Disodium EDTA was purchased from Fisher Scientific (Fair Lawn, NJ). Sodium acetate and glacial acetic acid were purchased from J. T. Baker (Phillipsburg, NJ). Acetonitrile, 2-propanol, L-ascorbic acid (AA), serotonin hydrochloride, 3-methoxytyramine hydrochloride (3-MT), and sodium 1-octanesulfonate (SOS) were purchased from Sigma (St. Louis, MO). All the chemicals were used as received without any further purification. Ultra-pure water was obtained from a Millipore Milli-Q Synthesis A10 system (Bedford, MA).

3.2.2 Chromatographic system

Homemade capillary columns were slurry packed with 1.7 μm BEH C 18 reversed-phase particles (Waters, Milford, MA) using 100 or 150 μm i.d., 360 μm o.d. fused-silica capillaries as the column blank (Polymicro Technologies, Pheonix, AZ). Column frits were made by sintering 2 μm borosilicate particles (Thermo Scientific, Fremont, CA) which were pushed into the ends of the columns by pressing the capillary into the particle powder. A Model DSF-150-C1 air driven fluid pump (Haskel, Burbank, CA) was used for packing columns with a packing pressure

of 12 000 psi. The packed capillary columns were connected directly to the injector and flushed overnight with mobile phase before use.

A UHPLC pump (Model nanoLC-Ultra 1D, Eksigent, Dublin, CA), with a maximum pump pressure of 10 000 psi, was used to deliver mobile phase in the flow rate range of 0.1-12 μL/min. A 10 port nanobore injector was used for consecutive injections (Valco Instruments, Houston, TX). Injection loops were fused silica capillaries. The typical sample volume was 500 nL. Column frits were made on the inlet side of the injection capillary to remove any particulates from dialysate samples and protect the column from being blocked.

Two homemade heating assemblies controlled the temperature of the injector and the capillary column. Two proportional-integral-derivative (PID) controllers (Model CT15122, Minco Products, inc., Minneapolis, MN) drove Kapton polyimide heat film (Minco Products, inc., Minneapolis, MN) to heat the column and injector separately. For the capillary column, the heat film covered the surface of an aluminum cylinder with insulation which transferred the heat to the capillary column. The temperature sensor was placed inside the aluminum block, and the signal was fed back to the controller. For the injector, a standoff assembly was used to insulate the actuator from the valve which was covered by the heat film with insulation so the electronic part of the injector was not heated. The temperature sensor was placed in contact with the surface of the valve. The precision of the temperature control is about 0.1 ℃ in the range from room temperature to 100 ℃.

Chromatographic condition: separations of serotonin were achieved using ion-pair reverse phase liquid chromatography. The mobile phase was prepared by mixing an aqueous buffer with acetonitrile with a 96:4 volume ratio. The aqueous buffer contains 100 mM sodium acetate, 0.15 mM disodium EDTA and 10.0 mM SOS. The pH of the buffers was adjusted to 4.0

with glacial acetic acid. The mobile phase was passed through a 0.22 μm Nylon filter (Osmonics, Minnetonka, MN).

Sample preparation: stock solutions of 1.0 mM analytes were prepared in 0.1 M acetic acid and stored frozen at -20 ℃. Analyte solutions with a desired concentration were prepared by successive dilution in 0.1 M acetic acid expect for the final dilution in artificial cerebrospinal fluid (aCSF) with 7 μM AA which mimicked the sample matrix of the microdialysis sample. The aCSF solution contained NaCl 144 mM, KCl 2.7 mM, $CaCl_2$ 1.2 mM, $MgCl_2$ 1 mM, NaH_2PO_4 2 mM at pH 7.4.

3.2.3 Electrochemical detection

A homemade working electrode block was used with a BASi radial-style thin-layer auxiliary electrode. The 1 mm diameter glassy carbon working electrode (HTW Hochtemperatur-Werkstoffe GmbH, Thierhaupten, Germany) was sealed in a Kel-F block with Spurr low visocosity epoxy resin (Polyscience, Inc., Warrington, PA). Electrical contact was made by connecting the working electrode to a metal pin with silver epoxy H20E (Epoxy Technology Inc., Billerica, MA). The flow channel was defined by a 13 μm thick Teflon spacer. Before each day's experiments, the working electrode was wet polished with 0.05 μm γ-alumina slurry (Buehler Ltd., Lake Bluff, IL) and sonicated in Milli-Q water. The working electrode at 700 mV vs Ag/AgCl reference electrode was located directly opposite to the flow inlet. The detector was connected to the capillary column through a piece of 10-cm-long 25-μm-i.d. capillary tubing. Potential control and data collection were done by a BASi Epsilon potentiostat (West Lafayette, IN).

3.2.4 Animals and surgical procedures

All procedures involving animals were carried out with the approval of the Institutional Animal Care and Use Committee of the University of Pittsburgh. Male Sprague-Dawley rats (Hilltop; Scottsdale, PA) (250-375 g) were anesthetized with isoflurane (2% by volume) (Halocarbon Products Corporation; North Augusta, SC) and wrapped in a homoeothermic blanket (EKEG Electronics; Vancouver, BC, Canada) to maintain a body temperature of 37 ℃. The rats were placed in a stereotaxic frame (David Kopf Instruments; Tujunga, CA). Holes were drilled through the skull in the appropriate positions to expose the underlying dura and brain tissue. The dura was removed with a scalpel to allow for placement of the microdialysis probe into the brain tissue with minimal disruption to the surrounding blood vessels.

3.2.5 Guide cannula implantation

Rats underwent surgical preparation three days prior to microdialysis probe placement. Surgery was performed under aseptic conditions. Animals were positioned in a stereotaxic frame according to the atlas of Paxinos and Watson.[108] In addition to the holes in the skull for passage of a guide cannula (BASI, West Lafayette, IN) into the brain, four additional holes were drilled to accept four jeweler's screws. The cannula was anchored in place with acrylic dental cement. Animals were housed individually until they recovered from the surgery.

3.2.6 Microdialysis

Four millimeter membrane microdialysis probes were purchased (30 KDa, MD-2204, BASi, West Lafayette, IN) and conditioned prior to insertion by flushing with aCSF for 1 hour. FEP tubing 0.65 mm OD x 0.12 mm ID was used to connect the inlet and outlet ends of the microdialysis probe to a 1.0 mL gas-tight syringe. Microdialysis probes were lowered into the striatum using flat-skull coordinates (0.75 mm anterior to bregma, 2.5 mm lateral from midline and 7.0 mm below dura) over a 30 minute period. All probes were perfused with aCSF with 7 μM of AA, pH 7.4, at a rate of 0.586 μL/min. After a 2-h equilibration period, two baseline samples were collected at 1-h each and analyzed by HPLC. All baseline samples contained a final concentration of 0.05 M acetic acid. To elicited spreading depression (high K^+ concentrations), the microdialysis probe was perfused with 120 mM K^+ aCSF (NaCl 26.7 mM, KCl 120.0 mM, $CaCl_2$ 1.2 mM, $MgCl_2$ 1 mM, NaH_2PO_4 2 mM) in 7 μM of AA for 20 minutes at rate of 0.586 μL/min. During this time, 5 samples were collected at 20 minutes each in tubes containing 0.05 M acetic acid. After 20 minutes the perfusate was switched back to aCSF in 7 μM of AA till the end of the experiment. Two additional samples were collected at 1 hour post high K^+ perfusion. All samples were placed on dry ice until analyzed by HPLC later on the same day, usually within an hour.

3.3 RESULTS AND DISCUSSION

3.3.1 Theory for optimization of a chromatographic system operating at maximum pressure and with a choice of particle diameter

This section is a brief recapitulation of Carr et al. [99] to establish certain relationships among variables. In that work, and Poppe's work, one can find the optimum values of column length L and interstitial linear velocity u_e to give the maximum N once d_p, t_0, and P are specified. Alternatively, one could find the optimum values of L and u_e to give the minimum t_0 once d_p, N, and P are specified.

Eq. 8 gives interstitial linear velocity u_e, as a function of void time t_0 and column length L:

$$u_e = \frac{u}{\lambda} = \frac{L}{\lambda t_0} \tag{8}$$

where λ is the ratio of interstitial and total porosity. Interstitial linear velocity u_e is used here in accordance with Carr's work[99] and for its relevance to mass transport in relationships between plate height and mobile phase velocity. Eq. 9 gives length, L, as a function of pressure drop over the whole column, P, particle diameter, d_p, and u_e.

$$L = \frac{d_p^2 P}{\phi \eta(T) u_e} \tag{9}$$

Here, ϕ is the flow resistance factor (relating specifically to u_e), and $\eta(T)$ is the mobile phase viscosity at temperature T. Then u_e and L can be expressed as functions of t_0 and d_p (and other parameters) below derived from Eqs. 8 and 9.

$$u_e(t_0, d_p, T) = \sqrt{\frac{P}{\phi\eta(T)\lambda t_0}} d_p \tag{10}$$

$$L(t_0, d_p, T) = \sqrt{\frac{P\lambda t_0}{\phi\eta(T)}} d_p \tag{11}$$

For the best chromatographic performance, we will operate at a certain maximum pressure,

$$P = P_{\max} \tag{12}$$

The plate number generated by a column with length L and velocity u_e is shown in Eq. (13),

$$N = \frac{L}{H} = \frac{L}{hd_p} = \frac{L}{d_p(A + \frac{B}{v} + Cv)} = \frac{L}{d_p(A + \frac{BD_m(T)}{u_e d_p} + \frac{Cu_e d_p}{D_m(T)})} \tag{13}$$

Where H is the plate height, h is the reduced plate height, v is the reduced linear velocity, A, B, C are dimensionless terms in the van Deemter equation expressed in terms of reduced velocity, and $D_m(T)$ is the solute diffusion coefficient in the mobile phase at temperature T. Using Eqs. 10-12 in Eq. 13 leads to Eq. 14.

$$N(t_0, d_p, T) = \frac{\sqrt{\frac{P_{\max}\lambda t_0}{\phi\eta(T)}}}{A + \frac{BD_m(T)}{d_p^2}\sqrt{\frac{\phi\eta(T)\lambda t_0}{P_{\max}}} + \frac{Cd_p^2}{D_m(T)}\sqrt{\frac{P_{\max}}{\phi\eta(T)\lambda t_0}}} \tag{14}$$

Note that Eq. 14, which is equivalent to Eq. (13) of [99], is now a function of t_0, d_p, and P_{max}, as well as other parameters. As in Carr et al.,[99] we use the van Deemter equation instead of Knox equation for algebraic simplicity. Using reduced A, B, and C is convenient because it allows Eq. 14 explicitly to show variables (e.g., d_p) that are important in optimization, and simplifies the application of a final result to a column with known parameters. Below we show that the fits of

the two equations to the data are statistically the same. This equation could be used to determine the number of theoretical plates achievable with a particular d_p and t_0 (with the remaining parameters: $D_m(T)$, $\eta(T)$, λ, A, B, C, ϕ, and P_{max} known). Column length and mobile phase velocity are calculated using Eqs. 10 and 11. In the current context, we do not expect to realize N theoretical plates; rather, we expect some increased band spreading from volume overload which we accept for achieving a certain sensitivity of the analysis. In this case, we will realize an apparent theoretical plate number, N_a, that will be sufficient for the separation but lower than the intrinsic plate number of the column, N, because of the volume overload required to maximize detection sensitivity.

3.3.2 Column diameter: an important variable

The following discussion is based on work by Poppe et al.[104] and Colin and Guiochon.[103] We turn our attention to the degradation of column performance by volume overload in an isocratic chromatography system. Based on the column's intrinsic properties, given by variance σ_{col}^2, and additional variance from overload, σ_{ol}^2, we define the apparent number of theoretical plates, N_a. Eq. 15, describes the relationship between N_a and the intrinsic plate number generated by the column, N:

$$N_a = N\left(1-\frac{\sigma_{ol}^2}{\sigma_{ol}^2+\sigma_{col}^2}\right) = N(1-\theta^2) \tag{15}$$

where θ^2 is the fractional contribution to the observed band variance from the extra-column effect. Other contributions to extra-column peak variance such as postcolumn reactor volume[78] are not included here. We need the relationship for the volume-based variance of the peak, σ_v^2, based on the number of theoretical plates in terms of retention volume, V_r, (Eq. 16)

$$\sigma_v^2 = \frac{V_r^2}{N} \tag{16}$$

Eq. 17 relates injection volume to the sacrifice in column efficiency represented by θ and other column parameters.[103] It arises from using Eq.17 in the definition of θ with the assumption that σ_{ol}^2 is small compared to σ_{col}^2

$$V_{inj} = \frac{K\theta\pi\varepsilon d_c^2 L(k'+1)}{4\sqrt{N}} \tag{17}$$

V_{inj} is the injection volume which gives a particular contribution (θ) to the band dispersion. K is a constant depending on the injection technique, ε is column porosity, L is the column length, and k' is the retention factor of the solute. Eq. 17 is valid when the sample solvent and the injection solvent are the same. When the injected sample solvent has less eluting strength compared to the mobile phase, the injection volume V_{inj} for a particular θ increased by a factor of k_0'/k' where k_0' is the value of the retention factor in the sample solvent. [104,109] Solutes in the sample solvent concentrate at the head of the column which improves the concentration detection sensitivity due to the higher retention factor in the sample solvent and the compression arising from the step-gradient by the following higher eluting strength mobile phase. This preconcentration process is called on-column focusing. [104]Thus, the injection volume under on-column focusing is

$$V_{inj} = \frac{K\theta\pi\varepsilon d_c^2 L(k'+1)k_0'}{4\sqrt{N}k'} \tag{18}$$

From Eq. 18, we can find a relationship for θ which when used with Eq. 15 gives rise to the relationship between achieved plate number and injection volume

$$N_a = N - \frac{16k'^2 N^2 V_{inj}^2}{K^2\pi^2\varepsilon^2(k'+1)^2 k_0'^2 L^2 d_c^4} = N - \frac{N^2 V_{inj}^2}{X^2 L^2 d_c^4} = N - \frac{N^2 V_{inj}^2}{X^2 \frac{t_0}{\tau(T)} d_p^2 d_c^4} \tag{19}$$

Where

$$X = \frac{K\pi\varepsilon}{4}\frac{(k'+1)k_0'}{k'}$$

and

$$\frac{\phi\eta(T)}{P_{\max}\lambda} = \tau(T)$$

Eq. 19 shows that the column diameter and volume injected as well as t_0 and d_p are used to define N_a, whereas the intrinsic power of the column, expressed as N, only depends on t_0 and d_p (and other parameters that for a particular solute, mobile phase, and temperature are constants: X, P_{max}, $\tau(T)$, ϕ, $D_m(T)$, and the terms in the van Deemter equation).

The foregoing is completely general. In the context of the problem we posed in the introduction, N_a is a known quantity – the number of theoretical plates required for quantitative determination of the analyte. Thus, we derive Eq. 20 from Eqs. 11, 15, 18 and 19. This expression for d_c depends on t_0, d_p, T, and V_{inj} (and other parameters that for a particular solute, mobile phase, and temperature are constants: X, P_{max}, $\tau(T)$, ϕ, $D_m(T)$, and the terms in the van Deemter equation).

$$d_c(t_0, d_p, V_{inj}, T) = \sqrt{\frac{4\sqrt{N}k'V_{inj}}{K\theta\pi\varepsilon L(k'+1)k_0'}} = \sqrt{\frac{V_{inj}}{X\sqrt{\frac{t_0}{\tau(T)}}d_p}\frac{N(t_0, d_p, T)}{\sqrt{N(t_0, d_p, T) - N_a}}} \qquad (20)$$

3.3.3 Influence of chromatographic optimization on sensitivity

We now consider the sensitivity of the detector and its relationship to the chromatography. We use an electrochemical detector, but we will derive the necessary relationships in general terms. We use the symbol i generically for "signal". The instantaneous signal depends on the mobile phase flow rate F_m to some power, α.

$$i = kC_{in}F_m^{\alpha} \tag{21}$$

where k is a sensitivity factor that need not concern us and C_{in} is the analyte concentration in the mobile phase entering the detector. The observed concentration sensitivity is the ratio of the signal to the concentration in the injected sample

$$S = \frac{i}{C_s} = \frac{kC_{in}F_m^{\alpha}}{C_s} \tag{22}$$

where C_s is the analyte concentration. Eq. 22 expresses the well-known fact that the observed concentration sensitivity is influenced by chromatographic bandspreading and may be dependent on the flow rate of the chromatographic mobile phase. We can relate the concentration in the detector, conceptually, to the number of moles of analyte injected into the column and the peak volume. The peak volume is proportional to the volume standard deviation, σ_v, regardless of the details of the peak shape. We do not lose insight from calculating proportionalities rather than equalities, so we can drop the unknown detector sensitivity factor and the proportionality between peak standard deviation and peak volume that depends on peak shape.

$$S \propto \frac{C_{in}F_m^{\alpha}}{C_s} \tag{23}$$

We can express C_{in} as being proportional to the moles injected divided by the peak volume, $\frac{C_s V_{inj}}{\sigma_v}$

$$S \propto \frac{C_s V_{inj} F_m^{\alpha}}{C_s \sigma_v} = \frac{V_{inj} F_m^{\alpha}}{\sigma_v} \tag{24}$$

The volume standard deviation can be expressed in terms of theoretical plate count and retention volume as in Eq. 16, except that here we are considering the peak width in an actual analysis, so N_a, replaces N. In addition, we write the retention volume as $t_0(k'+1)F_m$.

$$S \propto \frac{\sqrt{N_a} V_{inj} F_m^{\alpha}}{t_0 (k'+1) F_m} \tag{25}$$

And finally, combining the flow rate terms, we have Eq. 26.

$$S \propto \frac{\sqrt{N_a} V_{inj} F_m^{\alpha-1}}{t_0 (k'+1)} \tag{26}$$

What remains is to replace flow rate with its equivalent in terms of other variables (here ε is the total column porosity):

$$F_m = \frac{u_e \lambda \pi \varepsilon d_c^2}{4} \propto u_e \lambda \varepsilon d_c^2 \propto \sqrt{\frac{P\lambda}{\phi \eta(T) t_0}} d_p \varepsilon d_c^2 \propto \sqrt{\frac{1}{\tau(T) t_0}} d_p \varepsilon d_c^2 \tag{27}$$

$$S \propto \frac{\sqrt{N_a} V_{inj} (\sqrt{\frac{1}{\tau(T) t_0}} d_p \varepsilon d_c^2)^{\alpha-1}}{t_0 (k'+1)} \tag{28}$$

For the electrochemical detector under many conditions the value of α is 1/3.[105-107] Thus, for the electrochemical detector, the sensitivity is

$$S_{el}(t_0, d_p, V_{inj}, T) \propto \frac{\sqrt{N_a} V_{inj} \tau(T)^{1/3}}{t_0^{2/3} (k'+1) (d_p \varepsilon d_c(t_0, d_p, V_{inj}, T)^2)^{2/3}} \tag{29}$$

In Eq. 29, sensitivity is a function of the independent variables t_0, d_p, V_{inj} and T. To achieve any combination of t_0, d_p, and T, we will work at the column length and velocity determined by Eqs. 10 and 11. This length and velocity will generate N theoretical plates (Eq. 14) in the limit of small injection volume. For an injected sample volume V_{inj} and required

apparent plate number N_a, we will work at the column diameter determined by Eq. 20. The incorporation of column diameter d_c adds another degree of freedom for the optimization.

Table 6. Fixed parameters involved in the optimization

Parameter	Determination	Value
Φ	Pressure vs u_e at T=343 K	289
A, B, C	h vs v at T=343 K	See Table 2
N_a	Experience	2200
P_{max}	Instrument	41.4 MPa (6 kpsi)
λ	Literature	0.625
D(298K)	Literature	5.4×10^{-10} $m^2 s^{-1}$ (T= 298K)
$\eta(T)$	Literature	See Eq. 24
X	N_a vs V_{inj} at T=343 K	87.94, see Fig. 2

3.3.4 Experimental determination of fixed parameter values

Table 6 shows the fixed parameters, how they were determined, and the parameter values. Eq. 9 shows that the slope of a P vs u_e plot will yield the column flow resistance factor for a column at 70 ℃ (constant d_p, $\eta(T)$ and L). This value, relating to mobile phase linear velocity, u, is 462. Thus, the flow resistance factor, ϕ, relating to u_e is 289. The A, B, and C terms were experimentally determined by building up a van Deemter plot (incorporating reduced variables) followed by regression (Figure. 9, Table 7). The van Deemter and Knox fits are both good and have essentially identical values of R^2. From our previous experience, N_a is 2200 for sufficient separation. Thus, A, B, C, ϕ and N_a are determined by experience or experiment. P_{max}, 41.37 MPa (6000 psi), is governed by our equipment. Although the maximum pressure capability of the

pump is 10,000 psi, the pressure generated from the pump's internal flow path is as high as 2100 psi at a flow rate of 12 μL/min. In consideration of this and that we want to work at a pressure a little lower than the pressure limit, *P* was chosen as 6000 psi in the calculation. Typical values of λ are in the range of 0.6-0.7 so here we use 0.625. For viscosity, we used the form of an empirical relationship for viscosity as a function of composition and temperature.[110] A nonlinear regression of that empirical function with the apparent integral viscosities at 400 bar for water-acetonitrile between 20 and 100 ℃ from Billen et al. [111] resulted in Eq. 30

$$\eta = 10^{(-2.533+(742/T)-0.452X_{acn}+(235/T)X_{acn}+1.573X_{acn}^2-(691/T)X_{acn}^2)} \tag{30}$$

where X_{acn} is the volume fraction of acetonitrile in the mobile phase. The diffusion coefficient D_m of 5-HT is $5.4\times10^{-6} cm^2/s$ at 298 K.[112] D_m at other temperatures is calculated based on empirical Eq. 31.

$$D_m(T) = 5.4\times10^{-6}\times\frac{T\times\eta(298)}{298\times\eta(T)} cm^2/s \tag{31}$$

Finally, we have experimentally determined the effect of injection volume on efficiency based on Eq. 19. A regression of N_a on V_{inj}^2 will reveal the lumped parameter *X* which can then be used in optimization (Figure. 10). The regression yields the relationship (V_{inj} is in nanoliters)

$$N_a = 6005 - 0.0187V_{inj}^2 \ (R^2 = 0.928) \tag{32}$$

and

$$X = \frac{K\pi\varepsilon(k'+1)k_0'}{4k'} = 87.94$$

at 343 K. Our primary conclusions are for T = 343 K, so X can be considered as a constant. In practice, changes in temperature are often accompanied by changes in mobile phase composition, so that k' may be more or less constant. However, k_0' will be temperature dependent. Thus, X is temperature dependent in general.

Table 7. Nonlinear fit of the van Deemter plot using theoretical equations

	A	B	C	R^2	Equations
Van Deemter	1.4 ± 0.2	9.4 ± 0.4	0.12 ± 0.01	0.968	$h = 1.4 + 9.4/v + 0.12v$
Knox	0.8 ± 0.1	10.3 ± 0.3	0.08 ± 0.01	0.960	$h = 0.8v^{1/3} + 10.3/v + 0.08v$

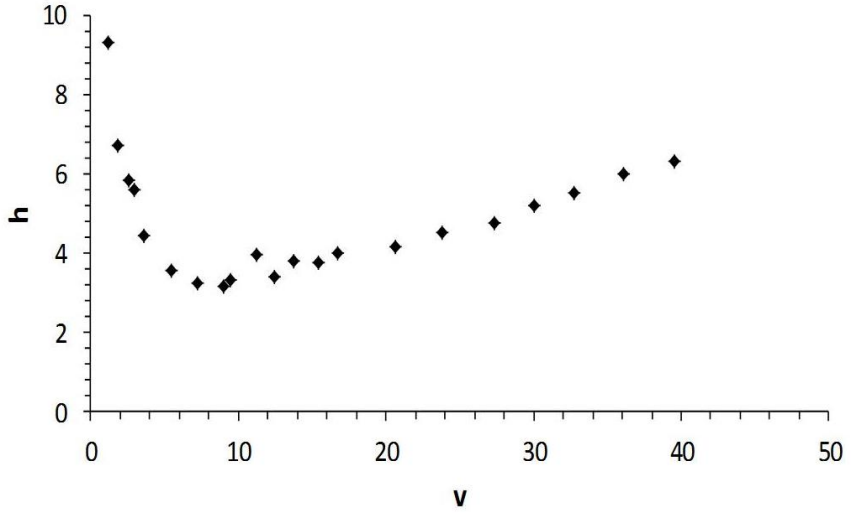

Figure 9. The reduced plate height vs reduced velocity (interstital) generated from a column

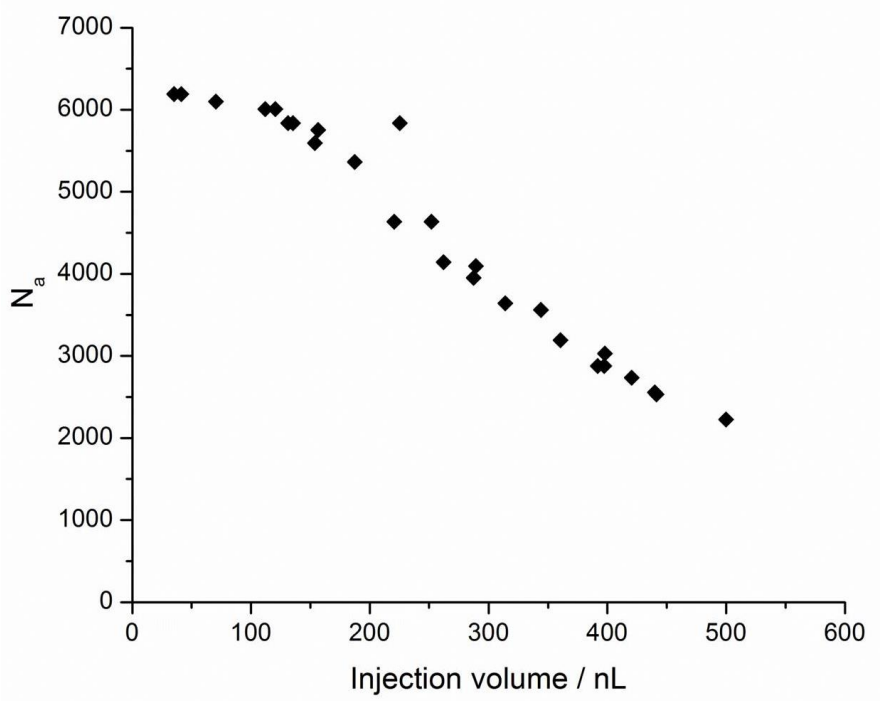

Figure 10. Apparent plate number measured at different injection volume

Column: 100 μm inside diamter, 5.0 cm long capillary column packed with 1.7 μm BEH C 18 particles. Mobile phase: 100 mM sodium acetate, 0.15 mM disodium EDTA, 10.0 mM SOS, pH=4.0, mixed with 4% (v/v) acetonitrile. Flow rate: 4.0 μL/min. Column temperature T = 343 K.

3.3.5 Finding the optimum conditions

Now that we have all the parameters, we will first explore briefly the variables T, V_{inj}, and d_p. Figure. 11 encapsulates, with just a few curves, the effect of these variables on sensitivity and speed according to Eq. 29. Note that each curve has a clear maximum, dropping off steeply to the short time side. We find the maximum sensitivity at a t_0 that is near the minimum accessible value. Thus, striving for maximum sensitivity does not require a significant sacrifice in speed. Comparison of the green and red curves shows that the higher temperature (383 K) permits a higher sensitivity and a potentially faster separation in comparison to the lower temperature (343

K) all else being equal. Comparison of the red and black curves shows that a modest change (red: 500 nL; black: 250 nL) in injected volume decreases the sensitivity, but has little effect on the speed. Comparison of the red (1.7 µm d_p) and blue (2.6 µm d_p) curves show that the smaller particle diameter improves speed and sensitivity. Therefore, we can conclude that with the goal of higher sensitivity and speed, we should work at conditions with the highest practical T, largest V_{inj}, and smallest d_p. Prior work guided us to choose 70 ºC (343 K) as the column temperature which is the highest working temperature with good column selectivity and stability.[100] Although larger sample volume benefits the detection sensitivity, it also relates to the time resolution of the analysis. Here, a sample volume of 500 nL was used based on experience which provides a sampling time resolution of less than 1 minute for typical microdialysis flow rates. Also, the sub-2 µm porous particles are currently the smallest commercially available porous particles which is our best choice. Given the pragmatic constraints mentioned above, we will choose to operate at T = 343 K, use 1.7 µm particles, and inject 500 nL.

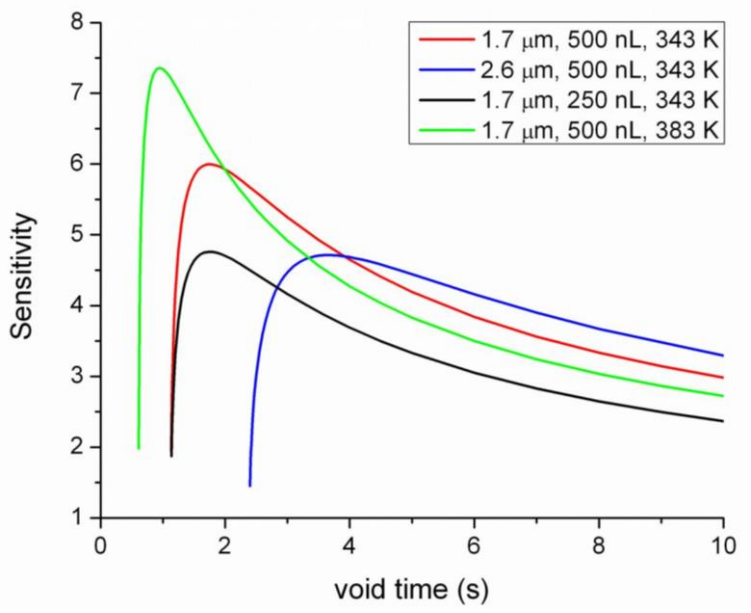

Figure 11. Effect of particle size, injection volume and column temperature on concentration sensitivity and separation speed (void time t_0)

The column diameter is a key parameter in this optimization. In the current context where we seek optimum conditions, it is not independently variable. It depends, like sensitivity, on t_0, d_p, V_{inj}, and T (as well as the parameters in Table 6). For a given temperature and injection volume, there is a single value of S_{el} corresponding to a pair of values (t_0, d_p). The same is true of column diameter. Thus, it is instructive to consider S_{el} and d_c as a function of t_0 given d_p, V_{inj}, and T. Figure 12a shows how sensitivity (with V_{inj} and T fixed at the values stated above) depends on column diameter and void time. Each curve corresponds to a different particle diameter. It is hard to visualize the curve in three dimensions, so we have plotted in Figure 12b the projections of each curve on the three two-dimensional planes. Table 8 shows the range of laboratory parameters that will provide sensitivity within 3% of the maximum.

Some general observations may be made. Smaller particle diameter results in higher sensitivity at optimum conditions. The column diameter is an important variable. Note that in Figure 12 significant sensitivity is lost by using columns with a diameter of 500 μm. On the other hand, when the column diameter is too small the column length must increase to avoid volume overload and maintain N_a. This is reflected in the simultaneous decrease in sensitivity and increase in void time when column diameter becomes small. Note that the void time is completely independent of the column diameter for column diameters larger than some value that depends on the particle diameter. This reflects the point where volume overload is negligible, *i.e.*, $N = N_a$.

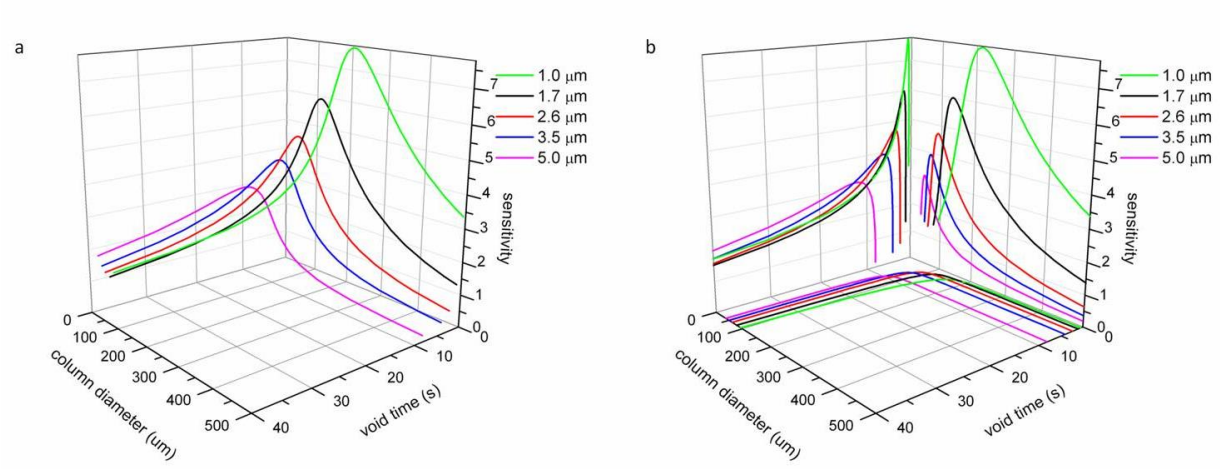

Figure 12. Concentration sensitivity as a function of void time t_0 and column diameter d_c

Left: a line for each particle diameter in three dimensions. Right: projections of each of the latter curves in each of the two-dimensional planes.

Table 8. Optimum chromatographic parameters' rang for 97-100% of maximum sensitivity

Injection volume: 500; working temperature: 343 K.

d_p (µm)	Sensitivity	u_e (cm/s)	L (cm)	t_0 (s)	d_c (µm)
1.0	7.5-7.7	1.8-1.4	1.2-1.4	0.67-1.0	238-195
1.7	5.8-6.0	2.0-1.7	3.0-3.6	1.5-2.2	148-122
2.6	4.6-4.7	2.1-1.8	6.6-7.9	3.1-4.5	99-82
3.5	3.8-3.9	2.2-1.8	12-14	5.4-7.8	74-62
5.0	3.1-3.2	2.2-1.8	23-28	10.6-15.2	53-44

3.3.6 Application of the optimized system to microdialysis

We use 1.7 µm BEH C 18 particles. Considering both sensitivity and speed from Figure 12 and Table 8, the column diameter is 150 µm with a length of 3.1 cm. Figure 13 demonstrates results from this column. The total analysis time for 5-HT and 3-MT was reduced to about 0.6 minutes with t_0 of 1.5 s and a plate number of 2450. The flow rate is 12 µL/min and the reduced linear velocity v is 32. The total pressure is 8354 psi while the back pressure generated by the column is 6204 psi. We note that the plate count and column pressure are close to the values specified in the optimization (2200 and 6000 psi, resp.). This supports the reproducibility of our column packing, as Figure 9 and Figure 10 are from different columns created before packing the optimally sized columns.

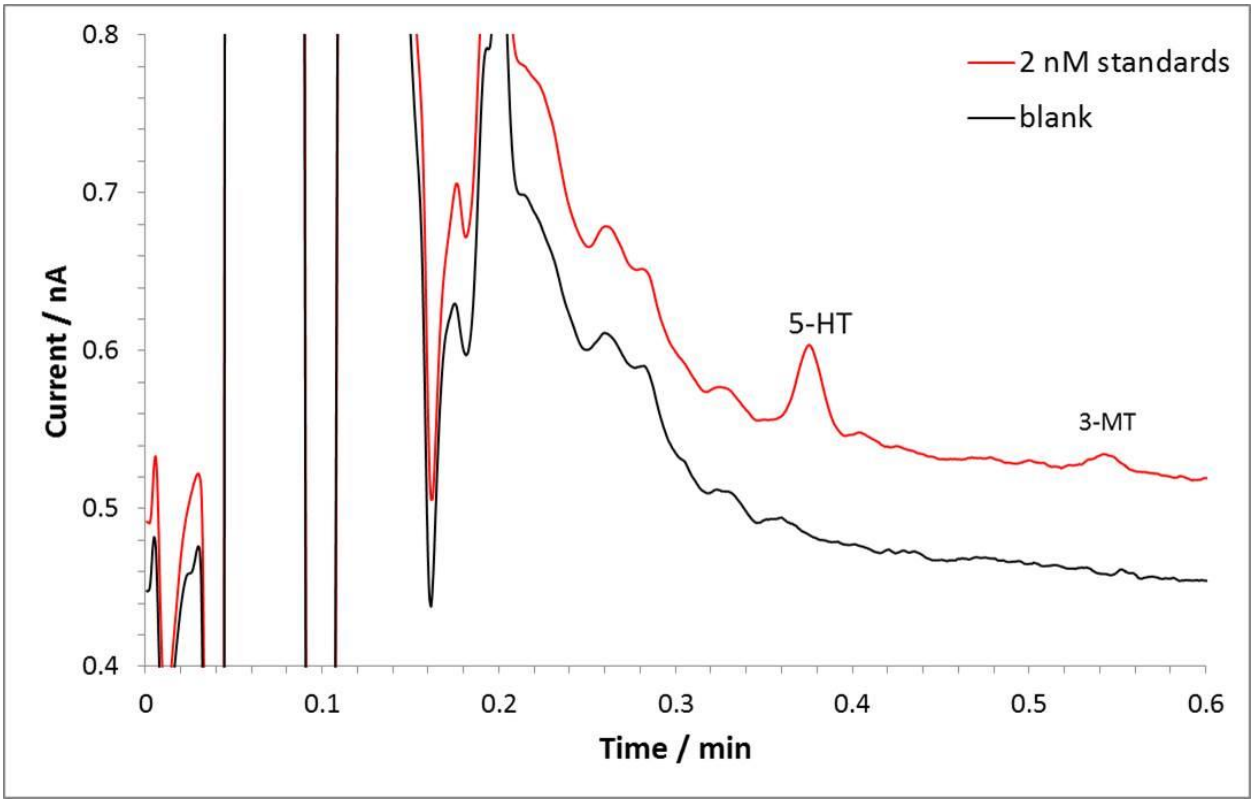

Figure 13. Typical chromatogram of a 500 nL standard injection sample

Red: standard sample containing 2 nM 5-HT, 2 nM 3-MT and 7 μM AA. Black: blank aCSF solution. Column: 150-μ-i.d., 3.1-cm-length capillary column packed with BEH C 18 particles. Mobile phase: 100 mM sodium acetate, 0.15 mM disodium EDTA, 10.0 mM SOS, pH=4.0, mixed with 4% (v/v) acetonitrile. Flow rate: 12.0 μL/min. Column temperature: 70 ℃. Electrochemical detection.

We first applied the system to offline measurements. The system proved excellent within-day retention and sensitivity reproducibility. The average retention time of 5-HT peaks in standards and dialysate samples from one typical day-long experiment is 22.5 ± 0.1 s based on 47 injections. One concern often expressed about electrochemical detection is a slow decrease in sensitivity commonly attributed to electrode fouling. The change in the active electrode surface area and surface properties may cause this sensitivity drift. Therefore, the detection sensitivity at the beginning and end of a whole day's experimentation (typically 7-9 hours, 50-80 injections) was investigated. The sensitivity loss for 5-HT was in the range of 2-5%. This relatively small sensitivity change of about 0.5% per hour can be ignored for experiments requiring an hour or less. For longer experiments, pre- and postcalibration should be used.

The electrochemical detector responds linearly in the concentration range from 0.5 nM to 100 nM (5-HT: R^2=0.9992; 3-MT: R^2=0.9994). Therefore, one point at the very high concentration (100 nM) was used for 5-HT and 3-MT concentration calibration. Limits of detection for 5-HT and 3-MT are 0.3 nM and 1.0 nM respectively (signal three times greater than rms noise).

With the conditions and method established, we then determined 5-HT in rat brain microdialysate (Figure 14). The total analysis time is about 36 s with 5-HT eluting at 22.7 s and 3-MT eluting at 33.3 s. The basal 5-HT and 3-MT concentrations are 0.67 nM and 2.62 nM. Confirmation of the 5-HT peak was done by spiking samples with an equal volume of a 5 nM

standard (Figure 14). Confirmation of the peak identity can also be done using the physiological response to elevated extracellular K^+ concentration. Samples were collected before, during and after high K^+ stimulation at 20-min intervals (Figure 15). The increased extracellular K^+ concentration induced a significant increase of the 5-HT concentration in the dialysate.[113]

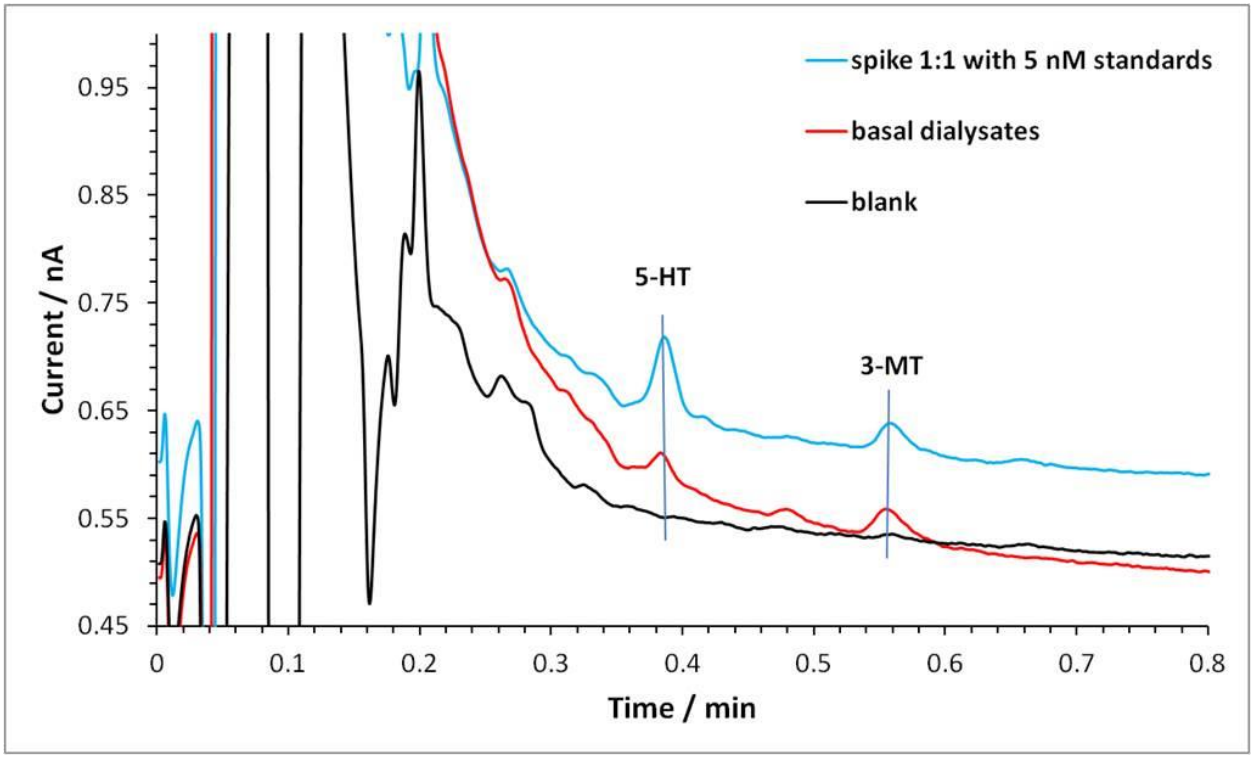

Figure 14. Determination of basal 5-HT and 3-MT in rat brain microdialysate

Separation conditions were the same as in Figure 5. Black: blank aCSF solution. Red: basal microdialysate sample collected from striatum of rat brain with a perfusion flow rate of 0.6 μL/min. Blue: 1:1 volume ratio mixture of basal microdialysate sample and 5 nM standard.

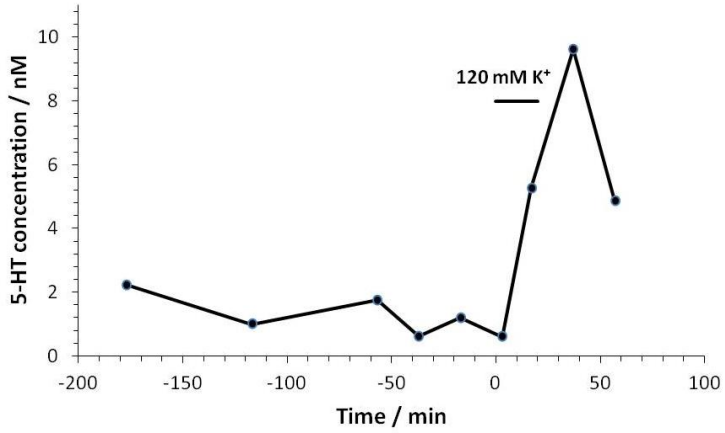

Figure 15. Monitoring of 5-HT concentration followed by high K^+ stimulation

Administration: 120 mM K^+ aCSF solution for 20 min. Samples were collected and analyzed offline. Separation and sampling conditions were the same as in Figure 6.

The temporal resolution of the 5-HT separation is now 36 s with 500 nL dialysate samples. This makes it possible to imagine online measurements every 36 s with a perfusate flow rate of 0.83 µL per minute (*i.e.*, 500 nL/0.6 minutes). Since our goal is online analysis, the feasibility of continuous analysis was done by making 5 consecutive injections of basal dialysate samples with 0.6-min time intervals (Figure 16). The average 5-HT concentration was 0.66 ± 0.03 nM and the average 5-HT peak retention time was 22.7 ± 0.1 s based on the five injections. The small standard error shows excellent reproducibility of sample loading, separation and detector response which are important parameters for online analysis. There are no late-eluting peaks from early injections that impact later injections.

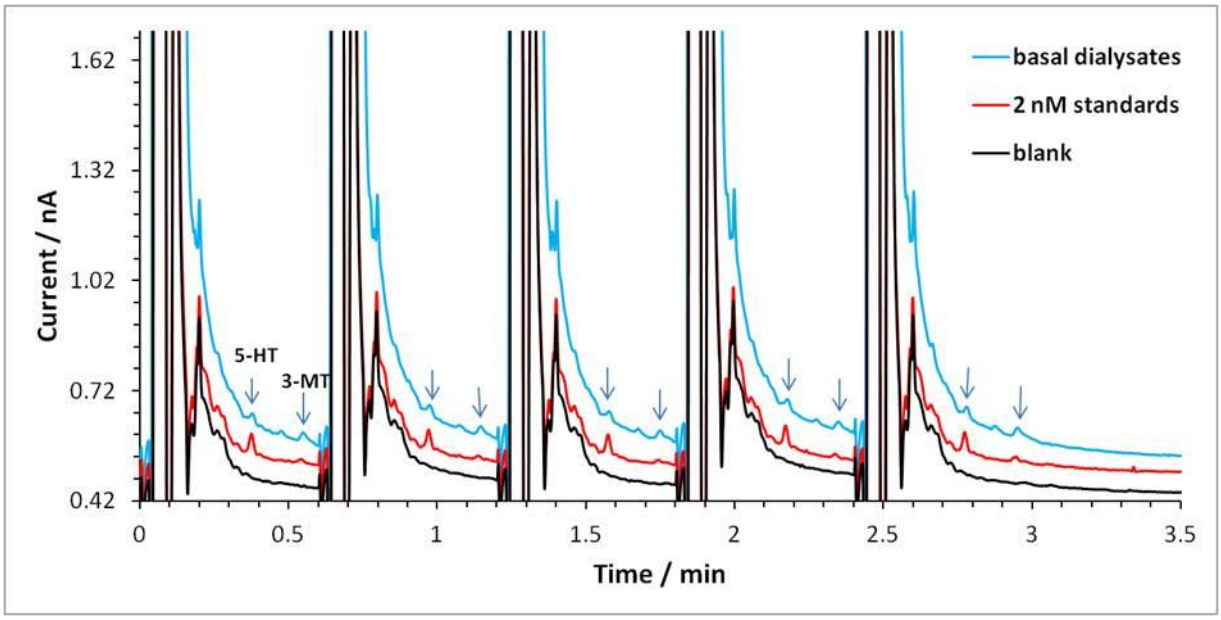

Figure 16. Chromatograms of samples with consecutive injections

Injection intervals: 0.6 minutes. Separation and sampling conditions were the same as in Figure 6.

3.4 CONCLUSIONS

The optimization of an HPLC system generally pursues the speed or efficiency of a separation However, the theory regarding optimization, as valuable as it is, does not optimize conditions for an isocratic trace analytical method based on chromatography. Specifically, we take into account the ubiquitous procedure of on-column preconcentration as part of the overall optimization. A sample volume that is too large will sacrifice the separation speed, separation efficiency and analysis temporal resolution when sampling from flowing streams at a constant rate. A sample volume that is too small may result in undetected compounds. We demonstrate that the column diameter is an important parameter in the optimization of conditions to attain high speed and the best possible sensitivity for a given sample volume with a certain required number of theoretical

plates. For an electrochemical detector, the maximum concentration sensitivity is achieved with a particular t_0 and corresponding d_c. Smaller particle size and higher temperature provides smaller optimum t_0 and greater sensitivity which means higher speed and better detection limit. The theory was successfully used for optimization of serotonin measurements using online microdialysis coupled with capillary HPLC-EC. Careful optimization is required because our goal is to improve temporal resolution, but we must not reduce the method's concentration sensitivity since the sample size is limited and concentration detection limit is important. With the optimized system, we demonstrated basal 5-HT measurements in rat microdialysate samples offline in 36 s. The consecutive analysis provides strong support for successful online analysis.

4.0 *IN VIVO* MONITORING OF SEROTONIN IN THE STRIATUM OF FREELY-MOVING RATS WITH ONE-MINUTE TEMPORAL RESOLUTION BY ONLINE MICRODIALYSIS-CAPILLARY HIGH PERFORMANCE LIQUID CHROMATOGRAPHY AT ELEVATED TEMPERATURE AND PRESSURE

The following work has been published in *Analytical Chemistry* **2013**, *85*, 9889-9897.

Online monitoring of serotonin in striatal dialysate from freely moving rats was carried out for more than sixteen hours at one-minute time resolution using microdialysis coupled online to a capillary HPLC system operating at about 500 bar and 50 ^{o}C. Several aspects of the system were optimized towards robust, *in vivo* online measurements. A two-loop, eight-port rotary injection valve demonstrated better consistency of continuous injections than the more commonly used two-loop, ten-port valve. A six-port loop injector for introducing stimulating solutions (stimulus injector) was placed in-line between the syringe pump and microdialysis probe. We minimized solute dispersion by using capillary tubing (75 μm i.d., 70 cm long) for the probe inlet and outlet. *In vitro* assessment of concentration dispersion during transport with 30-s time resolution showed that the dispersion standard deviation for serotonin was well within the desired system temporal resolution. Each 30- or 60-second measurement reflects the integral of the true time response over the measurement time. We have accounted for this mathematically in determining

the concentration dispersion during transport. The delay time between a concentration change at the probe and its detection is seven minutes. The timing of injections from the stimulus injector and the cycle time for the HPLC monitoring of the flow stream was controlled. The electrochemical detector contained a 13 μm spacer to minimize detector dead volume. During *in vivo* experiments, retention time and separation efficiency were stable and reproducible. There was no statistically significant change over 5.5 hours in the electrochemical detector sensitivity factor for serotonin. Dialysate serotonin concentrations change significantly in response to a 120 mM K^+ stimulus. Release of serotonin evoked by a ten-minute, 120 mM K^+ stimulation, but not for other K^+ stimuli, exhibited a reproducible, oscillating profile of dialysate serotonin concentration vs. time. Infusion of fluoxetine, a serotonin uptake inhibitor, increased dialysate serotonin concentrations and stimulated release magnitude. Transient serotonin increases were observed in response to the stress associated with unexpected handling. This system is simple, efficient, reliable, and suitable for study of serotonin neurochemistry associated with emotion and behavior.

4.1 INTRODUCTION

Online sampling/analysis is highly desirable for many applications, for example high throughput screening,[114] analysis of synthetic reactions in microreactors,[86] environmental[115] and biological[116] substance monitoring, and process analytical chemistry.[117] Online sampling especially benefits the analysis of small volume samples since it avoids sample handling procedures. Another area in which it excels is in monitoring dynamic processes such as those

occurring in the brain.[6] Increasing the temporal resolution of online sampling/analysis will provide more details of dynamic processes.

Serotonin (5-hydroxytryptamine, 5-HT) together with the 5-HT transporter and receptors modulate many brain functions[2-4,118] and intestinal activities.[119] Neurological disorders like depression and anxiety are associated with abnormalities of the serotonergic system. Two major tools to study 5-HT neurochemistry in the brain are fast scan cyclic voltammetry[13,77,120] and microdialysis/HPLC. These techniques are complementary. The former has sub-second time resolution while microdialysis-HPLC can perform multi-analyte detection over long timescales with the potential for unambiguous analyte identification.

Online measurements following microdialysis are continuous, e.g., using sensors,[121] or discrete, e.g., using a separation.[7,52,122,123] Here, we focus on the latter. Conventional microdialysis-HPLC is carried out with low temporal resolution. Temporal resolution can be improved by decreasing the scale of the separation method, e.g., capillary HPLC and capillary electrophoresis.[27,29,32,124] Kennedy and Bowser measured changes in neurotransmitter concentrations (e.g., dopamine, glutamate, aspartate) in response to a stimulus using online microdialysis-capillary electrophoresis with online fluorescent derivatization.[75] The temporal resolution was as high as 11 s for amino acids[124] and 90 s for dopamine.[32] While capillary electrophoresis is powerful, within the neuroscience community HPLC has become the preferred method for research on low concentration neurotransmitters like dopamine and 5-HT[125,126] because of its reliability and reproducibility. Using microdialysis-HPLC, Newton and Justice[27] studied dopamine dynamics with one-minute temporal resolution by using small, 1 μL samples in conjunction with a 0.5-mm-inner diameter (i.d.) microbore column. Richter et al.[127] studied 5-HT and other neurotransmitters with a temporal resolution of 1.5 minutes using 3 μL samples in

conjunction with a 2-mm-i.d. column. These researchers recognized the advantage of small diameter columns: they minimize sample dilution during the separation permitting reliable quantitation with small volume injections. However, they performed the chromatography offline. Using even smaller i.d. capillary columns offline Parrot et al.[26] with 1 μL samples and Jung et al.[28] with 0.5 μL samples achieved low detection limits for 5-HT, but the separations were performed offline and were approximately ten minutes long.

The Andrews lab[128] recently reported *in vivo*, online monitoring of 5-HT with a temporal resolution of three minutes. This is a significant advance. The work was done with commercially available equipment. They applied this fast microdialysis approach to awake animals for times long enough to perceive circadian changes.

When considering the design of an online separation-based analysis system, it is important to understand the relationships that define and indeed connect the system's figures of merit. Scheme 1 shows that the concentration of analyte 5-HT *in the detector* following a separation consists of two independent components: the animal/microdialysis part of the experiment defines the number of *moles* injected into the separation system and the separation system (here chromatography) dictates the *volume* of the solution in which the injected moles are found in the detector. We will call the latter volume the *peak volume*. The number of moles collected in each sample depends on the sample volume and the dialysate concentration, itself a function of the actual concentration in the brain and the microdialysis recovery. The peak volume is defined by the retention time and a number of other parameters related to column efficiency, (which may include extracolumn effects and overloading) as well as the inside diameter of the column. Ultimately, the moles acquired divided by the peak volume must exceed the concentration detection limit of the detector used. The integral relationship between sampling

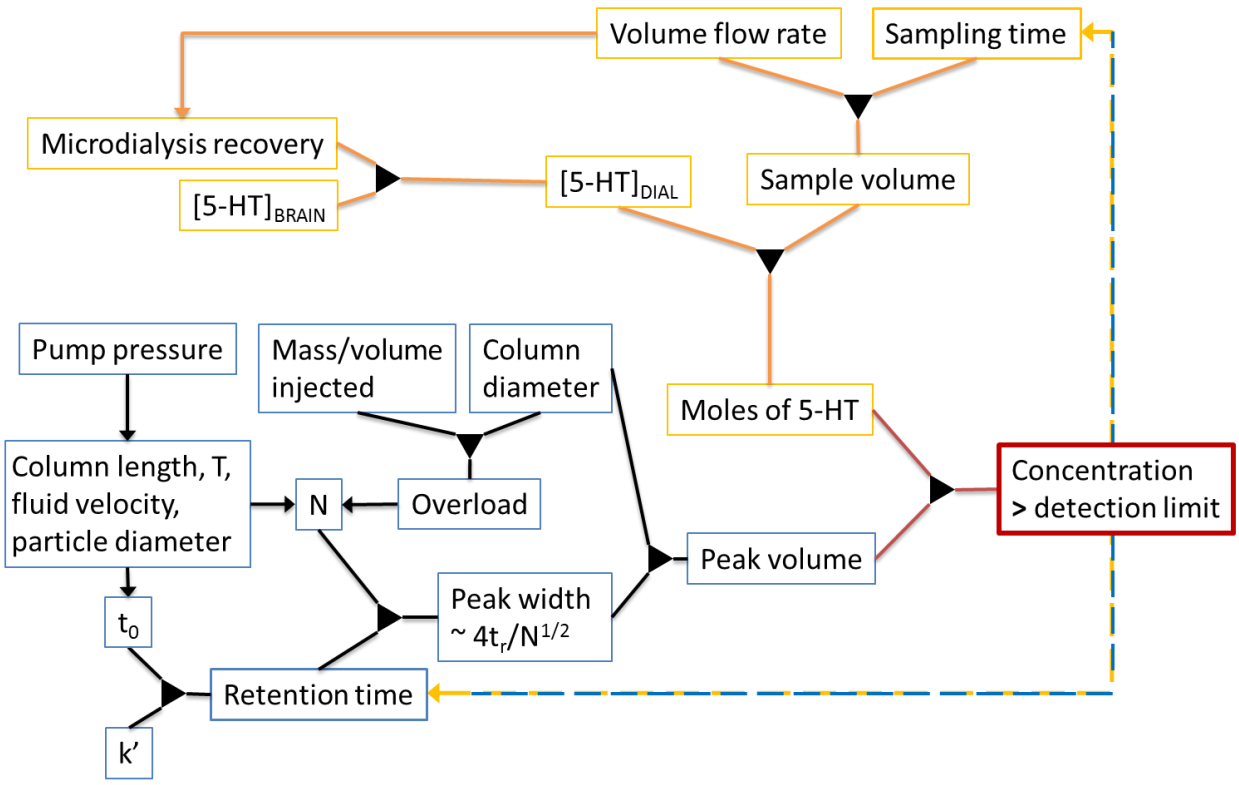

Scheme 1. Factors that determine the concentration of analyte 5-HT in the detector following a separation

Yellow outlined boxes correspond to microdialysis; blue boxes correspond to the chromatography. Arrows imply "controls" or "affects". Black triangles with two "inputs" and one "output" imply "define". The 5-HT concentration in the brain with the microdialysis recovery gives rise to a dialysate. Microdialysis recovery depends on dialysate flow rate. The flow rate of the dialysate and desired sampling time together define the sample volume. The sample volume and dialysate concentration give the moles of 5-HT in one sample. Column parameters at a particular temperature, *T*, limited by available pump pressure, control the number of theoretical plates, *N*, and the void time, t_0. The value of N will be decreased by injecting too much mass or volume. The reduction in efficiency that results from either type of overload depends on the column volume. The void time and the retention factor, *k'*, give the retention time of the analyte. The chromatographic system yields a peak with a particular volume (peak volume) dependent on a peak width related to bandspreading and column inside diameter. The peak volume and the moles of 5-HT from the dialysis give a concentration in the detector that must be greater than the detection limit of the detector. Note that in the optimal case, the sampling time and retention time are similar as well (blue yellow dashed line).

and measurement is even deeper. The microdialysis sample volume and flow rate define the sampling time and thus the temporal resolution. Ideally, the speed of the chromatographic system and the sampling time will "match" so that one chromatogram is achievable in the same time required to collect the sample. The constraints on an optimized system are therefore that *under conditions where the sampling time is approximately equal to the separation time, the ratio of moles collected during the sampling time to the peak volume in the separation system must exceed the detector's detection limit by some factor*. While the foregoing is accurate, it should be borne in mind that the system's time resolution may be limited by the dispersion within the microdialysis flow path (to be discussed below).

Recently, Liu et al.[100] and Zhang et al.[126] improved the HPLC analysis speed of 5-HT to the sub-minute level using elevated column pressure and temperature, a capillary column packed with sub-2-μm particles, and a sensitive, low dead-volume electrochemical detector. Using the smallest commercially available packing material at the time, Zhang et al. optimized a chromatographic system as described in Scheme 1 for maximum sensitivity given a required separation power (theoretical plate count), desired separation speed, and sample size. The column diameter is a key parameter and has an optimum value. This is the first time that both the microdialysis sampling time and the analysis time for 5-HT are one minute or less laying the groundwork for *in vivo* online microdialysis coupled to capillary UHPLC with electrochemical detection (UHPLC-EC) (here we use the rather ill-defined term UHPLC to represent our use of elevated temperature and pressure conditions). In this work, we carried out *in vivo* online microdialysis coupled to capillary UHPLC to monitor basal 5-HT concentrations and the subsequent changes in response to a stimulus with one-minute temporal resolution in the striatum of freely-moving rats. Optimization of both sampling and analysis were carried out, with

emphasis on temporal resolution, long time continuous analysis sensitivity, and robustness. We observed basal concentrations and dynamic changes of 5-HT for up to sixteen hours and forty minutes.

4.2 EXPERIMENTAL SECTION

4.2.1 Chemicals and materials

Chemicals and sources were: disodium EDTA, Fisher Scientific (Fair Lawn, NJ); ethanol, Pharmco-AAPER (Shelbyville, KY); sodium acetate and glacial acetic acid, J. T. Baker (Phillipsburg, NJ); acetonitrile, 2-propanol, l-ascorbic acid, serotonin hydrochloride, fluoxetine hydrochloride, and sodium 1-octanesulfonate (SOS), Sigma (St. Louis, MO). All the chemicals were used as received without further purification. Ultra-pure water was obtained from a Millipore Milli-Q Synthesis A10 system (Bedford, MA). Fused silica capillaries were from Polymicro Technologies (Pheonix, AZ).

4.2.2 Chromatography

Capillary columns were packed according to a previously reported procedure.[126] Briefly, columns were slurry packed with 1.7 μm BEH C 18 reversed-phase particles (Waters, Milford, MA) using 150 μm i.d., 360 μm outer diameter (o.d.) capillaries as the column blank. The packed capillary columns were connected directly to the injector and flushed with mobile phase overnight before use.

A UHPLC pump (Model nanoLC-Ultra 1D, Eksigent, Dublin, CA), with a maximum pressure limit of 700 bar, was used. The outlet of the pump was connected to an eight-port nanobore injector equipped with two 500 nL sample loops (Valco Instruments, Houston, TX). Isocratic separations of 5-HT were achieved using ion-pair, reversed phase liquid chromatography. The mobile phase was aqueous buffer:acetonitrile in a 96:4 (v/v). The aqueous buffer contained 100 mM sodium acetate, 0.15 mM disodium EDTA and 10.0 mM SOS and glacial acetic acid sufficient to create pH = 4.00. Mobile phase was filtered before use (0.22 μm Nylon filter, Osmonics, Minnetonka, MN). The mobile phase flow rate for the *in vivo* experiments was 10 μL/min and the operating temperature of the injector and the capillary column was maintained at 50 ℃ using two homemade heating assemblies[126] unless stated otherwise. Analytes were detected at 700 mV vs Ag/AgCl reference electrode by a BASi radial-style electrochemical detection flow cell (West Lafayette, IN) with a 13 μm Teflon gasket. The cell was connected to the column with a 10-cm-long, 25-μm-i.d. capillary. Potential control and data acquisition were done by a BASi Epsilon potentiostat (West Lafayette, IN). Instrument control and data collection was achieved using a PeakSimple Chromatographic Data System (SRI Instruments, Torrance, CA).

4.2.3 Microdialysis probe fabrication

Microdialysis probes[129] were prepared with Spectra-Por RC hollow fiber dialysis membrane (4 mm long; 200-μm i.d., 216-μm o.d.; molecular weight cut-off (MWCO) 13 kD; Spectrum Laboratories Inc., Rancho Dominguez, CA) and fused-silica inlet/outlet tubing (70 cm long; 75 μm i.d., 150 μm o.d.), which were sealed in a 3.5-cm-long stainless steel hypodermic tubing body (B000FMWJWK, Small Parts, Logansport, IN) with 2 Ton epoxy (ITW Devcon, Danvers,

MA). The hollow fiber membrane is shipped filled with a water-insoluble ester (isopropyl myristate) to prevent membrane deformation. Probes were activated by flushing with 1.0 mL ethanol to remove the long chain ester before use. The alcohol was removed by rinsing with artificial cerebrospinal fluid (aCSF) (containing NaCl 144 mM, KCl 2.7 mM, $CaCl_2$ 1.2 mM, $MgCl_2$ 1 mM, NaH_2PO_4 2 mM at pH 7.4).

4.2.4 *In vitro* online microdialysis coupled to a capillary UHPLC-EC system

A microdialysis probe was placed in a 100 mL beaker filled with aCSF solution (Figure S1). A concentration step was generated through the addition of a concentrated 5-HT solution to the stirred contents of the beaker. The 5-HT concentration was monitored with a 30 seconds analysis time interval. The chromatographic conditions were slightly different from the *in vivo* experiments in order to achieve the 30 s time resolution. Mobile phase flow rate was 12 µL/min with column and injector temperatures at 70 ℃.

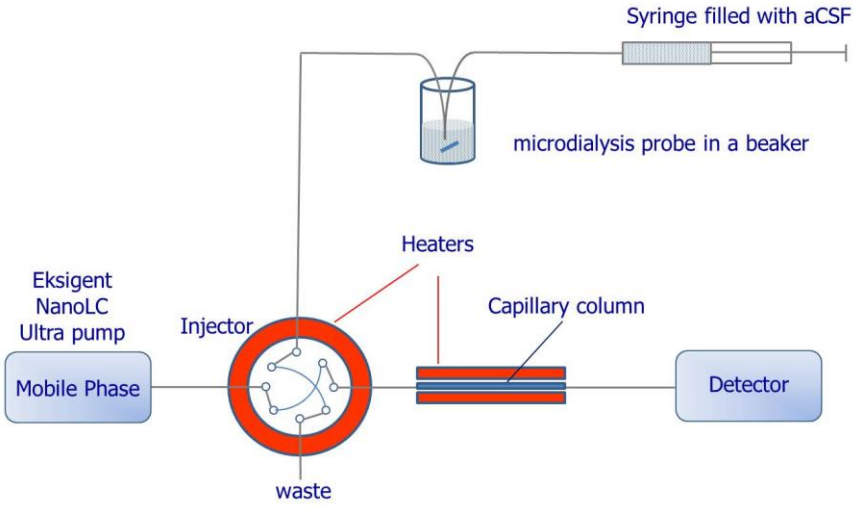

Figure 17. *In vitro* online microdialysis-UHPLC-EC experimental set up

4.2.5 *In vitro* assessment of solute dispersion during sample transfer

The microdialysis probe was replaced by a loop injector fitted with a 6 µL injection loop. The concentration profile resulting from injecting the loop contents into the outlet capillary was monitored with one-minute time resolution. It is important to control the time of the injection with respect to the continuous, one-minute cycle time of the monitoring. In this experiment, we altered the time between the injection and the UHPLC injection cycle to 5 s, 25 s and 45 s for three separate concentration steps.

4.2.6 Surgical procedure

All procedures involving animals were carried out with the approval of the Institutional Animal Care and Use Committee of the University of Pittsburgh. Male Sprague-Dawley rats (250-375 g, Hilltop, Scottsdale, PA) were anesthetized with isoflurane (0.5% by volume, Baxter Healthcare, Deerfield, IL). A homoeothermic blanket (EKEG Electronics; Vancouver, BC, Canada) kept the body temperature at 37 ^{o}C. A stereotaxic frame (David Kopf Instruments; Tujunga, CA) was used for all surgeries. (over the striatum. A guide cannula MD-2251, Bioanalytical Systems Inc.; West Lafayette, IN) was implanted into the striatum (1.2 mm anterior of bregma, 2.5 mm lateral of bregma), and lowered to 1 mm beneath the surface of the brain. Jeweler's screws with dental cement were used to hold the cannula in place. Rats recovered for a minimum of three days. Then a second procedure was performed to implant the microdialysis probe. Rats were anesthetized with isoflurane and microdialysis probes were slowly lowered vertically over thirty minutes into the striatum (7.0 mm below dura) and secured to the guide cannula with epoxy

cement. Once the probe was implanted, anesthesia was removed and the rats were placed in a Raturn chamber (Bioanalytical Systems, West Lafayette, IN) for the duration of the experiment.

4.2.7 *In vivo* online microdialysis coupled with capillary UHPLC-EC system

Figure 18 shows a diagram for the *in vivo* online microdialysis-UHPLC-EC system. A PicoPlus syringe pump (Harvard Apparatus, Holliston, MA) with a 1.0 mL gas-tight syringe delivered the microdialysis perfusion fluid, aCSF. A two-position "stimulus" loop injector was placed between the syringe and dialysis probe for the introduction of another solution. To minimize Taylor-Aris dispersion and other sources of dispersion, 75 μm i.d. capillary tubing (10 cm) connected the stimulus valve to the microdialysis inlet capillary, the inlet capillary (70 cm) to the dialysis tubing, the outlet capillary (70 cm) to a connector capillary (10 cm) connected to the HPLC injection valve. All connections were made with MicroTight Unions (IDEX Health & Science, Oak Harbor, WA).

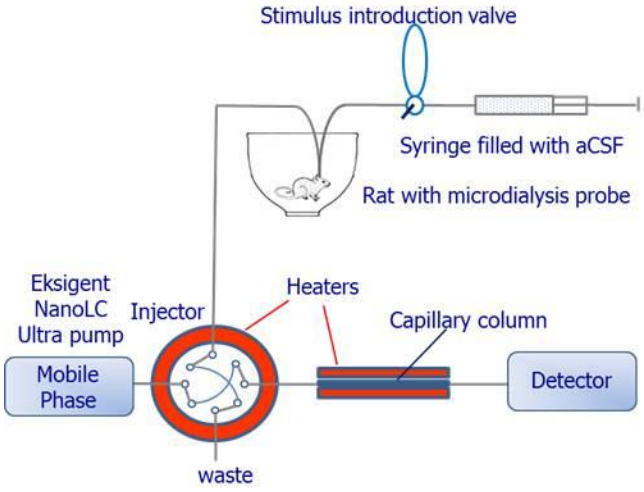

Figure 18. *In vivo* online microdialysis-UHPLC-EC experimental set up

Probe implantation was done early in the morning and online experiments were initiated in the afternoon of the same day. Probes were perfused with aCSF at 0.6 μL/min for at least 2 hours after implantation prior to connection to the online chromatographic system. Standards (100 nM 5-HT) were analyzed before and after the online experiments for calibration. The sampling volume was 600 nL which was selected to slightly overfill the 500 nL sample loop volume to increase injection volume precision.[130] Stable basal 5-HT concentrations were observed for at least twenty minutes prior to carrying out an experiment such as K^+ stimulation. Potassium stimulations of three or ten minutes were conducted with either 70 mM K^+ or 120 mM K^+. The selective serotonin reuptake inhibitor fluoxetine was introduced by perfusion with 10 μM fluoxetine dissolved in aCSF.

Peak area was used for concentration calibration. To integrate the areas under the 5-HT peaks, a standard Savitzky-Golay, second derivative, quadratic smooth was employed, using an 81 point window.[131,132] Prior to determining the integration limits, an approximate window defined to contain the eluted peak was identified. The start integration point and the stop integration point were manually determined. A linear baseline between the start and stop points was created and the integration routine was programmed in the MATLAB environment (Mathworks, Natick, MA).

4.3 RESULTS AND DISCUSSION

4.3.1 Valve selection and stimulus introduction

For continuous sampling/analysis, two-position, electronically actuated valves with dual sample loops are employed. Each of the valve positions dictates which loop is in the "load" position while the other is in the "inject" position. Our initial online experiments had a ten-port injection valve. However, the ten-port valve was found to be less desirable than an eight-port injection valve. The ten-port valve has an extra length of tubing, a so-called jumper loop (Figure 19). During the injection process, the jumper loop's contents, mobile phase, follow the contents of the sample loop in the "A" position. However, the jumper loop's contents precede, and thus mix with the leading edge of, injections from the "B" position. We speculate that the additional extra-column bandspreading seen when injecting from the "B" position resulted from poor on-column focusing resulting from the higher eluting strength of the mixed sample/mobile phase as it enters the column while the leading edge of the samples injected from the "A" position were not mixed with mobile phase prior to entering the column. While peak areas are not significantly different, peak heights for 5-HT standards injected from the "A" and "B" positions were different (paired Student's *t*, $p < 0.05$). The eight-port injection valve has an asymmetrical flow path but no jumper loop (Figure 18). Using the eight-port valve, peak heights for 5-HT standards injected from the A and B loops were not found to be statistically different (paired Student's *t*, $p > 0.05$).

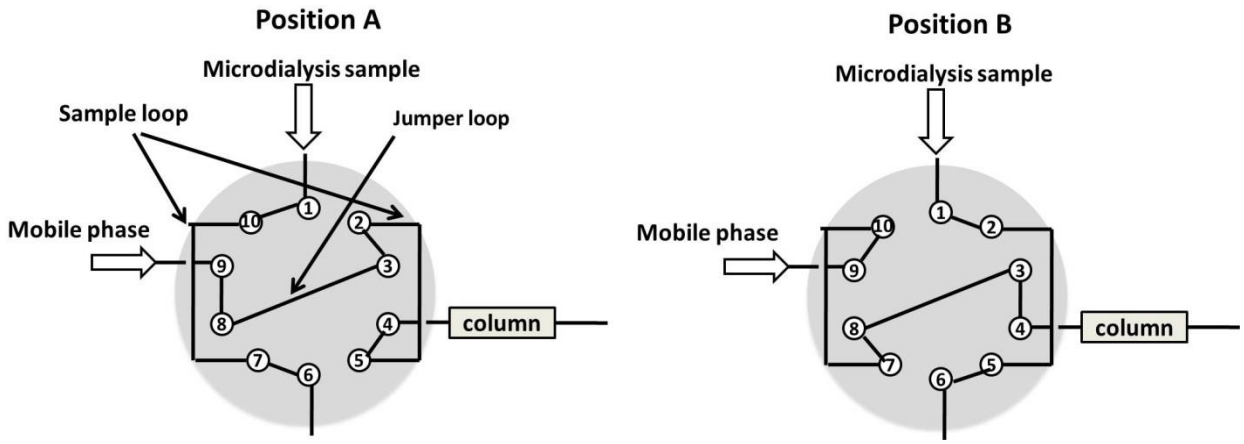

Figure 19. Flow path design for continuous analysis using a ten-port valve

Initially, we set up the perfusion system with a pair of syringes in a syringe pump connected to a four-port switching valve to switch between syringes. However, we noted that three- and five-minute K^+ stimulations in awake animals both gave increased 5-HT over a nine-minute period. We speculate that two factors contribute to this. One is the large, 12.4 µL swept volume of the four-position switching valve. The other is the change in back pressure felt by the syringe that is switched into the flow stream. We replaced the two-syringe-pump arrangement with a single syringe followed by a low dead-volume (90 nL), six-port loop injection valve (Figure 18) with a loop made from tubing with a larger i.d. (150 µm) than the inlet and outlet tubing (75 µm i.d.). The loop is also shorter than the transport tubing. Recall that for constant flow rate, the change in pressure is proportional to the *fourth power* of the change in radius. Thus a factor of two change in radius corresponds to a factor of sixteen in pressure. In combination with the shorter length, we estimate that the backpressure with the loop inline is only 2% larger than with the loop out of the flow path. Therefore, the microdialysis flow rate remains stable and the introduction of a chemical stimulus is reproducible.

4.3.2 In-house microdialysis probe characterization and system temporal resolution

Initially, we used commercial microdialysis probes, but observed column pressure increases, and significant solute dispersion due to the relatively large outlet tubing (120 μm i.d.) in *in vivo* experiments. Dispersion during transport of the samples from the dialysis probe to the analysis system needs to be carefully controlled because it can be the limiting factor[121,123,133] in the overall temporal resolution of online measurements as sampling and analysis speeds are improved. In general, use of smaller microdialysis probe internal volume, shorter, narrower i.d. outlet tubing with fewer connections and zero dead-volume connectors will help to minimize the concentration dispersion during transport of samples from the brain to the instrument. On the other hand, the microdialysis probe is prone to clogging for outlet tubing with internal diameters less than 25 μm. Also, the pressure stemming from narrow outlet tubing can have an impact on both the relative and absolute recoveries of the probe.[134] Therefore, the outlet tubing i.d. and internal volume of the microdialysis probe itself should be carefully chosen. Figure 20 demonstrates a rapid response to concentration changes using the in-house microdialysis probe with a 75 μm i.d., 70 cm long outlet tubing. Data were acquired at 30 seconds intervals using a 200 nL sample loop at a microdialysis flow rate of 0.6 μL/min. Seven minutes after the change in 5-HT concentration in the beaker the change was detected in the UHPLC system. Solute dispersion resulted chiefly from two factors, namely inside the hollow fiber probe itself and within the outlet tubing. Assuming that the concentration changes as an instantaneous step function from 0 to C_0 in the beaker, the normalized concentration C/C_0 vs. time function when the step arrives at the UHPLC injector will be an error function,[135] Eq. 33, as expected for Taylor-Aris dispersion.[136] C is the concentration at time t, t_c is the time at the inflection point

of the error function, and σ is the concentration dispersion standard deviation in units of time. Because each injection has the number of moles of 5-HT in a particular 200 nL segment of the flow stream, each UHPLC peak's magnitude is proportional to the area under a particular segment of the concentration-time function. The area (A) from the integration of the normalized concentration C/C_0 profile for a certain time window (t_1 to t_2) in Eq. 34 represents the measured concentration for a single peak in the chromatogram. Using the solver function in Excel, the concentration dispersion standard deviation σ was found to be 11.6 s by fitting Eq. 34 to the measured concentration distribution. This means that it took about 46.4s (-2σ to 2σ) for a concentration change to reach steady state (~ 2% to ~ 98% of maximum), well within the one minute temporal resolution of the system.

$$\frac{C(t,t_c,\sigma)}{C_0} = \frac{1+erf(\frac{t-t_c}{\sqrt{2}\sigma})}{2} \tag{33}$$

$$A(t_1,t_2,t_c,\sigma) = \frac{t_2-t_1}{2} + \frac{(t_2-t_c)}{2}erf(\frac{t_2-t_c}{\sqrt{2}\sigma}) - \frac{(t_1-t_c)}{2}erf(\frac{t_1-t_c}{\sqrt{2}\sigma}) + \frac{\sigma}{\sqrt{2\pi}}(e^{\frac{-(t_2-t_c)^2}{2\sigma^2}} - e^{\frac{-(t_1-t_c)^2}{2\sigma^2}}) \tag{34}$$

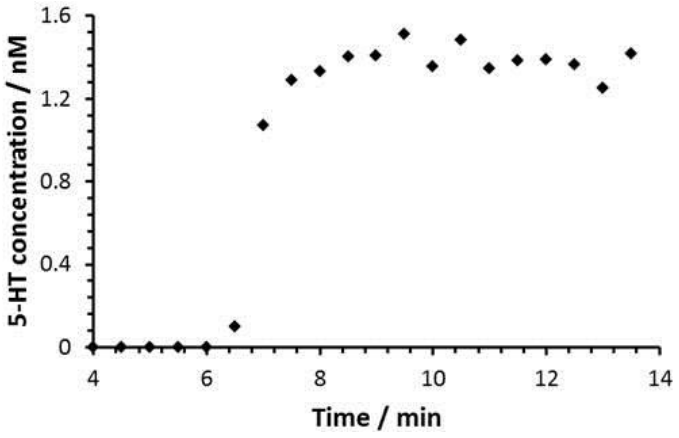

Figure 20. Solute dispersion of a concentration step by using an in-house microdialysis probe

Concentration changes were measured at 30 s intervals

We also studied the solute dispersion in the outlet tubing and connections alone by creating a concentration step using a six-port loop injector injecting directly into the 75 μm i.d., 70 cm long outlet capillary. Here we also explored attaining greater time resolution by observing multiple transients with different phase shift compared to a one-minute separation cycle time (Figure 21). Three consecutive concentration steps were created with 5 s, 25 s, and 45 s between 5-HT injections and the UHPLC injection cycle (Figure 22). The concentration values in the transient region were dependent on the phase difference between the injection time and the UHPLC injection cycle. Combination of the three concentration step profiles gave a concentration step with 20 s resolution (Figure 23). This demonstrates how to increase the time resolution when the experiment involves the introduction of a change in concentration at a known time. These data (Figure 23) tell us about dispersion in the outlet tube alone. Using the solver function in Excel, the concentration dispersion standard deviation was found to be 7.6 s by fitting Eq. 34 to the measured concentration distribution. This was in reasonable agreement with a calculated value of the standard deviation from Taylor dispersion, 6.2 s, based on a diffusion coefficient[112] for 5-HT of 5.4 x 10^{-10} m^2s^{-1} in aqueous samples. If we make the assumption that the observed total solute dispersion has independent contributions from the hollow fiber probe and the capillary tubing, then the variances from each contribution will add to yield the total observed variance of 134.6 s^2 (*i.e.*, (11.6 s)^2) We can thus deduce that the hollow fiber probe's concentration dispersion standard deviation is 8.7 s. Note that these dispersion experiments used concentrations of 5-HT in the physiological range (~1.5 nM), important to get a realistic measurement. The response time can be concentration dependent when the solute adsorbs to sampling system components. Use of a high concentration will lead to lower dispersion, and an overly optimistic picture.

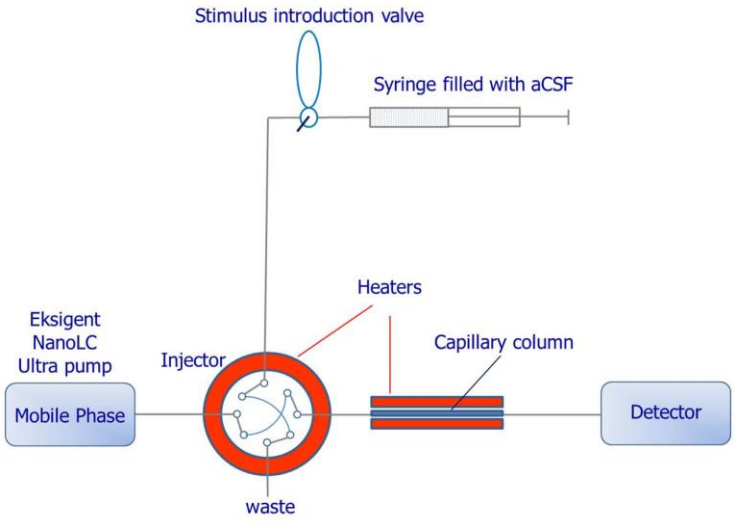

Figure 21. Experimental set up for monitoring of concentration steps created by the stimulus introduction vavle

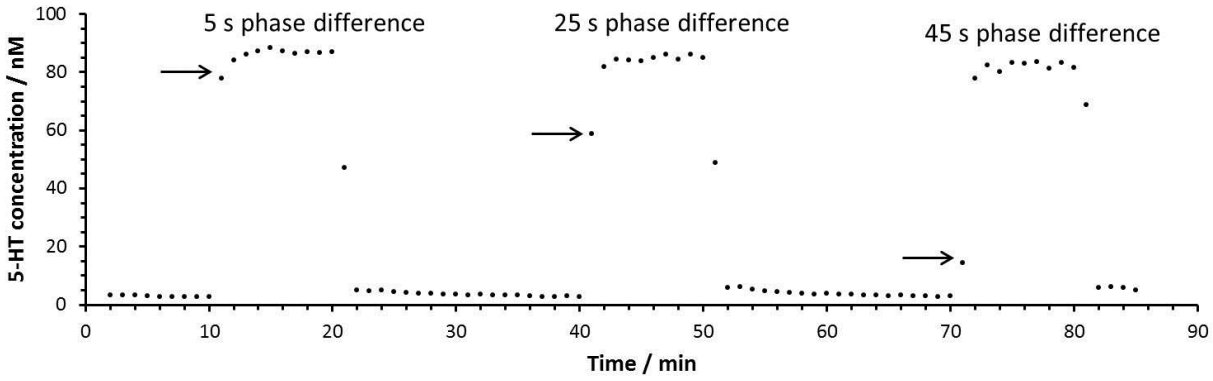

Figure 22. 5-HT concentration profile for monitoring of concentration steps created by the six-point injector valve The time intervals between the 5-HT standard injection and UHPLC injection cycle are 5 s, 25 s and 45 s. Arrows indicate the 5-HT peak in the transient region

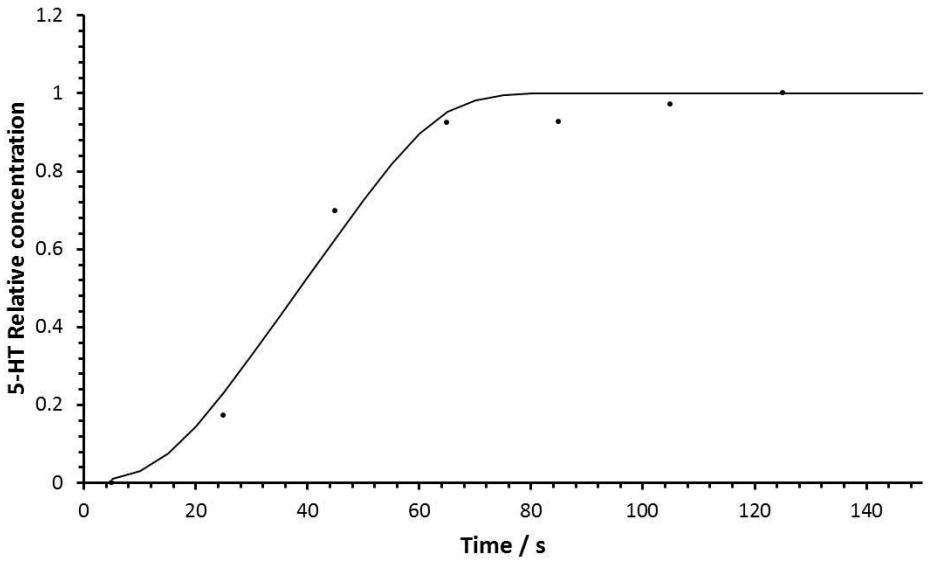

Figure 23. Combined concentration profile with 20 s resolution resulted from the three concentration steps in Figure 22

Switching to the in-house probe also solved the column clogging problem[137] present with the commercial probes (30 kDa MWCO, 4 mm long poly(acrylonitrile). The problem of the sample clogging the column is more severe when using capillary columns because the sample is not significantly diluted upon injection. The *in vitro* recovery of 5-HT with these microdialysis probes was about 35% at a perfusion flow rate of 0.6 μL/min. In total, fourteen in-house probes were used for *in vivo* online experiments. Twelve out of the fourteen showed no column clogging.

4.3.3 Online measurement of basal serotonin concentration in striatum

Microdialysate contains electroactive components at concentrations greater than 5-HT. Many of them are anionic, eluting prior to 5-HT, e.g., 5-hydroxyindole-3-acetic acid (5-HIAA), 3,4-dihydroxyphenylacetic aicd (DOPAC), and homovanillic acid (HVA) which are usually in the

200 nM to 5 μM range. However, one particular anionic compound, ascorbate, was the most bothersome during the initial chromatographic optimization experiments. For clarity, this discussion will refer to "ascorbate" and an "ascorbate peak" recognizing that in fact all of the anionic, electroactive components of the sample contribute to the low-retention-time signal. As seen in Figure 24 (dotted line), ascorbate is poorly retained. The concentration of ascorbate in the microdialysate is roughly 50 μM. The peak appears wide especially when observed with detection sensitivity sufficient to see 5-HT at about 10^5 lower concentration. The ascorbate peak tails with the result that the "baseline" for 5-HT is actually part of the tail of the ascorbate peak. This tail leads to signal drift in the region of 5-HT elution. This problem was not seen for offline analysis with commercial probes in our previous study[100,126] (Figure 24 solid line) where ascorbate was apparently at a much lower concentration due to the reduction in observed peak tailing. We also found that the ascorbate concentration was in between these two extremes for online analysis with commercial probes (Figure 24 dashed line). We think this ascorbate tailing is particularly associated with using capillary columns in which mass capacity is low compared to conventional columns. Ascorbate is oxidized by O_2 during sample transfer in the outlet tubing, and in offline collection and storage of the microdialysis sample. The oxidation rate depends on oxygen partial pressure, temperature,[138] pH[139] and oxygen permeability of the tubing wall materials.[140] Offline microdialysis samples are usually acidified[141] in the collection vial and stored frozen before analysis which decreases but cannot completely stop ascorbate oxidation/degradation. The Teflon tubing used by most commercial microdialysis probes is O_2 permeable, and the large surface area to volume ratio of the outlet tubing creates an ideal environment for ascorbate oxidation. In our current online experiment, the transfer from microdialysis to capillary UHPLC takes only about seven minutes and the outlet tubing is fused

silica which is not O_2 permeable. As seen in Figure 25, the baseline is sloping and the 5-HT peak is not quantifiable with a column temperature of 60 ℃. To solve this problem, 5-HT retention was increased by lowering the column temperature to 50 ℃ so it will elute at a later time (0.9 minutes) where the contribution of ascorbate is not as significant.

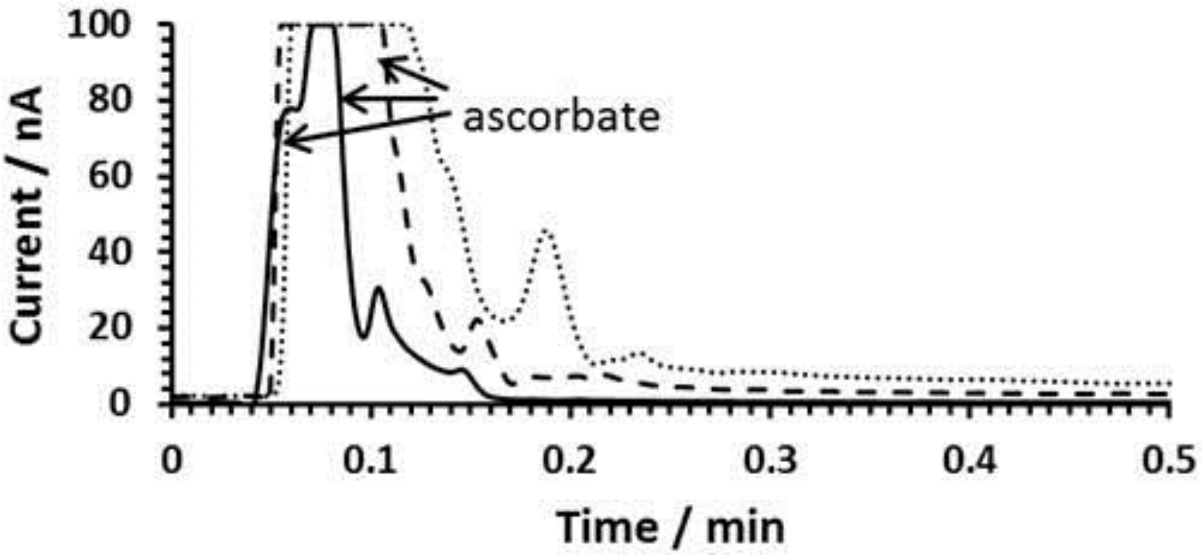

Figure 24. Ascorbate levels in microdialysis samples

The large peaks starting from about 0.05 minutes include ascorbic acid, the most abundant oxidizable molecule in the chromatogram. Dotted line: online UHPLC analysis of microdialysis samples using an in-house microdialysis probe. Dashed line: online UHPLC analysis of microdialysis samples using a commercial microdialysis probe. Solid line: offline UHPLC analysis of microdialysis samples using a commercial microdialysis probe.

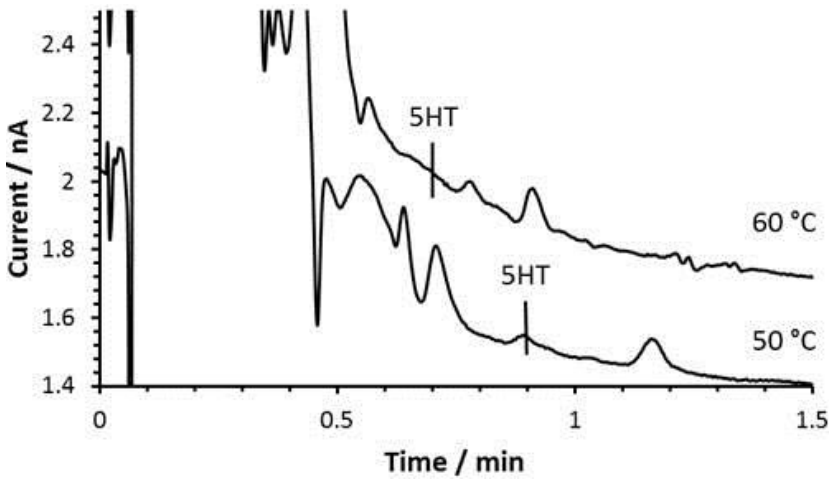

Figure 25. Chromatograms of microdialysis samples analyzed at 50 ℃ and 60 ℃

4.3.4 System stability

Column performance deterioration and detection sensitivity loss with time is a concern for *in vivo* experiments. We did four injections of a 100 nM standard before and after 5.5 hours of continuous *in vivo* experiments. Table 9 shows that the 5-HT retention time, peak width, and column plate number were reproducible. There was no significant change in the peak area when comparing standard injections before and after the *in vivo* experiments (Student's *t* test, $p > 0.05$, Table 10).

Table 9. Column performance evaluation before and after *in vivo* measurements

	Retention (time/s)	Fwh (m/s)	Plate number
Before	52.0 ± 0.3	2.2	3089 ± 37
After	51.8 ± 0.1	2.2	3071 ± 15

Table 10. Comparison of peak area before and after the *in vivo* experiments

	Mean	SD	N	t	$t_{0.95}$ (df = 6)
A_{before}	1.26×10^5	1×10^3	4	0.915	1.943
A_{after}	1.26×10^5	9×10^2	4		

4.3.5 *In vivo* monitoring and serotonin dynamics in response to a stimulus

Concentrations were determined using external calibration without correction for the probe recovery. A linear calibration curve was created using peak area vs 5-HT standard concentration from 0 to 100 nM ($r^2 = 0.998$). The detection limit for 5-HT was 0.16 nM (signal three times greater than rms noise). Figure 26 is part of a series of chromatograms showing 5-HT concentration changes caused by a three-minute 120 mM K^+ stimulation. The basal 5-HT concentration measured for this rat was 0.64 ± 0.04 nM (standard error based on eight samples). Introduction of 120 mM K^+ induces 5-HT release into the extracellular space resulting in the microdialysate concentration increasing to 29.2 nM.

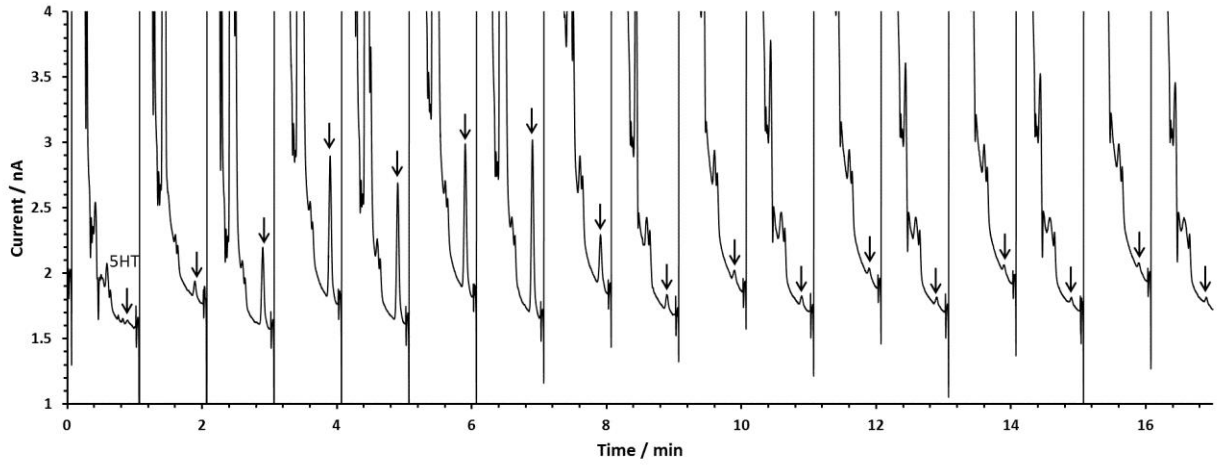

Figure 26. Typical chromatogram of continuous 5-HT measurements

Arrows indicate the 5-HT peak. The rat was under three-minute high K^+ stimulation which resulted in 5-HT release.

Figure 27 shows a typical run of nearly six hours. Each data point represents a single chromatogram. The figure shows several 5-HT transients caused by K^+ stimulation. Typically, the increase in the 5-HT concentration was about four times higher for three-minute 120 mM K^+ stimuli than for a three-minute 70 mM K^+ stimulus. We will return to the ten-minute 120 mM K^+ below. To confirm that we are measuring 5-HT, we infused an SSRI, fluoxetine and observed increased 5-HT concentration[79] (Figure 28). Infusion of fluoxetine also increased transient 5-HT concentration from high potassium stimulation (Figure 29), and decreased extraction efficiency of infused 5-HT (Figure 30).

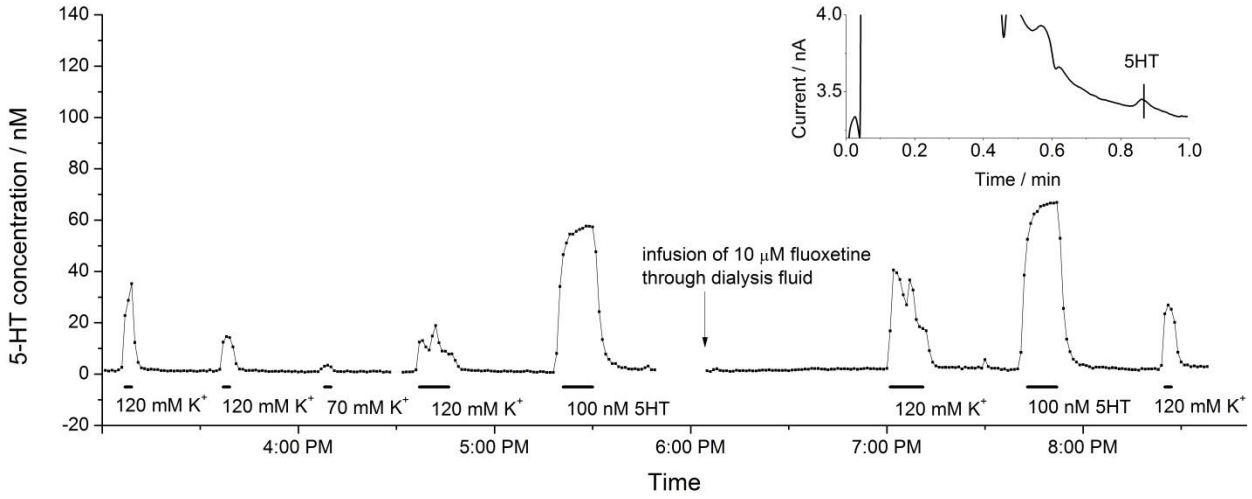

Figure 27. Typical online *in vivo* 5-HT measurement of one rat

Three-minute 70 mM K^+, three-minute and ten-minute 120 mM K^+ stimulations were carried out. Perfusion of aCSF containing 10 μM fluoxetine started at 06:05 PM. 6 μL 100 nM 5-HT standard was introduced to the perfusate by the six-port injector valve at 07:43 PM. A typical chromatogram for basal 5-HT is shown in the up right corner.

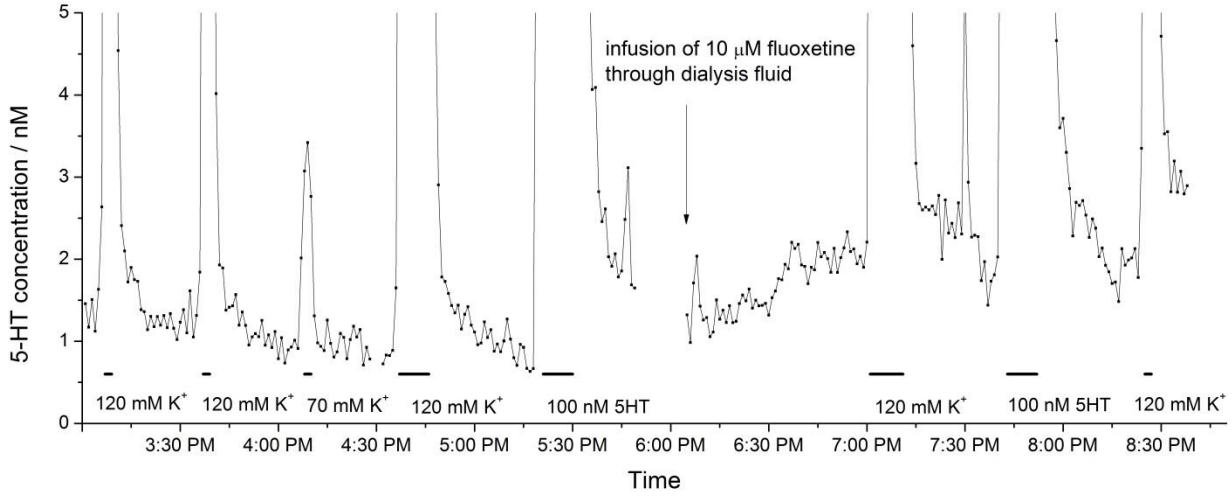

Figure 28. 5-HT increase in dialysate after infusion of 10 μM fluoxetine

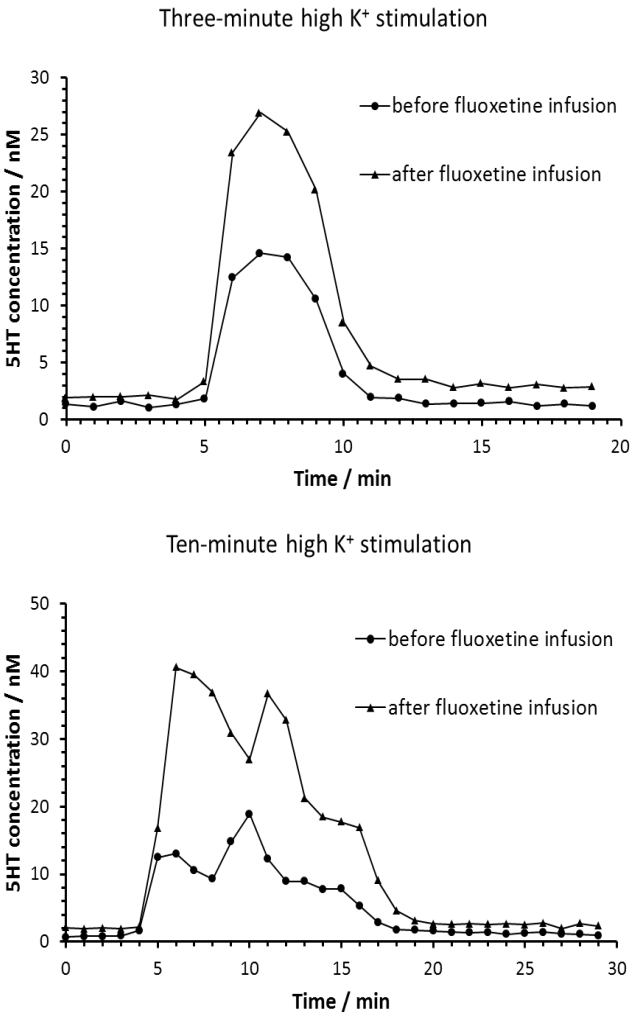

Figure 29. The effect of fluoxetine on 5-HT release resulted from K^+ stimulation

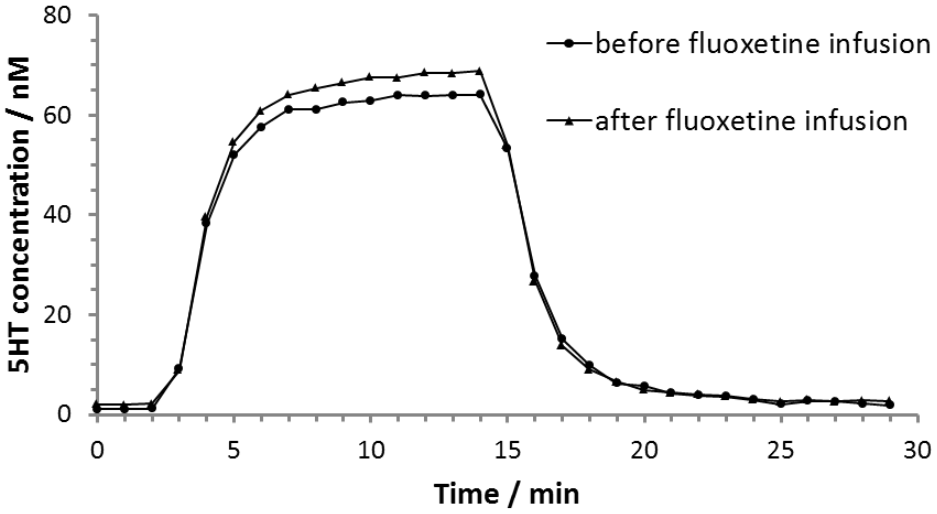

Figure 30. Concentration at the outlet of the probe from infused 5-HT

Figure 31 shows a portion of a set of data (full 16.7 h trace is Figure 32). We noticed that the 120 mM K^+, ten minute stimulation led to transient changes in the 5-HT concentration during 5-HT release. These, to our knowledge, have not been observed before. We controlled the time between stimulation and the UHPLC injection cycle to 5 seconds for all K^+ stimulations. Because of this, samples were acquired with a consistent time relationship to the onset of the stimulus. When we overlaid the four responses from the high potassium, ten minute stimulations seen in Figure 31, we found that the 5-HT oscillations were quite reproducible for repeated stimulations (Figure 33). The reproducibility coupled with the absence of similar fluctuations for three-minute infusions of K^+, and for ten-minute 5-HT infusions suggests that these observations represent real changes in extracellular 5-HT rather than an experimental artifact. We further extended the stimulation time to 20 minutes and confirmed the periodical reoccurrence of local 5-HT release maxima (Figure 34).

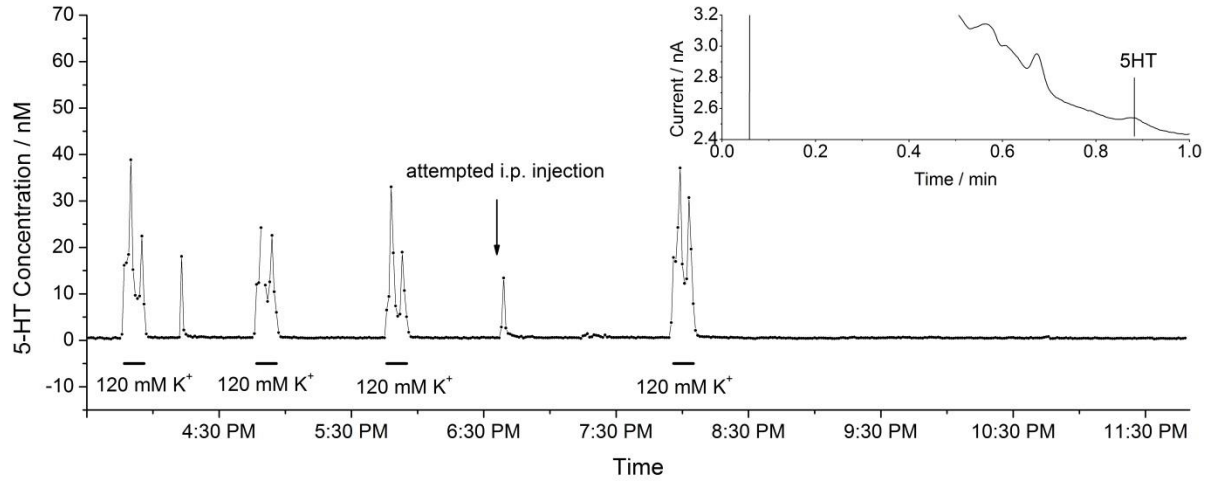

Figure 31. Online *in vivo* 5-HT measurements with attempted i.p. injection and repeated ten-minute 120 mM K^+ stimulation

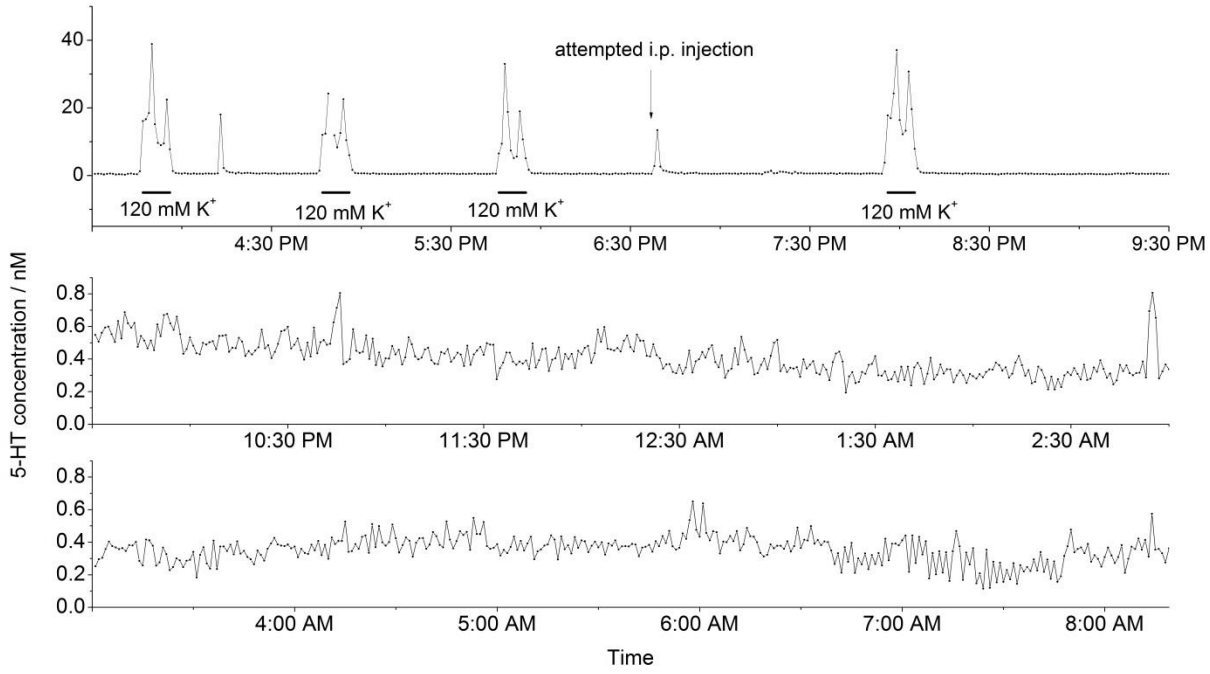

Figure 32. *In vivo* monitoring of 5-HT up to 16 hours and forty minutes

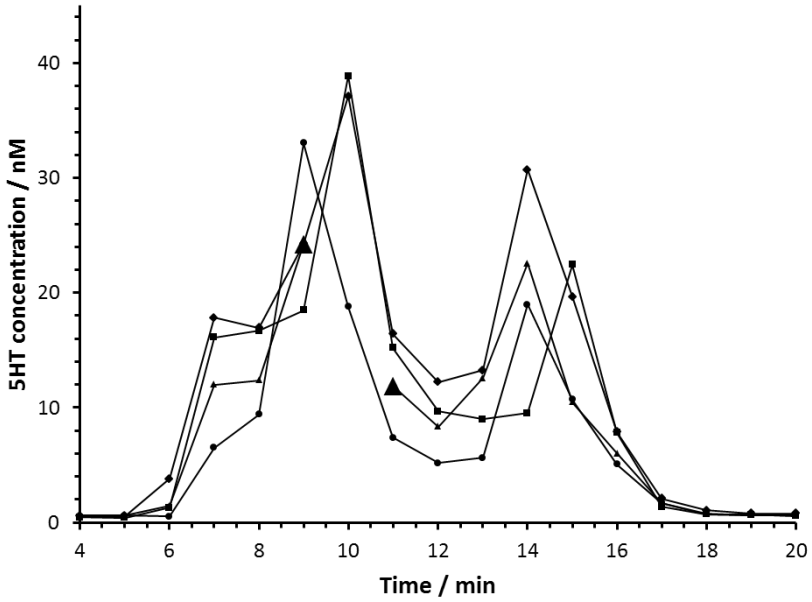

Figure 33. Comparison of the 5-HT release in response to four ten-minute 120 mM K^+ stimulations

One of the 5-HT release profile (triangle) missed a data point because the UHPLC system stopped to refill the reservoir so there was no analysis for that sample. The data before and after that missing data are emphasized by enlarged triangles. Curves are cubic splines

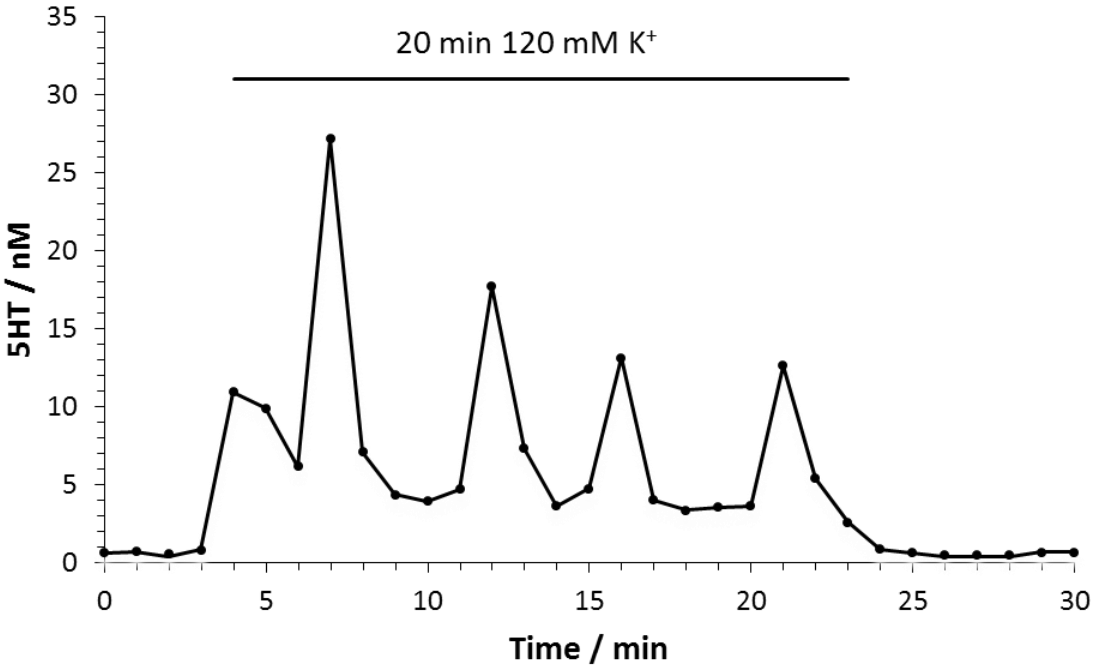

Figure 34. Monitoring of 5-HT concentration during 20 minute 120 mM K^+ stimulation

We made an interesting, if accidental, observation. None of the rats used in the experiments were accustomed to handling, thus it was not unusual to notice some unwillingness on the part of a particular animal during the handling required to make an intraperitoneal (i.p.) injection. We noticed considerable animal-to-animal variability in the signs of stress during handling. The 5-HT vs. time trace showed a transient elevation of 5-HT concentration correlated with the handling of one animal. Fortuitously, another animal undergoing the same handling appeared relaxed and exhibited no signs of stress, and there was no 5-HT elevation observed. A third animal exhibited less stress than the first animal, and this animal's 5-HT also spiked transiently as shown in Figure 32. We do not attempt to draw biological conclusions from these observations. The point is that the rapid response time of the system reveals such correlations. These observations are similar to those of Yang et al. who recently pointed out the value of six minute, on-line sampling by observing transients from i.p. injections of saline which could not be observed for longer sampling times.[128]

4.4 CONCLUSIONS

The potential for higher time resolution over long times in awake animals has been in existence for some time. We have realized this potential based on prior work on optimizing chromatographic conditions.[100,126] Of course, speeding up the chromatography is necessary but not sufficient to establish a useful method. All components of the system must be compatible with the higher time resolution and the smaller column volume. As discussed by Yang et al.,[128] the higher time resolution may make possible the investigation of some aspects of 5-HT dynamics and also changes in 5-HT during behavior.

5.0 *IN VIVO* MONITORING OF DOPAMINE IN THE STRIATUM OF FREELY-MOVING RATS WITH ONE MINUTE TEMPORAL RESOLUTION AND ITS APPLICATIONS

We developed an online microdialysis/LC system to carry out *in vivo* monitoring of dopamine in the extracellular space of the striatum of freely-moving rats. Dopamine basal levels and dynamic changes were measured with a one-minute time resolution. Spreading depression, caused by K^+, which occurs in the space of minutes, was the process of choice for the study of dopamine dynamics here using our system. Periodic dopamine fluctuations, with a time interval of 5 minutes, were observed following stimulation with 120 mM K^+. Stimulation using lower concentrations of K^+ was also carried out. The peak concentration of dopamine release was exponentially proportional to the K^+ concentration, which was in the range of 20 to 100 mM. Our online system proved useful in sharing key data during the monitoring of a biological event/brain injury phenomenon (spreading depression process).

5.1 INTRODUCTION

The dopaminergic system is widely investigated using a variety of methods, including electrophysiology,[142,143] voltammetry[12,144-146] and dialysis[147,148]. Electrophysiology records the electric activity of neurons, and is widely used to study dopamine neurotransmission and

associated behaviors in response to external stimuli. Voltammetry and dialysis gather information about the extracellular dopamine levels, thereby giving insight into mechanisms of dopamine release, reuptake, and the regulation of dopamine neurotransmission and associated behaviors.

Microdialysis sampling coupled with HPLC is commonly used in the study of the dopaminergic system; namely, the regulation of neurotransmission pathways, effects of drug intake and interactions between different neurotransmitter systems. However, typical temporal resolution of microdialysis sampling coupled with HPLC is 10-20 minutes. It is difficult to make any semi-quantitative/quantitative conclusions as the dynamic changes in extracellular dopamine concentrations are greatly diluted, and thus lost, in most of the microdialysis sample collected – microdialysate containing the basal dopamine levels. Newton and Justice[27] previously conducted one-minute sampling (1 μL microdialysate), using microdialysis followed with microbore column separation. They measured dopamine dynamics in response to cocaine administration by retrodialysis. However, the overall throughput was limited by the time-consuming separation process. In another study, where temporal resolution was improved (one minute), Young[149] successfully demonstrated changes in extracellular dopamine concentrations of different magnitudes in response to conditioned aversive stimuli.

Compared to offline analysis, online microdialysis/HPLC is less common, yet is preferable to the former in several aspects: it provides continuous, near real-time measurement and instant results (effectively guiding further experiments); it avoids the need of handing small volumes of microdialysate samples; and it avoids the issue of potential degradation and contamination. Cheng et al.[150] measured dopamine efflux induced by appetitive classical conditioning, using online microdialysis at a rate of 7.5 min/per sample. Online microdialysis for

dopamine was then shown to have better temporal resolution when coupled with capillary electrophoresis. Parrot et al.[151] investigated the interaction between excitatory amino acids and dopamine in anaesthetized rats using microdialysis/CE with a one-minute temporal resolution. Shou et al.[32] monitored dopamine levels with a one-minute temporal resolution in the striatum of free-moving rats and correlated dopamine changes with drug-induced behaviors. Although employment of CE for such studies was found to provide better temporal resolution, the HPLC system is significantly more reliable and reproducible, for which reasons it was used here. Our group developed an online microdialysis/capillary HPLC system for the purpose of studing the serotoninergic system.[100,126,152] By using elevated temperature and ultrahigh column pressure, we accelerated the separation speed and achieved one minute measurements of serotonin. Further optimization allowed online monitoring of serotonin in the striatum of freely-moving rats. Taking advantage of the one minute temporal resolution, dynamic details of serotonin levels under spreading depression were then revealed.

Here we applied this analytical system to the study of the dopaminergic system. Basal dopamine levels, as well changes in dopamine concentration during activity, are shown to be much higher than those of serotonin in the extracellular space of the striatum. Using dopamine as a monitoring molecule, we systemically studied brain processes and neuronal depolarization induced by K^+.

5.2 EXPERIMENTAL SECTION

5.2.1 Chemicals and materials

Chemicals and sources were: disodium EDTA, Fisher Scientific (Fair Lawn, NJ); ethanol, Pharmco-AAPER (Shelbyville, KY); sodium acetate and glacial acetic acid, J. T. Baker (Phillipsburg, NJ); acetonitrile, 2-propanol, l-ascorbic acid, dopamine hydrochloride, quinpirole dihydrochloride, and sodium 1-octanesulfonate (SOS), Sigma (St. Louis, MO). All chemicals were used without any further purification. Ultrapure water was obtained from a Millipore Milli-Q Synthesis A10 system (Bedford, MA). Fused silica capillaries were obtained from Polymicro Technologies (Phoenix, AZ).

5.2.2 Chromatography

The chromatographic system consisted of a UHPLC pump (Model nanoLC-Ultra 1D, Eksigent, Dublin, CA) with a maximum pressure limit of 700 bar, a Valco eight-port injection valve (Valco Instruments, Houston, TX), two heating assemblies for the capillary column and the injection valve. A lab-made capillary column packed with 1.7 μm BEH C 18 reversed-phase particles (Waters, Milford, MA). The column dimensions were as follows: 150 μm inner diameter (i.d.), 360 μm outer diameter (o.d.), and 3 cm length. The detection was carried out using a BASi electrochemical detection flow cell (West Lafayette, IN) composed of a radial-style thin-layer auxiliary electrode, a 13 μm Teflon gasket and a 3 mm diameter glassy carbon working electrode. Analytes were detected at 700 mV vs Ag/AgCl reference electrode. The flow cell was connected to the column with a 10-cm-long, 25-μm-i.d. capillary tubing. Potential and

instrument control, and data acquisition, were carried out using a BASi Epsilon potentiostat (West Lafayette, IN) and a PeakSimple Chromatographic Data System (SRI Instruments, Torrance, CA).

The chromatographic separations were performed at 35 ℃, with a mobile phase flow rate of 8 μL/min, unless stated otherwise. For each analysis, the sample volume was 500 nL, which was defined by the total volume of the capillary sample loop. The mobile phase was aqueous buffer:acetonitrile in a 96:4 (v/v). The aqueous buffer contained 100 mM sodium acetate, 0.15 mM disodium EDTA, 10.0 mM SOS and glacial acetic acid (buffered to pH 4.0). The mobile phase was filtered prior to use, using a 0.22 μm Nylon filter (Osmonics, Minnetonka, MN).

5.2.3 Microdialysis probe fabrication

Microdialysis probes[129] were prepared using a Spectra-Por RC hollow fiber dialysis membrane (4 mm long; 200-μm i.d., 216-μm o.d.; molecular weight cut-off (MWCO) of 13 kDa; Spectrum Laboratories Inc., Rancho Dominguez, CA) and fused-silica inlet/outlet tubing (70 cm long; 75 μm i.d., 150 μm o.d.) sealed in a 3.5-cm stainless steel hypodermic tubing body (B000FMWJWK, Small Parts, Logansport, IN) with 2 Ton epoxy (ITW Devcon, Danvers, MA). The hollow fiber membrane arrived filled with a water-insoluble ester, isopropyl myristate, to prevent membrane deformation. Probes were activated by flushing with 1.0 mL ethanol to remove the long chain ester, prior to experimentation. The alcohol was removed by rinsing probes with artificial cerebrospinal fluid (aCSF) containing 144 mM NaCl, 2.7 mM KCl, 1.2 mM $CaCl_2$, 1.0 mM $MgCl_2$, and 2 mM NaH_2PO_4, at pH 7.4).

5.2.4 Surgical procedure

All procedures involving animals were carried out with the approval of the Institutional Animal Care and Use Committee of the University of Pittsburgh. Male Sprague-Dawley rats (250-375 g, Hilltop, Scottsdale, PA) were anesthetized with isoflurane (0.5% by volume, Baxter Healthcare, Deerfield, IL). A homoeothermic blanket (EKEG Electronics; Vancouver, BC, Canada) kept the rats' body temperature at 37 ^{o}C. A stereotaxic frame (David Kopf Instruments; Tujunga, CA) was used for all surgeries. (over the striatum. A guide cannula MD-2251, Bioanalytical Systems Inc.; West Lafayette, IN) was implanted into the striatum (1.2 mm anterior of bregma, 2.5 mm lateral of bregma) and lowered to 1 mm beneath the surface of the brain. Jeweler's screws with dental cement were used to hold the cannula in place. Rats recovered for a minimum of three days, following which a second procedure was performed to implant the microdialysis probe. Rats were anesthetized with isoflurane and microdialysis probes were slowly lowered vertically, over thirty minutes, into the striatum (7.0 mm below dura) and secured to the guide cannula with epoxy cement. Once the probe was implanted, anesthesia was removed and rats were placed in a Raturn chamber (Bioanalytical Systems, West Lafayette, IN) for the duration of the experiment.

5.2.5 *In vivo* online microdialysis coupled with capillary UHPLC-EC system

Figure 18 shows a diagram for the *in vivo* online microdialysis-UHPLC-EC system. A PicoPlus syringe pump (Harvard Apparatus, Holliston, MA) with a 1.0 mL gas-tight syringe delivered the microdialysis perfusion fluid aCSF. A two-position "stimulus" loop injector was placed between the syringe and dialysis probe for the introduction of another solution. To minimize Taylor-Aris dispersion and other sources of dispersion, 75 μm i.d. capillary tubing (10 cm) connected the

stimulus valve to the microdialysis inlet capillary (70 cm), which was, in turn, connected to the dialysis tubing, the outlet capillary (70 cm), a connector capillary (10 cm) and the HPLC injection valve. All connections were made using MicroTight Unions (IDEX Health & Science, Oak Harbor, WA).

Probe implantation was carried out early in the morning, with online experiments initiated in the afternoon of the same day. Probes were perfused with aCSF at 0.6 μL/min for at least 2 hours after implantation prior to connection to the online chromatographic system. Standards (100 nM DA) were analyzed both before and after the online experiments, for the purpose of calibration. The sampling volume was 600 nL – selected to slightly overfill the 500 nL sample loop volume, in order to increase injection volume precision. Stable basal dopamine concentrations were observed for at least twenty minutes prior to carrying out an experiment such as K^+ stimulation. Following this, twenty minute stimulations with 20 mM, 50 mM, 70 mM, 100 mM and 120 mM K^+ were conducted. The dopamine D2/D3 receptor agonist quinpirole was then introduced by perfusion (10 μM in aCSF).

Peak area was used for concentration calibration. Tointegrate the areas under the dopamine peaks, a standard Savitzky-Golay, second derivative, quadratic smooth was employed, using an 81 point window.[131,132] Prior to determining the integration limits, an approximate window defined to contain the eluted peak was identified. The start and stop integration points were manually determined. A linear baseline between the start and stop points was created and the integration routine was programmed using MATLAB environment (Mathworks, Natick, MA).

5.3 RESULTS AND DISCUSSION

5.3.1 Separation conditions for online dopamine determination

Dopamine and serotonin coexist in the extracellular space of the striatum in rat brain. Compared to serotonin, dopamine is less hydrophobic due to a smaller aromatic ring and, therefore, exhibits notably smaller retention in ion-pair reverse phase HPLC. Dopamine was poorly retained using the original separation condition for serotonin and the basal level dopamine in microdialysate was beyond the detection limit. Therefore, we had to re-optimize the separation condition, in order to achieve proper retention and good detection limit for dopamine. In order to avoid the sloping baseline caused by the additional presence of a high concentration of ascorbate, we increased the retention time of dopamine to about 0.9 minutes (Figure 35), by adjusting the column temperature to 35 ℃ and mobile phase flow rate to 8 μL/min. The lower column temperature also helped with the dopamine on-column focusing process and improved the dopamine detection limit.

5.3.2 *In vivo* dopamine monitoring and dopamine dynamics in response to a stimulus

External calibration was done using 100 nM dopamine standards. The dopamine concentration in the probe was used directly, without probe recovery correction. Figure 35 shows a typical chromatogram for online measurement of basal dopamine concentrations in microdialysates collected from the striatum of freely-moving rats. Confirmation of dopamine peaks was done by perfusing with 10 μM quinpirole (section 5.2.5), which lead to decreased dopamine levels in the

extracellular space. Following this perfusion, a total loss of dopamine peaks was observed (Figure 35).

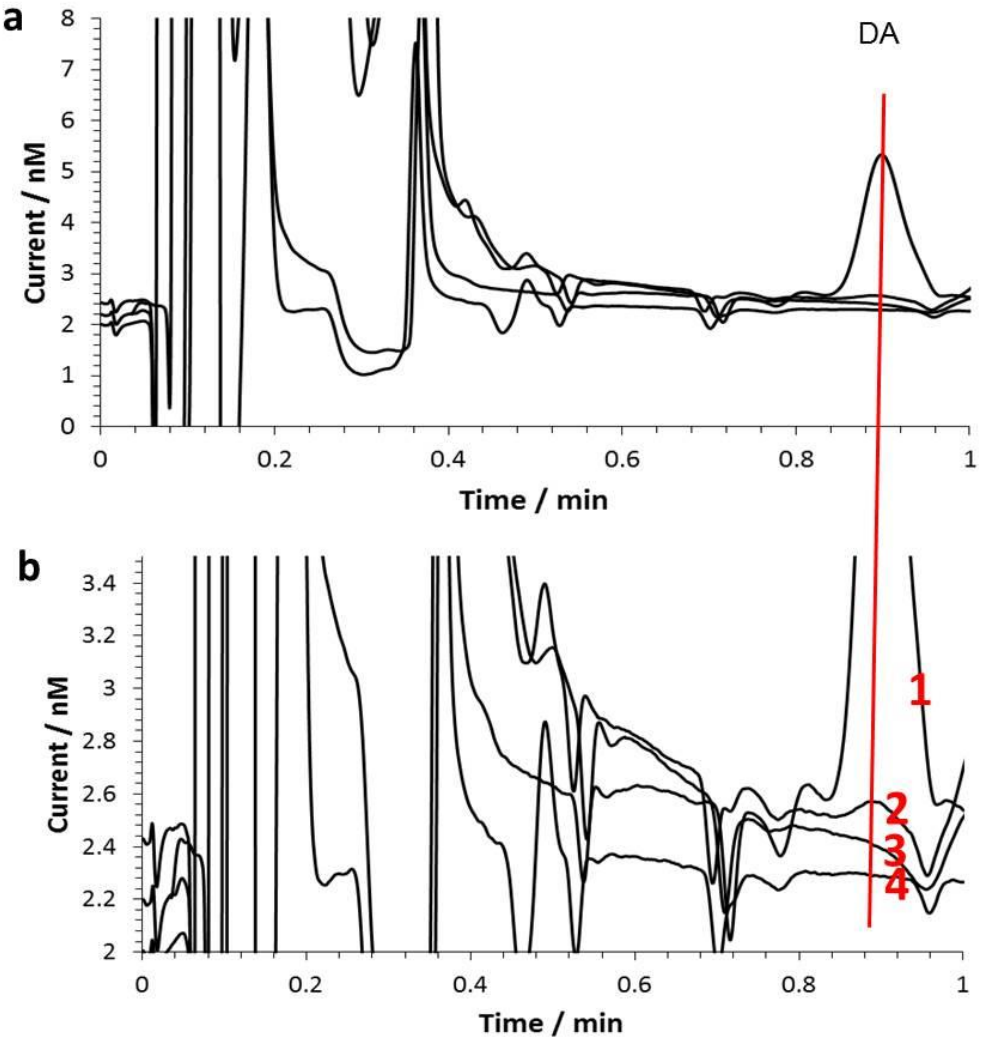

Figure 35. Confirmation of dopamine peak in the microdialysates

Chromatograms (a) and their local image (b) of a standard 100 nM DA sample (1); a baseline microdialysate sample (2); a baseline microdialysate sample after perfusing with 10 μM quinpirole (3); aCSF (4). Column: 150-μ-i.d., 3.0-cm-length capillary column packed with BEH C 18 particles. Mobile phase: 100 mM sodium acetate, 0.15 mM disodium EDTA, 10.0 mM SOS, pH=4.0, mixed with 4% (v/v) acetonitrile. Flow rate: 8.0 μL/min. Column temperature: 35 ℃. Injection volume: 500 nL. Electrochemical detection.

Spreading depression[153] is a wave of near-complete sustained depolarization of neurons and astrocytes, which propagates over cortical and subcortical structures. The occurrence of spreading depression is associated with massive ion/neurotransmitter efflux, enormous glucose consumption and increased cerebral blood flow, followed by oligemia. Spontaneous occurrences of spreading depression are clinically and experimentally observed in neurological disorders[154] and brain injury.[155] Of interest to this study, spreading depression can be artificially induced in experimental settings by electric stimulation, needle prick and K^+. Spreading depression is, most commonly, detected using electrophysiology and real-time imaging of blood flow. Rogers et al.[121] monitored changes in extracellular glucose and K^+ concentrations during spreading depression induced by needle prick, using microdialysis coupled with microfluidic sensors. With the help of a superior temporal resolution, it was revealed that the start of glucose consumption was synchronous with K^+ recovery, instead of K^+ release. Monitoring extracellular dopamine and serotonin allows investigation into, and understanding of, the response of the monoaminergic neurotransmission system under spreading depression. Compared to serotonin, dopamine occurs in significantly higher basal concentrations in the striatum and is more sensitive to stimuli, such as K^+. Following perfusion with 20 mM K^+, there was a detectable increase in extracellular dopamine; however, no statistically significant changes in serotonin were observed. This is likely to be due to the serotonin response being too small to reach the detection threshold.

It was previously reported that perfusion of high K^+ through microdialysis probes can induce recurrent waves of spreading depression.[156] Therefore, we expected dramatic changes in extracellular dopamine levels, resulting from massive dopamine efflux, caused by near-complete sustained depolarization with each wave of spreading depression. Perfusion of aCSF, containing six different K^+ concentrations, into the striatum area for twenty minutes elevated dopamine

levels in the microdialysates (Figure 36). At K^+ concentrations of 100 and 120 nM, periodical dopamine fluctuations with regional concentration maxima were observed, which represented recurrent near-complete neuronal depolarization characteristic of a spreading depression wave. Comparing neuron depolarization induced by 100 and 120 nM K^+, we found that the frequency of spreading depression waves positively correlated to K^+ concentration: higher K^+ concentrations induced higher frequency in spreading depression waves. On the other hand, relatively low K^+ concentrations (<= 70 nM) were associated with observed spikes in extracellular dopamine concentration, followed by a gradual decrease back to basal dopamine. The observation of dopamine spikes indicated that K^+ promotes dopamine release, as expected. After initial release, dopamine recovery by neurons accounted for the net dopamine change and reduction of extracellular dopamine levels. The data set for maximum dopamine release and K^+ concentration is shown to fit well in exponential regression analysis (R^2 = 0.9926; Table 11, Figure 37), before reaching the threshold of spreading depression.

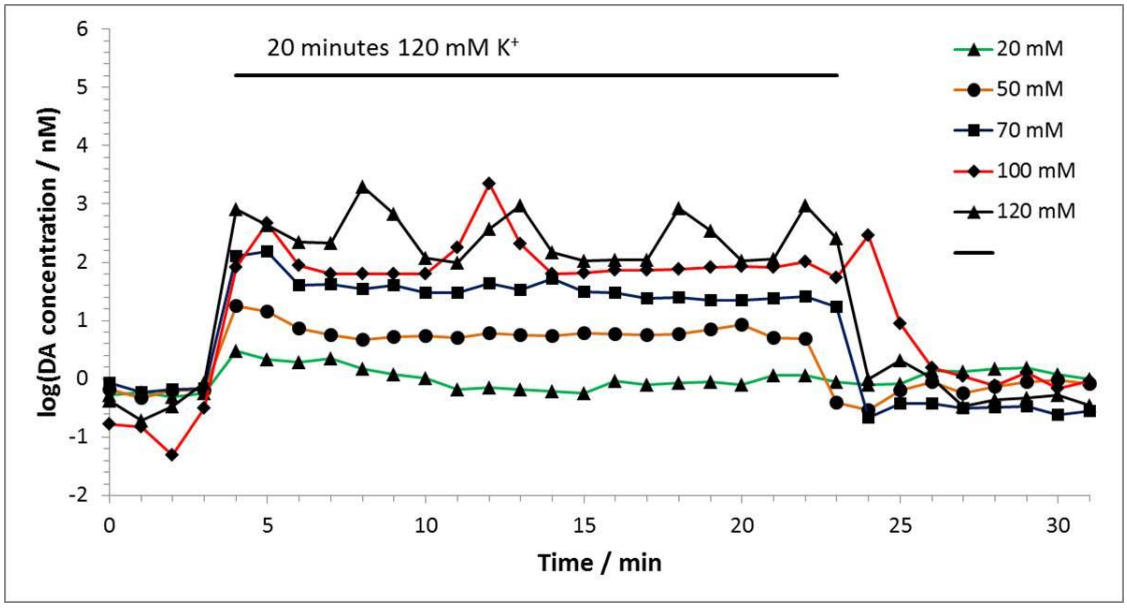

Figure 36. Online *in vivo* dopamine measurement under 20 minutes K^+ administration

Table 11. Dopamine maximum release in response to stimulation with different concentrations of K^+

K^+ (mM)	3.5	20	50	70	100	120
DA (nM)	0.5	3.0	18	155	2178	2014

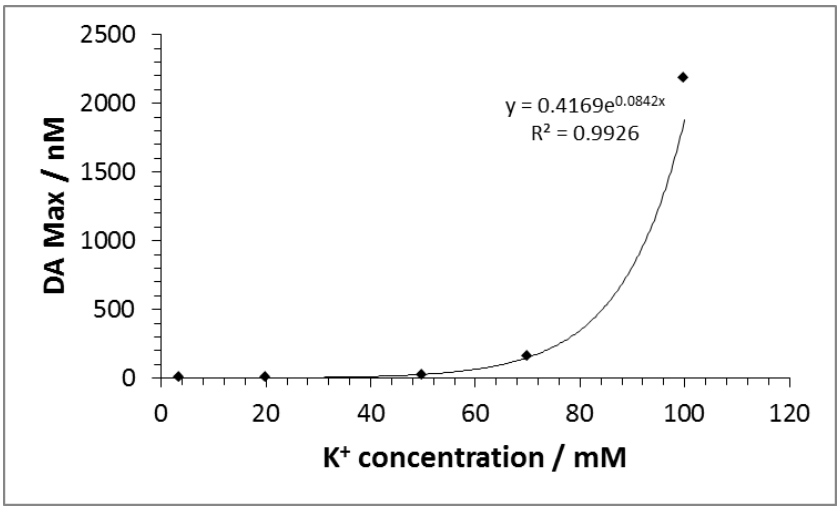

Figure 37. The relationship between maximum dopamine release and K^+ (stimulus) concentration

5.4 CONCLUSIONS

Our online microdialysis/HPLC system proved to be a robust method of monitoring extracellular levels and changes in monoamine neurotransmitters, dopamine and serotonin. The improved temporal resolution was found to yield new information on dynamics of these molecules, namely rapid changes in extracellular dopamine and serotonin, which can be used for elucidation of the role of monoamine neurotransmitters in physiologically relevant dynamic processes. We also suggest that this fast micoridialysis/HPLC system can uncover novel information on

dopaminergic and serotonergic neurochemistry, which could be useful in studying emotion, behavior, complex disorders and new therapeutic strategies for neurological conditions.

BIBLIOGRAPHY

(1) Schultz, W. *Annual review of neuroscience* **2007**, *30*, 259-288.
(2) Naughton, M.; Mulrooney, J. B.; Leonard, B. E. *Hum. Psychopharmacol.* **2000**, *15*, 397-415.
(3) Hahn, M. K.; Blakely, R. D. *Pharmacogenomics J.* **2002**, *2*, 217-235.
(4) Gainetdinov, R. R.; Caron, M. G. *Annu. Rev. Pharmacol. Toxicol.* **2003**, *43*, 261-284.
(5) Torres, G. E.; Gainetdinov, R. R.; Caron, M. G. *Nature reviews. Neuroscience* **2003**, *4*, 13-25.
(6) Schultz, K. N.; Kennedy, R. T. *Annu. Rev. Anal. Chem.* **2008**, *1*, 627-661.
(7) Perry, M.; Li, Q.; Kennedy, R. T. *Anal. Chim. Acta* **2009**, *653*, 1-22.
(8) Davies, M. I.; Cooper, J. D.; Desmond, S. S.; Lunte, C. E.; Lunte, S. M. *Adv. Drug Delivery Rev.* **2000**, *45*, 169-188.
(9) Stuart, J. N.; Hummon, A. B.; Sweedler, J. V. *Anal Chem* **2004**, *76*, 121A-128A.
(10) Phillips, P. E.; Stuber, G. D.; Heien, M. L.; Wightman, R. M.; Carelli, R. M. *Nature* **2003**, *422*, 614-618.
(11) Daws, L. C.; Toney, G. M.; Gerhardt, G. A.; Frazer, A. *The Journal of pharmacology and experimental therapeutics* **1998**, *286*, 967-976.
(12) Robinson, D. L.; Venton, B. J.; Heien, M. L.; Wightman, R. M. *Clin Chem* **2003**, *49*, 1763-1773.
(13) Hashemi, P.; Dankoski, E. C.; Petrovic, J.; Keithley, R. B.; Wightman, R. M. *Anal. Chem. (Washington, DC, U. S.)* **2009**, *81*, 9462-9471.
(14) Borue, X.; Cooper, S.; Hirsh, J.; Condron, B.; Venton, B. J. *Journal of neuroscience methods* **2009**, *179*, 300-308.
(15) Hentall, I. D.; Pinzon, A.; Noga, B. R. *Neuroscience* **2006**, *142*, 893-903.
(16) Zhou, F. M.; Liang, Y.; Salas, R.; Zhang, L.; De Biasi, M.; Dani, J. A. *Neuron* **2005**, *46*, 65-74.
(17) Mundorf, M. L.; Joseph, J. D.; Austin, C. M.; Caron, M. G.; Wightman, R. M. *J Neurochem* **2001**, *79*, 130-142.
(18) Kume-Kick, J.; Rice, M. E. *Journal of neuroscience methods* **1998**, *84*, 55-62.
(19) Wrona, M. Z.; Dryhurst, G. *Bioorg. Chem.* **1990**, *18*, 291-317.
(20) Parrot, S.; Neuzeret, P.-C.; Denoroy, L. *J. Chromatogr. B: Anal. Technol. Biomed. Life Sci.* **2011**, *879*, 3871-3878.
(21) Reinhoud, N. J.; Brouwer, H. J.; van Heerwaarden, L. M.; Korte-Bouws, G. A. *ACS chemical neuroscience* **2013**, *4*, 888-894.
(22) Ferry, B.; Gifu, E. P.; Sandu, I.; Denoroy, L.; Parrot, S. *Journal of chromatography. B, Analytical technologies in the biomedical and life sciences* **2014**, *951-952*, 52-57.
(23) Hasegawa, H.; Piacentini, M. F.; Sarre, S.; Michotte, Y.; Ishiwata, T.; Meeusen, R. *The Journal of physiology* **2008**, *586*, 141-149.

(24) Bosker, F. J.; Folgering, J. H.; Gladkevich, A. V.; Schmidt, A.; van der Hart, M. C.; Sprouse, J.; den Boer, J. A.; Westerink, B. H.; Cremers, T. I. *J Neurochem* **2009**, *108*, 1126-1135.
(25) McKenzie, J. A.; Watson, C. J.; Rostand, R. D.; German, I.; Witowski, S. R.; Kennedy, R. T. *Journal of chromatography. A* **2002**, *962*, 105-115.
(26) Parrot, S.; Lambas-Senas, L.; Sentenac, S.; Denoroy, L.; Renaud, B. *J. Chromatogr. B: Anal. Technol. Biomed. Life Sci.* **2007**, *850*, 303-309.
(27) Newton, A. P.; Justice, J. B., Jr. *Anal. Chem.* **1994**, *66*, 1468-1472.
(28) Jung, M. C.; Shi, G.; Borland, L.; Michael, A. C.; Weber, S. G. *Anal. Chem.* **2006**, *78*, 1755-1760.
(29) Wang, M.; Hershey, N. D.; Mabrouk, O. S.; Kennedy, R. T. *Anal. Bioanal. Chem.* **2011**, *400*, 2013-2023.
(30) Kennedy, R. T.; Watson, C. J.; Haskins, W. E.; Powell, D. H.; Strecker, R. E. *Curr Opin Chem Biol* **2002**, *6*, 659-665.
(31) Lada, M. W.; Kennedy, R. T. *Anal Chem* **1996**, *68*, 2790-2797.
(32) Shou, M.; Ferrario, C. R.; Schultz, K. N.; Robinson, T. E.; Kennedy, R. T. *Anal. Chem.* **2006**, *78*, 6717-6725.
(33) Hsieh, M. M.; Chang, H. T. *Electrophoresis* **2005**, *26*, 187-195.
(34) Tseng, W. L.; Chen, S. M.; Hsu, C. Y.; Hsieh, M. M. *Anal Chim Acta* **2008**, *613*, 108-115.
(35) Qi, S. D.; Tian, S. L.; Xu, H. X.; Sung, J. J.; Bian, Z. X. *Analytical and bioanalytical chemistry* **2009**, *393*, 2059-2066.
(36) Shippenberg, T. S.; Thompson, A. C. *Current Protocols in Neuroscience* **2001**, *7.1*, 1-27.
(37) Benveniste, H. *J Neurochem* **1989**, *52*, 1667-1679.
(38) Westerink, B. H.; Justice, J. B., Jr. In *Microdialysis in the Neurosciences*, Robinson, T. E.; Justice, J. B., Jr., Eds.; Elsevier Science Publishing: New York, 1991, pp 23-43.
(39) Bungay, P. M.; Morrison, P. F.; Dedrick, R. L. *Life Sci.* **1990**, *46*, 105-119.
(40) Ungerstedt, U. In *Measurement of Neurotransmitter Release In Vivo*, Marsden, C. A., Ed.; John Wiley & Sons: New York, 1984, pp 81-105.
(41) Herrera-Marschitz, M.; Arbuthnott, G.; Ungerstedt, U. *Progress in neurobiology* **2010**, *90*, 176-189.
(42) Cifuentes Castro, V. H.; Lopez Valenzuela, C. L.; Salazar Sanchez, J. C.; Pena, K. P.; Lopez Perez, S. J.; Ibarra, J. O.; Villagran, A. M. *Current neuropharmacology* **2014**, *12*, 490-508.
(43) Vissers, J. P. *Journal of chromatography. A* **1999**, *856*, 117-143.
(44) Edwards, J. L.; Edwards, R. L.; Reid, K. R.; Kennedy, R. T. *J. Chromatogr. A* **2007**, *1172*, 127-134.
(45) Vissers, J. P. C.; de, R. A. H.; Ursem, M.; Chervet, J.-P. *J. Chromatogr. A* **1996**, *746*, 1-7.
(46) Groskreutz, S. R.; Swenson, M. M.; Secor, L. B.; Stoll, D. R. *Journal of chromatography. A* **2012**, *1228*, 41-50.
(47) van Deemter, J. J.; Zuiderweg, F. J.; Klinkenberg, A. *Chem. Eng. Sci.* **1956**, *5*, 271-289.
(48) Hawkes, S. J. *J. Chem. Educ.* **1983**, *60*, 393-398.
(49) Crombeen, J. P.; Poppe, H.; Kraak, J. C. *Chromatographia* **1986**, *22*, 319-328.
(50) Gritti, F.; Guiochon, G. *Journal of chromatography. A* **2010**, *1217*, 1485-1495.
(51) Issaeva, T.; Kourganov, A.; Unger, K. *J. Chromatogr. A* **1999**, *846*, 13-23.
(52) Destefano, J. J.; Langlois, T. J.; Kirkland, J. J. *J Chromatogr Sci* **2008**, *46*, 254-260.
(53) Cunliffe, J. M.; Maloney, T. D. *J Sep Sci* **2007**, *30*, 3104-3109.
(54) Guiochon, G.; Gritti, F. *Journal of chromatography. A* **2011**, *1218*, 1915-1938.

(55) Guiochon, G. *Journal of chromatography. A* **2007**, *1168*, 101-168; discussion 100.
(56) Nakanishi, K.; Soga, N. *J. Am. Ceram. Soc.* **1991**, *74*, 2518-2530.
(57) Cabrera, K.; Wieland, G.; Lubda, D. *TrAC, Trends Anal. Chem.* **1998**, *17*, 50-53.
(58) Liu, K.; Aggarwal, P.; Lawson, J. S.; Tolley, H. D.; Lee, M. L. *J Sep Sci* **2013**, *36*, 2767-2781.
(59) Li, Y.; Lee, M. L. *J Sep Sci* **2009**, *32*, 3369-3378.
(60) Knox, J. H.; Saleem, M. *J. Chromatogr. Sci.* **1969**, *7*, 614-622.
(61) MacNair, J. E.; Lewis, K. C.; Jorgenson, J. W. *Anal Chem* **1997**, *69*, 983-989.
(62) Heinisch, S.; Rocca, J. L. *Journal of chromatography. A* **2009**, *1216*, 642-658.
(63) McNeff, C. V.; Yan, B.; Stoll, D. R.; Henry, R. A. *J Sep Sci* **2007**, *30*, 1672-1685.
(64) Teutenberg, T. *Anal Chim Acta* **2009**, *643*, 1-12.
(65) Thompson, J. D.; Brown, J. S.; Carr, P. W. *Anal Chem* **2001**, *73*, 3340-3347.
(66) Huang, J. X.; Stuart, J. D.; Melander, W. R.; Horvath, C. *J Chromatogr* **1984**, *316*, 151-161.
(67) Yang, Y. *LC-GC Europe* **2003**, 37-41.
(68) Stoll, D. R.; Carr, P. W. *J Am Chem Soc* **2005**, *127*, 5034-5035.
(69) Yan, B.; Zhao, J.; Brown, J. S.; Blackwell, J.; Carr, P. W. *Anal Chem* **2000**, *72*, 1253-1262.
(70) Yang, X.; Ma, L.; Carr, P. W. *Journal of chromatography. A* **2005**, *1079*, 213-220.
(71) Kephart, T. S.; Dasgupta, P. K. *Anal. Chim. Acta* **2000**, *414*, 71-78.
(72) Xiang, Y.; Yan, B.; Yue, B.; McNeff, C. V.; Carr, P. W.; Lee, M. L. *Journal of chromatography. A* **2003**, *983*, 83-89.
(73) Nguyen, D. T.; Guillarme, D.; Heinisch, S.; Barrioulet, M.; Rocca, J.; Rudaz, S.; Veuthey, J. *J. Chromatogr. A* **2007**, *1167*, 76-84.
(74) Plumb, R.; Mazzeo, J. R.; Grumbach, E. S.; Rainville, P.; Jones, M.; Wheat, T.; Neue, U. D.; Smith, B.; Johnson, K. A. *J Sep Sci* **2007**, *30*, 1158-1166.
(75) Bowser, M. T.; Kennedy, R. T. *Electrophoresis* **2001**, *22*, 3668-3676.
(76) Jung, M. C.; Weber, S. G. *Anal Chem* **2005**, *77*, 974-982.
(77) Jung, M. C.; Munro, N.; Shi, G.; Michael, A. C.; Weber, S. G. *Anal Chem* **2006**, *78*, 1761-1768.
(78) Xu, H.; Weber, S. G. *J. Chromatogr. A* **2009**, *1216*, 1346-1352.
(79) Xu, X.; Li, L.; Weber, S. G. *Trends in analytical chemistry : TRAC* **2007**, *26*, 68-79.
(80) Chen, J. G.; Weber, S. G.; Glavina, L. L.; Cantwell, F. F. *J Chromatogr* **1993**, *656*, 549-576.
(81) Dolan, J. W. *Journal of chromatography. A* **2002**, *965*, 195-205.
(82) Greibrokk, T.; Andersen, T. *Journal of chromatography. A* **2003**, *1000*, 743-755.
(83) McCalley, D. V. *Journal of chromatography. A* **2000**, *902*, 311-321.
(84) Bolliet, D.; Poole, C. F. *Analyst* **1998**, *123*, 295-299.
(85) Cukalovic, A.; Monbaliu, J.-C. M. R.; Stevens, C. V. *Top. Heterocycl. Chem.* **2010**, *23*, 161-198.
(86) Fang, H.; Xiao, Q.; Wu, F.; Floreancig, P. E.; Weber, S. G. *J. Org. Chem.* **2010**, *75*, 5619-5626.
(87) Frost, C. G.; Mutton, L. *Green Chem.* **2010**, *12*, 1687-1703.
(88) Weiler, A.; Junkers, M. *Pharm. Technol.* **2009**, *S6*, S10-S11.
(89) Wiles, C.; Watts, P. *Spec. Chem. Mag.* **2009**, *29*, 40-41.
(90) Wiles, C.; Watts, P. *Adv. Chem. Eng.* **2010**, *38*, 103-194.
(91) Davis, J. M.; Stoll, D. R.; Carr, P. W. *Anal. Chem.* **2008**, *80*, 461-473.
(92) Potts, L. W.; Stoll, D. R.; Li, X.; Carr, P. W. *J. Chromatogr. A* **2010**, *1217*, 5700-5709.
(93) Stoll, D. R. *Anal. Bioanal. Chem.* **2010**, *397*, 979-986.

(94) Nagata, T.; Nishiyama, A.; Yamato, T.; Obata, T.; Aomine, M. *Nutr. Neurosci.* **2011**, *14*, 96-105.
(95) Morita, M.; Nakayama, K. *Psychiatry Clin. Neurosci.* **2011**, *65*, 246-253.
(96) Kleijn, J.; Cremers, T. I. F. H.; Hofland, C. M.; Westerink, B. H. C. *Neurosci. Res.* **2011**, *70*, 334-337.
(97) Poppe, H. *J. Chromatogr. A* **1997**, *778*, 3-21.
(98) Desmet, G.; Clicq, D.; Gzil, P. *Anal. Chem.* **2005**, *77*, 4058-4070.
(99) Carr, P. W.; Wang, X.; Stoll, D. R. *Anal. Chem.* **2009**, *81*, 5342-5353.
(100) Liu, Y.; Zhang, J.; Xu, X.; Zhao, M. K.; Andrews, A. M.; Weber, S. G. *Anal. Chem.* **2010**, *82*, 9611-9616.
(101) Neue, U. D. *HPLC Columns: Theory, Technology, and Practice*; Wiley-VCH, 1997, p 393 pp.
(102) Poole, C. F.; Schuette, S. A. *Contemporary Practice of Chromatography*; Elsevier: Amsterdam, 1984, p 708 pp.
(103) Guiochon, G.; Colin, H. *Microcolumn High-Performance Liquid Chromatography*; Elsevier: Amsterdam, 1984; Vol. 28.
(104) Poppe, H.; Paanakker, J.; Bronckhorst, M. *J. Chromatogr. A* **1981**, *204*, 77-84.
(105) Weber, S. G. *J. Electroanal. Chem. Interfacial Electrochem.* **1983**, *145*, 1-7.
(106) Elbicki, J. M.; Morgan, D. M.; Weber, S. G. *Anal. Chem.* **1984**, *56*, 978-985.
(107) Weber, S. G.; Long, J. T. *Anal. Chem.* **1988**, *60*, 903A-904A, 906A-913A.
(108) Paxions, G.; Watson, C. *The Rat Brain in Stereotaxic Coordinates*; Academic Press: New York, 1998.
(109) Groskreutz, S. R.; Weber, S. G. *Journal of chromatography. A* **2015**.
(110) Guillarme, D.; Heinisch, S.; Rocca, J. L. *J Chromatogr. A* **2004**, *1052*, 39-51.
(111) Billen, J.; Broeckhoven, K.; Liekens, A.; Choikhet, K.; Rozing, G.; Desmet, G. *J Chromatogr. A* **2008**, *1210*, 30-44.
(112) Gerhardt, G.; Adams, R. N. *Anal. Chem.* **1982**, *54*, 2618-2620.
(113) Jackson, D.; Abercrombie, E. D. *J. Neurochem.* **1992**, *58*, 890-897.
(114) Zhou, J.-L.; An, J.-J.; Li, P.; Li, H.-J.; Jiang, Y.; Cheng, J.-F. *J. Chromatogr. A* **2009**, *1216*, 2394-2403.
(115) Sameenoi, Y.; Koehler, K.; Shapiro, J.; Boonsong, K.; Sun, Y.; Collett, J.; Volckens, J.; Henry, C. S. *J. Am. Chem. Soc.* **2012**, *134*, 10562-10568.
(116) Dishinger, J. F.; Kennedy, R. T. *Anal. Chem.* **2007**, *79*, 947-954.
(117) Workman, J.; Koch, M.; Lavine, B.; Chrisman, R. *Anal. Chem. (Washington, DC, U. S.)* **2009**, *81*, 4623-4643.
(118) Murphy, D. L.; Lesch, K.-P. *Nat. Rev. Neurosci.* **2008**, *9*, 85-96.
(119) Bian, X.; Patel, B.; Dai, X.; Galligan, J. J.; Swain, G. *Gastroenterology* **2007**, *132*, 2438-2447.
(120) Bunin, M. A.; Prioleau, C.; Mailman, R. B.; Wightman, R. M. *J. Neurochem.* **1998**, *70*, 1077-1087.
(121) Rogers, M. L.; Feuerstein, D.; Leong, C. L.; Takagaki, M.; Niu, X.; Graf, R.; Boutelle, M. G. *ACS Chem. Neurosci.* **2013**, *4*, 799-807.
(122) Nandi, P.; Lunte, S. M. *Anal. Chim. Acta* **2009**, *651*, 1-14.
(123) Nandi, P.; Scott, D. E.; Desai, D.; Lunte, S. M. *Electrophoresis* **2013**, *34*, 895-902.
(124) O'Brien, K. B.; Esguerra, M.; Miller, R. F.; Bowser, M. T. *Anal. Chem.* **2004**, *76*, 5069-5074.

(125) Jaquins-Gerstl, A.; Shu, Z.; Zhang, J.; Liu, Y.; Weber, S. G.; Michael, A. C. *Anal. Chem. (Washington, DC, U. S.)* **2011**, *83*, 7662-7667.
(126) Zhang, J.; Liu, Y.; Jaquins-Gerstl, A.; Shu, Z.; Michael, A. C.; Weber, S. G. *J. Chromatogr. A* **2012**, *1251*, 54-62.
(127) Richter, D. W.; Schmidt-Garcon, P.; Pierrefiche, O.; Bischoff, A. M.; Lalley, P. M. *The Journal of physiology* **1999**, *514 (Pt 2)*, 567-578.
(128) Yang, H.; Thompson, A. B.; McIntosh, B. J.; Altieri, S. C.; Andrews, A. M. *ACS Chem. Neurosci.* **2013**, *4*, 790-798.
(129) Stamford, J. A. In *Monitoring Neuronal Activity*; Oxford University Press: Oxford, 1992, pp 149-155.
(130) Dolan, J. W. *LC-GC* **1996**, *14*, 562-566.
(131) Savitzky, A.; Golay, M. J. E. *Anal. Chem.* **1964**, *36*, 1627-1639.
(132) Thekkudan, D. F.; Rutan, S. C. In *Comprehensive Chemometrics*, Brown, S.; Tauler, R.; Walczak, B., Eds.; Elseiver: Oxford, 2009, pp 9-24.
(133) Lada, M. W.; Vickroy, T. W.; Kennedy, R. T. *Anal. Chem.* **1997**, *69*, 4560-4565.
(134) Bungay, P. M.; Wang, T.; Yang, H.; Elmquist, W. F. *J. Membr. Sci.* **2010**, *348*, 131-149.
(135) Nunge, R. J.; Gill, W. N. *Ind. Eng. Chem.* **1969**, *61*, 33-49.
(136) Beisler, A. T.; Schaefer, K. E.; Weber, S. G. *J. Chromatogr., A* **2003**, *986*, 247-251.
(137) Chaurasia, C. S.; Chen, C.-E.; Ashby, C. R., Jr. *J. Pharm. Biomed. Anal.* **1999**, *19*, 413-422.
(138) Penicaud, C.; Bohuon, P.; Peyron, S.; Gontard, N.; Guillard, V. *Ind. Eng. Chem. Res.* **2012**, *51*, 1131-1142.
(139) Tikekar, R. V.; Anantheswaran, R. C.; LaBorde, L. F. *J. Food Sci.* **2011**, *76*, H62-H71.
(140) Dupertuis, Y. M.; Ramseyer, S.; Fathi, M.; Pichard, C. *JPEN J Parenter Enteral Nutr* **2005**, *29*, 125-130.
(141) Roig, M. G.; Rivera, Z. S.; Kennedy, J. F. *Int J Food Sci Nutr* **1995**, *46*, 107-115.
(142) Fiorillo, C. D.; Tobler, P. N.; Schultz, W. *Science (New York, N.Y.)* **2003**, *299*, 1898-1902.
(143) Fiorillo, C. D.; Newsome, W. T.; Schultz, W. *Nature neuroscience* **2008**, 966-973.
(144) Roitman, M. F.; Stuber, G. D.; Phillips, P. E.; Wightman, R. M.; Carelli, R. M. *The Journal of neuroscience : the official journal of the Society for Neuroscience* **2004**, *24*, 1265-1271.
(145) Hermans, A.; Keithley, R. B.; Kita, J. M.; Sombers, L. A.; Wightman, R. M. *Anal Chem* **2008**, *80*, 4040-4048.
(146) Roitman, M. F.; Wheeler, R. A.; Wightman, R. M.; Carelli, R. M. *Nature neuroscience* **2008**, *11*, 1376-1377.
(147) Watson, C. J.; Venton, B. J.; Kennedy, R. T. *Anal Chem* **2006**, *78*, 1391-1399.
(148) Tang, A.; Bungay, P. M.; Gonzales, R. A. *Journal of neuroscience methods* **2003**, *126*, 1-11.
(149) Young, A. M. *Journal of neuroscience methods* **2004**, *138*, 57-63.
(150) Cheng, J. J.; de Bruin, J. P.; Feenstra, M. G. *The European journal of neuroscience* **2003**, *18*, 1306-1314.
(151) Bert, L.; Parrot, S.; Robert, F.; Desvignes, C.; Denoroy, L.; Suaud-Chagny, M. F.; Renaud, B. *Neuropharmacology* **2002**, *43*, 825-835.
(152) Zhang, J.; Jaquins-Gerstl, A.; Nesbitt, K. M.; Rutan, S. C.; Michael, A. C.; Weber, S. G. *Anal Chem* **2013**, *85*, 9889-9897.
(153) Leao, A. A. P. *Journal of Neurophysiology* **1944**, *7*, 359-390.

(154) Lauritzen, M.; Dreier, J. P.; Fabricius, M.; Hartings, J. A.; Graf, R.; Strong, A. J. *Journal of cerebral blood flow and metabolism : official journal of the International Society of Cerebral Blood Flow and Metabolism* **2011**, *31*, 17-35.
(155) Strong, A. J.; Fabricius, M.; Boutelle, M. G.; Hibbins, S. J.; Hopwood, S. E.; Jones, R.; Parkin, M. C.; Lauritzen, M. *Stroke; a journal of cerebral circulation* **2002**, *33*, 2738-2743.
(156) Herreras, O.; Somjen, G. G.